ERDC/CHL TR-XX-DRAFT

Coastal and Hydraulics Laboratory

US Army Corps of Engineers®
Engineer Research and Development Center

ERDC
ENGINEER RESEARCH & DEVELOPMENT CENTER

Water Operations Technical Support Program

Simulation of Hydrology, Stream Flow, and Reservoir Levels in the Upper Russian River Watershed

In Support of Forecast Informed Reservoir Operations at Lake Mendocino

Charles W. Downer, Jaime Graulau-Santiago, Stephen J. Turnbull, Clay LaHatte, Michael Shaw, Nawa Raj Pradhan, Ahmad Tavakoly, Mark Wahl, Drew Loney, and Ricardo Vera

July 2020

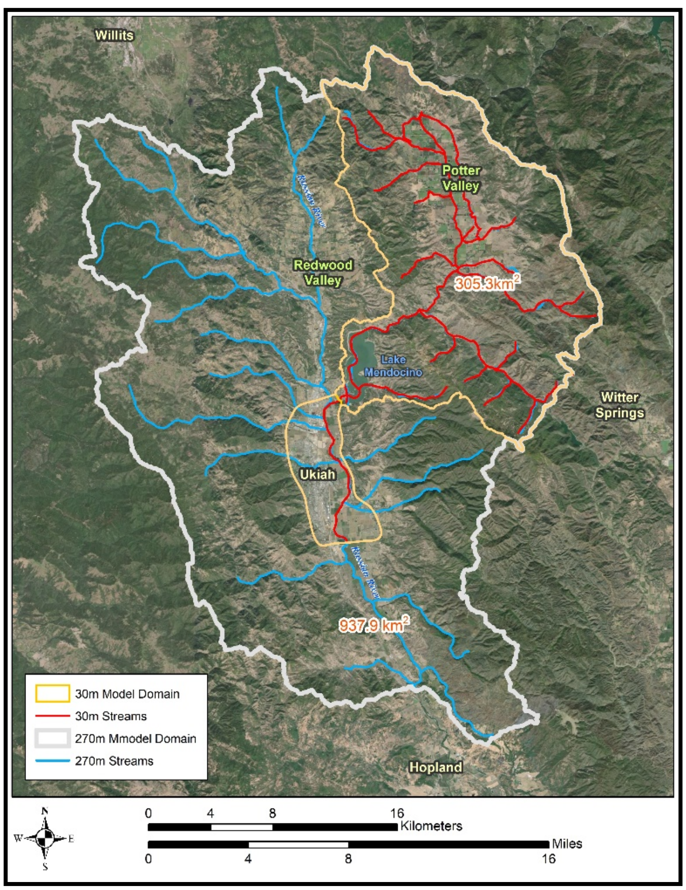

Simulation of Hydrology, Stream Flow, and Reservoir Levels in the Upper Russian River Watershed

In Support of Forecast Informed Reservoir Operations at Lake Mendocino

Downer C. W., Graulau-Santiago J., Turnbull S. J., LaHatte W. C., Shaw M., Pradhan N., Tavakoly A., Wahl M., Loney D., Vera R.

Coastal and Hydraulics Laboratory
U.S. Army Engineer Research and Development Center
2902 Newmark Drive
Champaign, IL 61822

Shaw M., Vera R

Cold Regions Research and Engineering Laboratory
U.S. Army Engineer Research and Development Center
72 Lyme Rd.
Hanover, NH 03755

Graulau-Santiago J

Jacksonville District USACE
701 San Marco Rd
Jacksonville, FL 33207

Final report

Prepared for Water Operations Technical Support Program
Vicksburg, Mississippi

Under Project ####, “Forecast Informed Reservoir Operations”

Abstract

The physics-based, fully-distributed Gridded Surface Subsurface Hydrologic Analysis (GSSHA) watershed model was used to simulate hydrology and lake levels in the Upper Russian River watershed as part of a multi-agency effort to develop Forecast Informed Reservoir Operations (FIRO) for Lake Mendocino in California.

Coupled surface/groundwater models were developed from point and spatially distributed data sets and were driven by precipitation and meteorological forcings from various data sources including the RHONET gauge network, the California/Nevada River Forecast Center (CNRFC) gage derived data, and meteorological forecasts from the Scripps Institute Center for Western Weather and Water Extremes' West-WRF model, a version of the mesoscale Weather Research and Forecast (WRF) model, set up specifically to provide forecasts for atmospheric rivers in the western United States. GSSHA models of various grid resolutions were calibrated to historical data sets and then verified to independent data.

The calibrated models were capable of reproducing US Geological Survey gauging station flows in the Upper Russian River watershed. Applying the calibrated model parameters to validation periods showed that these models are good predictors of the river flows and lake levels when compared to historical observations. The models were also useful for understanding hydrology in the basin as well as determining an annual water budget for the watershed and the reservoir.

A West-WRF driven GSSHA model was capable of reproducing flows and lake levels for a 1 day forecast lead time, but using forecast lead times longer than 1 day resulted in departures from the historical data sets. Physics-based hydrology models are sensitive to precipitation, and analysis of the West-WRF total seasonal precipitation indicated that the rainfall decreased as the forecast lead time increased, resulting in under prediction of flows to Lake Mendocino. The results indicate that an operational West-WRF/GSSHA model may be beneficial in providing information and guidance in a FIRO setting. Improvements to the West-WRF longer lead time precipitation forecasts could improve the utility of such a system. These are active research topics in the FIRO program.

Contents

Figures and Tables

Figures

Tables

Preface

This study was conducted for the US Army Corps of Engineers Forecast Informed Reservoir Operations program under [[[Funding information from title page/Form 7]]]. The technical monitor was Dr. Cary Talbot.

At the time of publication of this report, Dr. Hwai-Ping (Pearce) Cheng was Chief, Hydrologic Systems Branch, and Dr. Cary Talbot was Chief, Flood and Storm Protection Division of the US Army Engineer Research and Development Center, Coastal and Hydraulics Laboratory (ERDCCHL). The Deputy Director of ERDC-CHL was Mr. Jeffrey R. Eckstein, and Dr. Ty V. Wamsley was the Director. COL Teresa A. Schlosser was the Commander of ERDC, and the director was Dr. David Pittman.

The Commander of ERDC was COL Teresa A. Schlosser and the Director was Dr. David W. Pittman.

1 Introduction

1.1 Background

1.1.1 FIRO Project

In the Russian River Basin, a multi-agency effort termed the Forecast-Informed Reservoir Operations (FIRO) study has been underway to assess the potential for both improved streamflow predictions and upgraded (forecast-informed) reservoir operating rules to make water management more efficient in the face of extreme weather and climate events that typically lead to flooding or drought. A drought beginning in 2014, with the release of water from Lake Mendocino to satisfy the flood control operating rules, highlighted the need to consider the possible future conditions, when operating reservoirs. The drought that began in 2014 continued for years, with the reservoir never able to recover the targeted pool levels during that time. In addition, the Sonoma County Water Agency (SCWA), demonstrated that even for the years before the drought (2000-2014) the average water levels in the lake were well below the targeted values. Subsequent flooding in the region that broke the drought caused significant damage, further indicating the need to consider the future (forecast) when operating reservoirs.

1.1.2 FIRO Viability

FIRO consist of two stages: the preliminary viability assessment, and the final viability assessment. The preliminary viability assessment was conducted to determine if the concept of FIRO was theoretically possible. In that stage of the study, standard agency tools (Corps Water Management System (CWMS) models from the United States Army Corps of Engineers (USACE) Hydrologic Engineering Center (HEC), and forecasts from the California Nevada River Forecast Center (CNRFC)) were used to assess the possible viability of using forecasted atmospheric and hydrology products to modify operating rules for Lake Mendocino. In summary, that study indicated that the FIRO concept was indeed viable, and that Lake Mendocino could realistically be operated using forecasts for weather and hydrology while maintaining, or possibly improving flood protection, as well as increasing storage for water supply. With the concept proven sound, the Final Viability Assessment (FVA) was begun. While there are many components of the FVA, this report will focus on the scientific research components of the FVA, specifically the application of state of the art atmospheric and hydrology models at Lake Mendocino.

The system chosen to represent the state of the art in atmospheric and hydrologic modeling were the West-WRF meteorological forecasting and GSSHA hydrology models. The two models are coupled by passing West-WRF forecasted precipitation and hydro-meteorological forcings to drive the GSSHA model. A research-grade observation network in the Russian River Basin above Lake Mendocino provides additional forcing data and observations for tuning and assessing the hydrologic model.

1.1.3 Hydrologic Simulator

GSSHA is a physics-based, spatially explicit, hydrologic model with the capacity to simulate, on a continuous basis, numerous processes relevant to the hydrologic response of a watershed subject to meteorological forcings (Downer and Ogden, 2006). These processes can include, among others: rainfall distribution, plant interception, surface retention, evapotranspiration (ET), vertical infiltration, two-dimensional (2D) overland flow, one-dimensional (1D) channel flow, 2D groundwater flow for an unconfined aquifer system and related surface water-groundwater interaction, lake/reservoir levels, and snow accumulation and melt. Processes are treated with varying degrees of fidelity with related computational and input data requirements, allowing the modeler to choose a process solution method that is consistent with project requirements and/or to explore the potential tradeoffs between simulation accuracy and related resource requirements. Spatial data products, such as digital elevation models, surveyed channel cross sections, soil classification, vegetative cover, land use, and hydro-geological characterizations of the subsurface can readily be incorporated to support model development and model process parameterization.

For application at Lake Mendocino, GSSHA is potentially advantageous to current methods in that GSSHA represents a state-of-the art integrated hydrologic simulator for watershed analysis. In this application the watershed, stream network, and reservoir are simulated in an integrated fashion within one application.

In addition, GSSHA, with GSSHApy (a Python application to convert netCDF format datasets, including gridded weather forecast products, into GSSHA hydro-meteorological forcings) can be driven by weather models for forecasting purposes. Information on GSSHApy is also available on the gsshawiki.com website. In this application, the GSSHA model is driven by the West-WRF forecasting model as described below.

1.1.4 Atmospheric Simulator

As described in Martin et. al. (2018) the CW3E operational model, named West-WRF, has the primary goal of predicting extreme precipitation events (especially those associated with atmospheric rivers (ARs)) that are key to water supply and flooding in the region (Dettinger et al. 2011; Ralph and Dettinger 2012). The West-WRF model (maintained largely through the National Center for Atmospheric Research) is an application of the Weather Research and Forecast model (WRF), a mesoscale numerical weather prediction center configured with the Advanced Research WRF (ARW) dynamical solver (Skamarock 2008). The WRF model is used for a wide range of regional meteorological applications across scales ranging from meters to thousands of kilometers.

Forecasts of 3-hourly near-surface and atmospheric variables needed for GSSHA are obtained from daily West-WRF forecasts generated between December 1st and March 31st of each water year. The West-WRF model configuration includes two overlapping domains (or nests), with parent 9-km domain (25 to 45 N, 115 to 155 W), and a one-way nested 3-km resolution area centered over Northern California. Each domain contains a common vertical spacing of 36 model levels; multiple nested domains are useful for several reasons including; 1) the intermediate resolution (between coarser global model scales and finer, more detailed fine scale nest) can prevent issues with overly abrupt changes of resolved atmospheric wave modes, 2) narrowing the finer scale domain with its much higher fidelity can be more computationally efficient than it might be to attempt to resolve fine scales where such detail may not be necessary for purposes of the forecast or study. The parent domain extent was chosen based on a climatological analysis of the spatial extent of landfalling ARs at Bodega Bay, CA. The inner nest (3-km area) was configured to produce high-resolution forecasts of orographic precipitation and other meteorological details across California and Southern Oregon. Physics options in the two domains are similar except that the finer scale model resolves cloud dynamics, whereas the coarser model includes a cumulus cloud physics scheme with more statistical representation of convective cloud forms since many of their scales cannot be physically resolved at the coarser model mesh scales.

For each 10-day forecast used for this study, the coarse model's initial and boundary conditions are derived from the National Oceanic and Atmospheric Administration's (NOAA) Global Forecast System (GFS) 13 km grid. The 3-km resolution model derives initial and boundary conditions from the coarser model. At this relatively finer scale (when compared with other atmospheric models) and with the physics options selected, the West-WRF model is better able to capture orographic precipitation and other important meteorological details through dynamical downscaling and higher fidelity or more refined physical process representation than what is found in the global, so coarser, GFS; this is one of the purposes of mesoscale numerical weather prediction

(NWP) models versus global, more general circulation models. The 3-km data are further downscaled and temporally concatenated together to provide a continuous stream of input for GSSHA model hydrologic calibration and simulations at GSSHA scales.

1.1.5 Study Site - Lake Mendocino and Coyote Valley Dam (CVD)

Lake Mendocino is located on the East Fork of the Russian River in Mendocino County, California. Created in 1958 by the construction of the Coyote Valley Dam (CVD) impounds water on the East Fork of the Russian River providing flood control, water supply, recreation and stream flow regulation. The CVD and Lake Mendocino have been in operation since 1959. The U.S. Army Corps of Engineers (USACE) owns and operates the dam in accordance with the Lake Mendocino Water Control Manual (1959, revised in 1986) (unpublished). The Sonoma County Water Agency (Water Agency) is the local partner that manages water stored in Lake Mendocino for water supply.

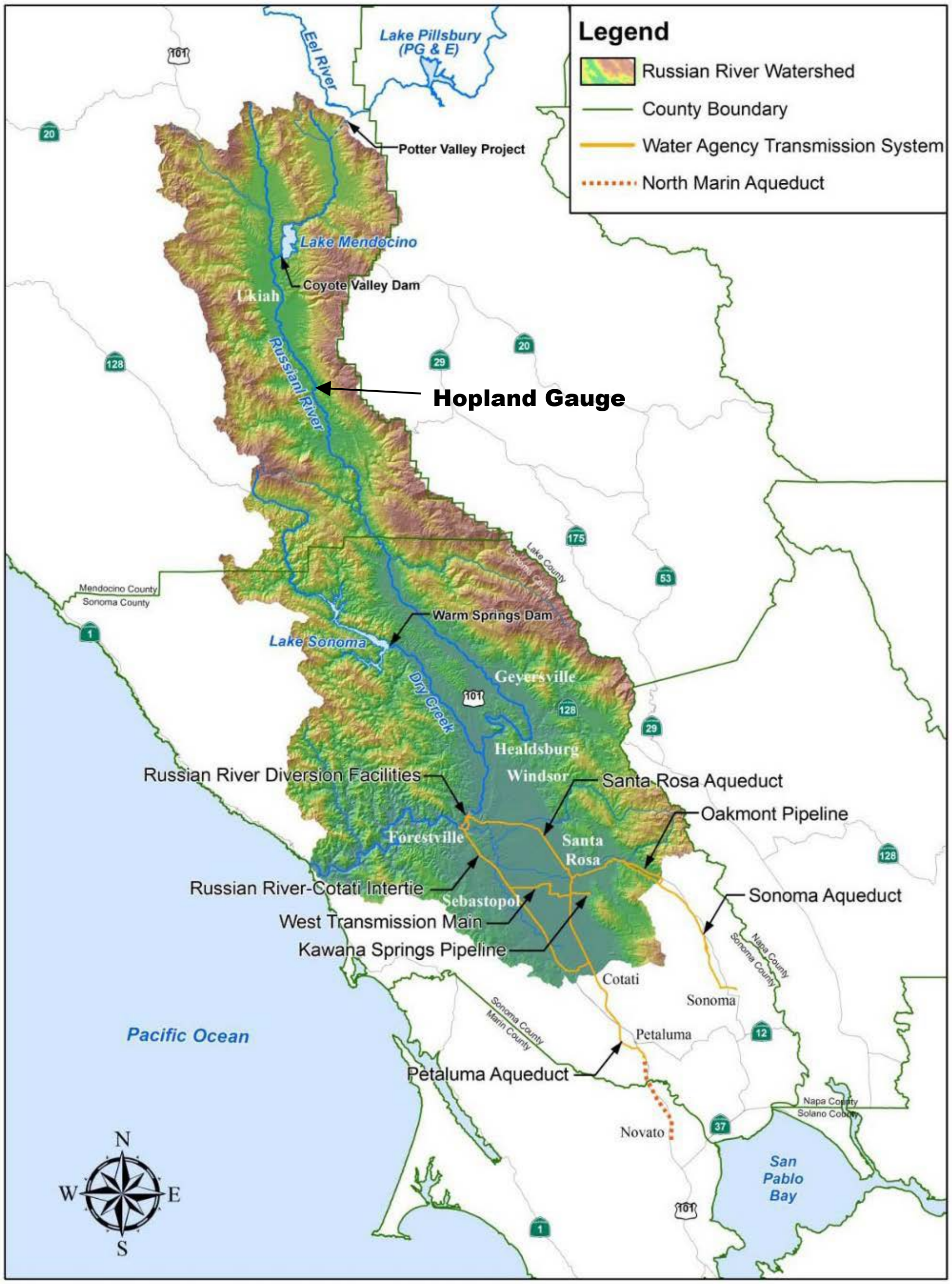

Figure 1. Map of Russian River watershed, including Sonoma County Water Agency transmission system. Source: Sonoma County Water Agency.

Lake Mendocino captures water from two sources: (1) runoff from a drainage area of approximately 105 square miles and (2) Eel River water diverted by Potter Valley Pacific Gas and Electric's (PG&E) Potter Valley Project (PVP). During the rainy season (November through April), natural drainage and stream flow (as opposed to reservoir releases) contribute the majority of the Russian River flow downstream of CVD and above Dry

Creek, the tributary from the Russian River to Lake Sonoma (Figure 1), the other major reservoir in the watershed. In contrast, during the drier months of May through October, water released from Lake Mendocino accounts for most of the water in the Russian River upstream of Dry Creek.

The Water Agency and the Mendocino Flood Control District have water rights permits authorizing storage up to the design capacity of 151101 hectare-meter per year (ha m yr^{-1}) in the reservoir. The Water Agency controls releases from the water supply pool in Lake Mendocino, which is currently specified to be 8437 ha m of storage. However, the USACE manages flood control releases when the water level exceeds the top of the water supply pool elevation. The USACE allows the Water Agency to encroach into the flood pool in the spring so that the summer water supply pool can be increased to 13,692 ha m (111,000 acre ft).

The Lake Mendocino Water Control Manual (unpublished) specifies elevations for an upper volume of reservoir storage that must be kept available for capturing storm runoff and reducing flood risk, and a lower volume of storage that may be used for water supply. During a flood event, runoff is captured by the reservoir and released soon after to create storage space for another potential storm. The Manual is based on typical historical weather patterns– wet during the winter, dry otherwise. The Lake Mendocino operating schedule, or rule curve, is shown in Figure 2.

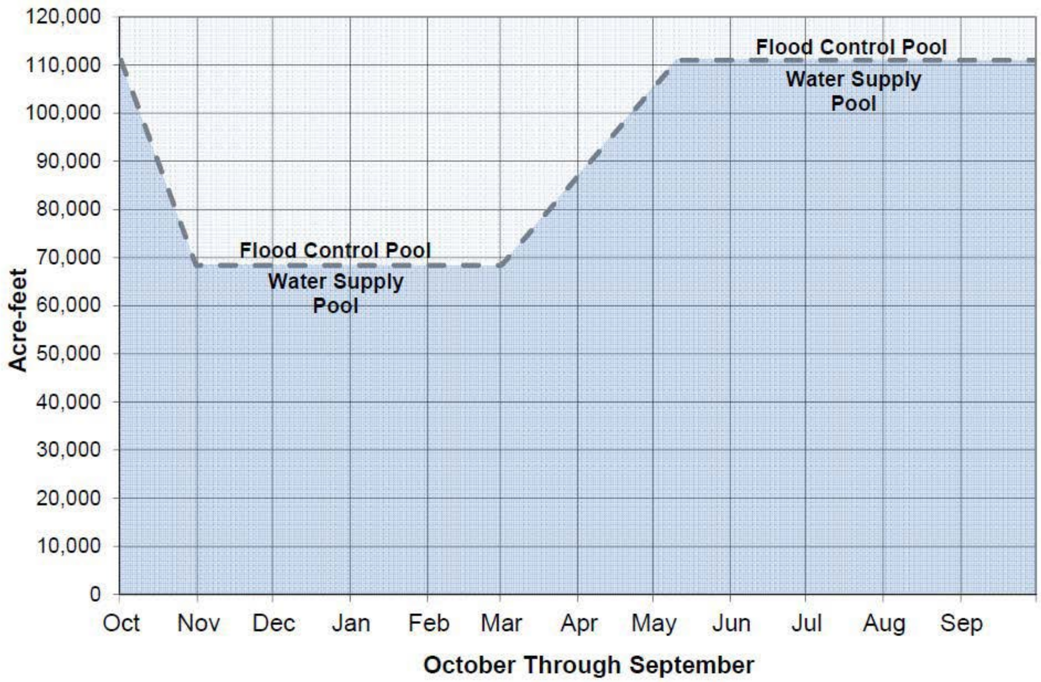

Figure 2. Lake Mendocino reservoir existing operating storage volumes.

1.1.6 Observation Network

The U.S. Geological Survey (USGS) currently monitors stream flow at 27 gage sites within the Russian River basin. Several agencies, including the Earth System Research Laboratory's Physical Sciences Division (ESRL-PSD), Department of Water Resources (DWR), Sonoma County Water Agency (SCWA), United States Geological Survey (USGS), and USACE collaborate in a precipitation and soil moisture monitoring program in the Russian River Watershed. ESRL-PSD installed both rain gauge and soil moisture monitoring sites above Lake Mendocino to monitor watershed conditions and augment the existing ESRL-PSD network in the Russian River Watershed.

As part of this effort, CW3E, as described by Sumargo et al. (2020), installed a network of surface meteorological, soil moisture, and stream gauges in the upper Russian River basin for the purposes of better understanding the hydrological processes in the basin and providing observed data for driving and assessing atmospheric and hydrologic models applied in the basin. For the purposes of this report, the Upper Russian River is defined as the portion above the Hopland USGS station, Figure 1.

The locations of the CW3E surface meteorology and soil moisture, and streamflow sites are shown on a topographic map of the Lake Mendocino watershed. Surface meteorology and soil moisture sites are shown with circles and streamflow sites are shown with triangles. Existing NOAA HMT and USGS sites are also shown in Figure 3.

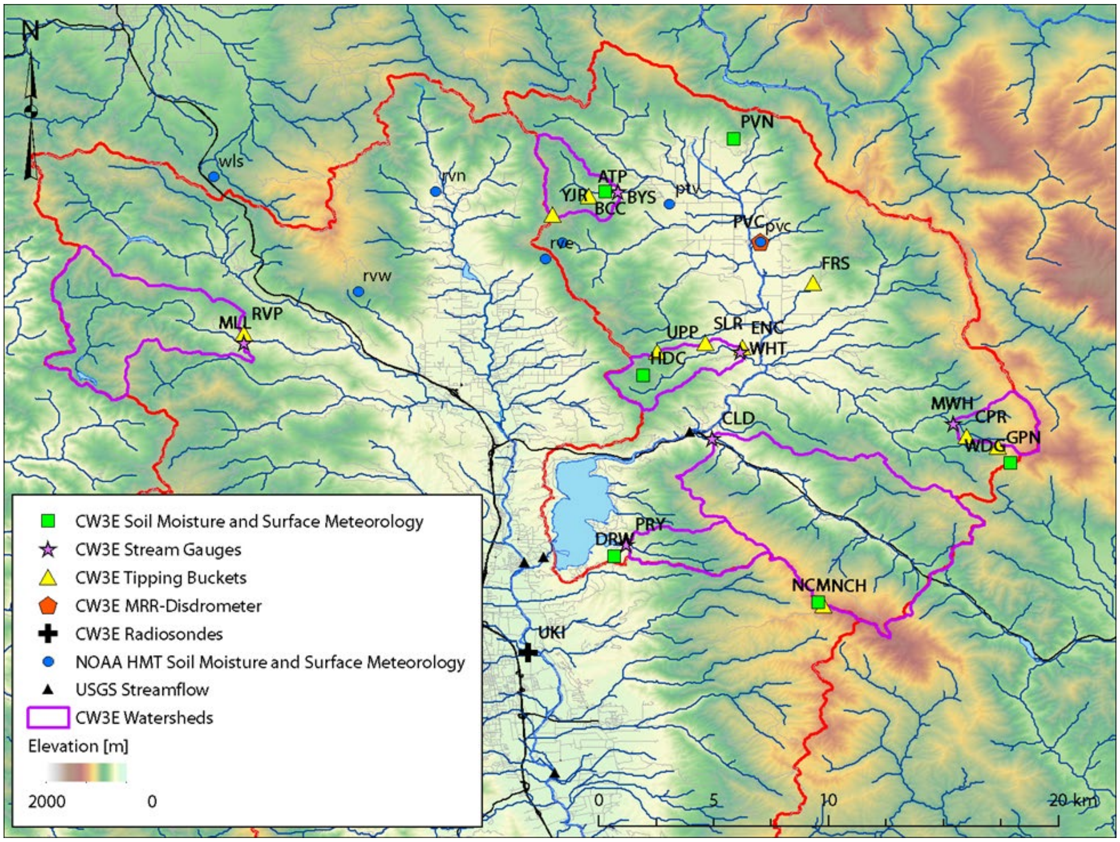

Figure 3. Observation network in the upper Russian River Basin (after Sumargo et al. (2020)).

While the CW3E precipitation sites are only operating during the rainy season, the NOAA and USGS stations operate year round and provide sufficient data for continuous simulations with the GSSHA models.

1.1.7 Objective(s)

This study is part of the Final Viability Assessment for Phase I of FIRO conducted as part of the overall FIRO research program. Research efforts in FIRO are meant to advance the overall FIRO objective, which is to more effectively operate reservoirs for authorized purposes utilizing precipitation and hydrologic forecasts.

The most basic research question we are trying to address is

> Can the application of state-of-the-art atmospheric and hydrologic models at Lake Mendocino improve the ability to simulate and forecast stream flows and lake levels, especially during large events?

In addition, several other research topics to be addressed as part of this study include:

1. Developing a better understanding of how the Upper Russian River watershed functions hydrologically.
2. Assessing how well an integrated physics based watershed model can simulate stream flow, lake level, and soil moisture in the basin.
3. Testing the effects of model spatial resolution on simulation accuracy.
4. Analyzing the effects of precipitation source/type/resolution on hydrologic model results and calibrated parameter values.
5. Testing the effects of forecast lead-time on hydrologic modeling results.

1.2 Approach

Critical elements in the study were:

- Gathering, analyzing, and preparing existing data.
- Filling in data gaps with the CW3E-led data collection effort.
- Developing hydrologic models of varying resolutions.
- Coupling the hydrologic models to the West-WRF meteorological model and other spatially distributed meteorological datasets (developed by the CNRFC).
- Calibrate the hydrologic models to stream flow.
- Validate the hydrologic models to stream flow, reservoir level, and soil moisture.

- Assess the ability of the models to simulate streamflow, and the possibly utility of the modeling system for providing forecast.

- Incorporate the GSSHA model into the University Corporation for Atmospheric Research (UCAR) data assimilation (DA) system.

- Assess the impact of utilizing DA for GSSHA modeling, specifically at Lake Mendocino.

2 Data

Because of the hydrologic model being applied and the research objectives, significant data were needed to build, force, and assess the models' capability. In general, spatially distributed data are used to develop the GSSHA models, and both spatially distributed and point data are used to force and assess the model.

2.1 Point Data

2.1.1 Precipitation

Going back to 1971 in the historical data record, 59 unique gauges were identified with some period of record recorded between 1971 and 2019. The number and location of the gauges varies over that time period. These gauges are a combination of hourly, and 15-minute recording stations. Beginning in 2017 CW3E installed 6 additional precipitation gauges (Figure 3). Nine additional gauges were installed in 2018. CW3E tipping bucket gauges record at 2-minute intervals.

2.1.2 Flows

The USGS maintains 4 main-stem gauges in the Upper Russian River Watershed: Calpella, Ukiah, Talmage, and Hopland (Figure 4), with relatively long records, though not necessarily continuous. In addition, CW3E installed 6 additional gauges on secondary and tertiary streams beginning in 2017 and continuing into 2018. All stream gauges in the basin record at 15-minute increments.

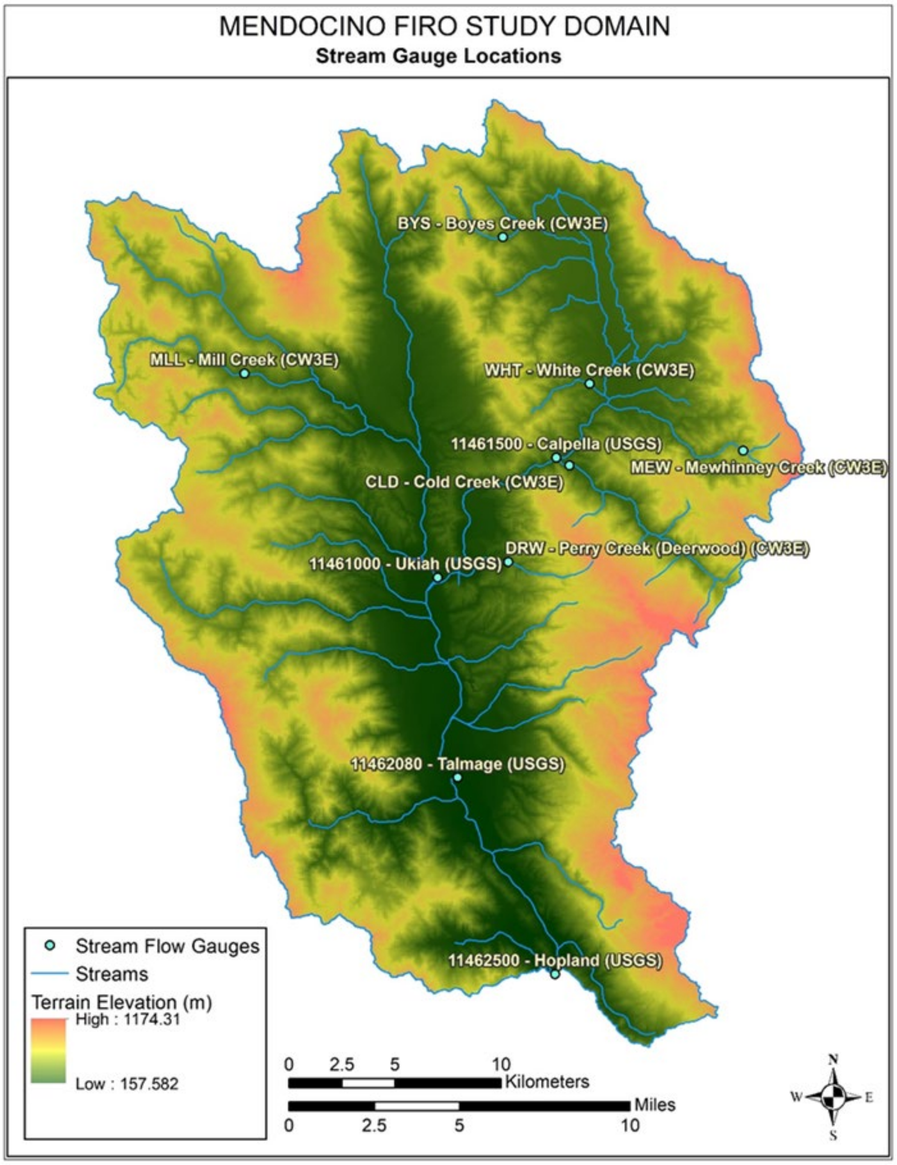

Figure 4. Location of stream gauging stations in the upper Russian River watershed, above Hopland.

Daily discharges from Lake Mendocino are measured by the USACE downstream of the dam, at CVD. Inter-basin transfers from the Eel River are measured daily at the Potter Valley Pacific Gas and Electric Station. Potter Valley flows were obtained from the Sonoma County Water Agency (SCWA).

2.1.3 Lake Levels

Daily lake levels were obtained from the USACE Los Angeles District.

2.1.4 Soil Moisture

Soil moistures are measured at 12 locations in the study area -- six NOAA stations, and six CW3E network stations (Figure 3). For the NOAA stations, data are collected at two depths, 10-cm and 100-cm. The CW3E soil moisture stations record soil moistures at multiple depths, from 5-cm to 100-cm (5, 10, 15, 20, 50, and 100 cm) at 2-minute intervals. All soil moisture data were collected and provided by CW3E.

2.1.5 HMET

Standard hydro-meteorological (surface airways) data were available from the Ukiah airport from 1973 to present. Hourly data were provided courtesy of the US Air Force.

2.2 Distributed Data

Development of the GSSHA model required spatial data. Data used to develop the models are discussed below.

2.2.1 Elevation

The digital elevation map (DEM) basis of the GSSHA model, 10m resolution data were obtained from the USGS Seamless Data Browser.

DEM data were supplemented by locally obtained Light Detection And Ranging (LiDAR) data within Lake Mendocino at 0.91 m resolution. The survey data points are shown in Figure 5. LiDAR data were provided by Sonoma County Water Agency (SCWA). Bathymetric survey data were collected in 2014.

Lake Mendocino survey derived bathymetry and elevation, area, storage curves were obtained from USACE SPL. The bathymetric data for Lake Mendocino were acquired as a point shapefile of longitudinal transects from the San Francisco District of the US Army Corps of Engineers, Figure 5.

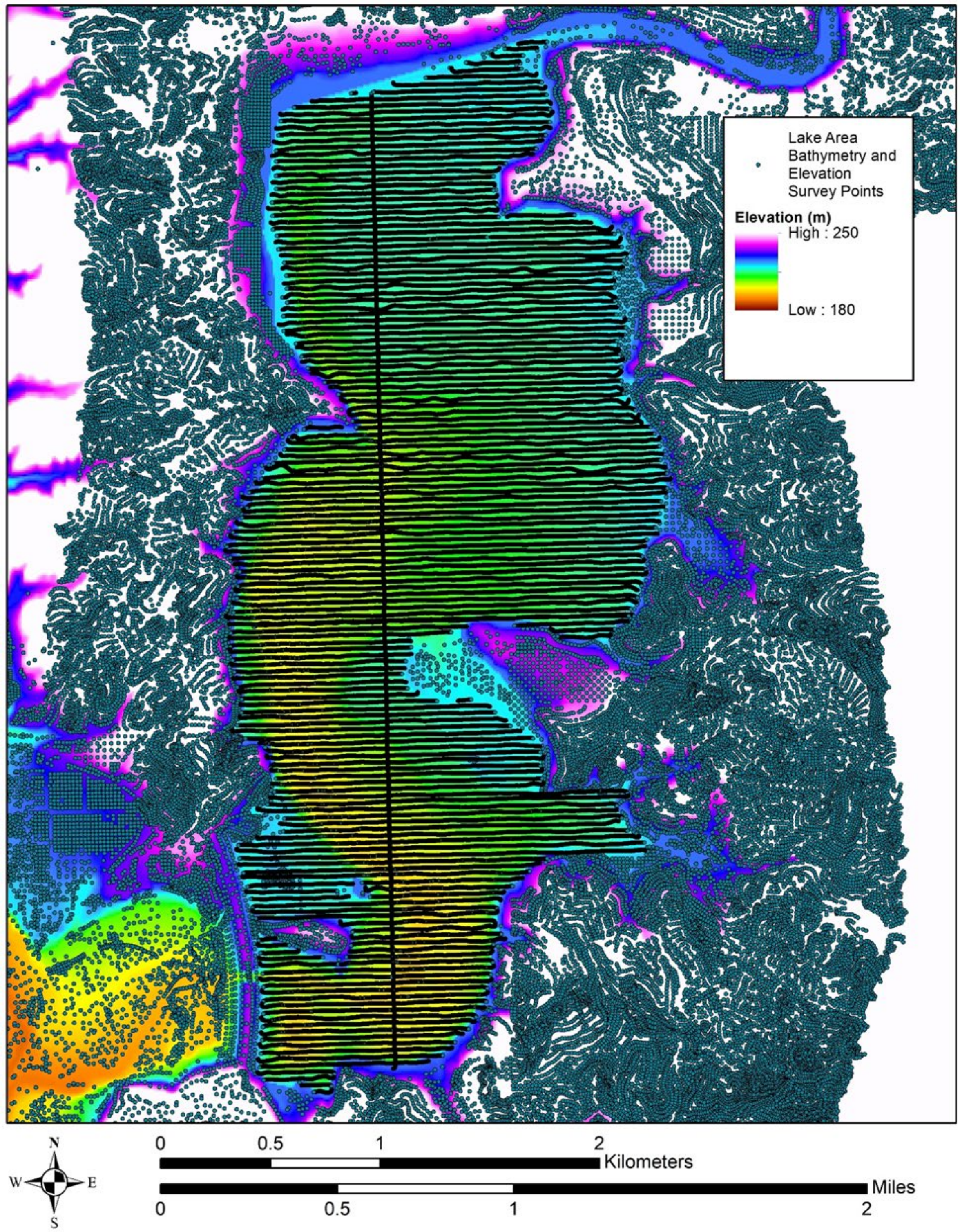

Figure 5. Location of LIDAR points and bathymetric survey cross sections.

2.2.2 Soils

Soils data in SSURGO form were obtained from the Natural Resources Conservation Service (NRCS 2020). SSURGO data are provided as polygons with soils information, including soil texture and soil series, as attributes. Soil survey data, also from NRCS, provides detailed information about depth of soils, soil layer, and physical and hydraulic properties.

2.2.3 Land Use

Land use data, at 30m resolution, was obtained from the SCWA website (NLCD 2011).

2.2.4 Bedrock

Information about the location of the bedrock was limited, but three sources of data were available -- USGS ground penetrating radar data, USGS borehole data, and NRCS data on soil layering and impervious layers. Under contract with USACE, the USGS collected supplemental ground penetrating radar in the Russian River watershed. These data were combined with borehole information and existing ground penetrating radar data to develop a depth to bedrock map for the Russian River.

3 Model Development

3.1 System Conceptualization

The Russian River watershed and the Upper Russian River watershed in particular, is a well-studied watershed in terms of observations, analysis and simulation. Due to the distribution of rainfall, streamflow is potentially high in the winter/spring wet season (Jan-May) and is typically low/absent in the prolonged dry season.

According to the Natural Resources Conservation Service (NRCS), soil depths in the upper Russian River basin range from less than 30 cm in many high elevations areas, to greater than 2 meters in valleys (Figure 6).

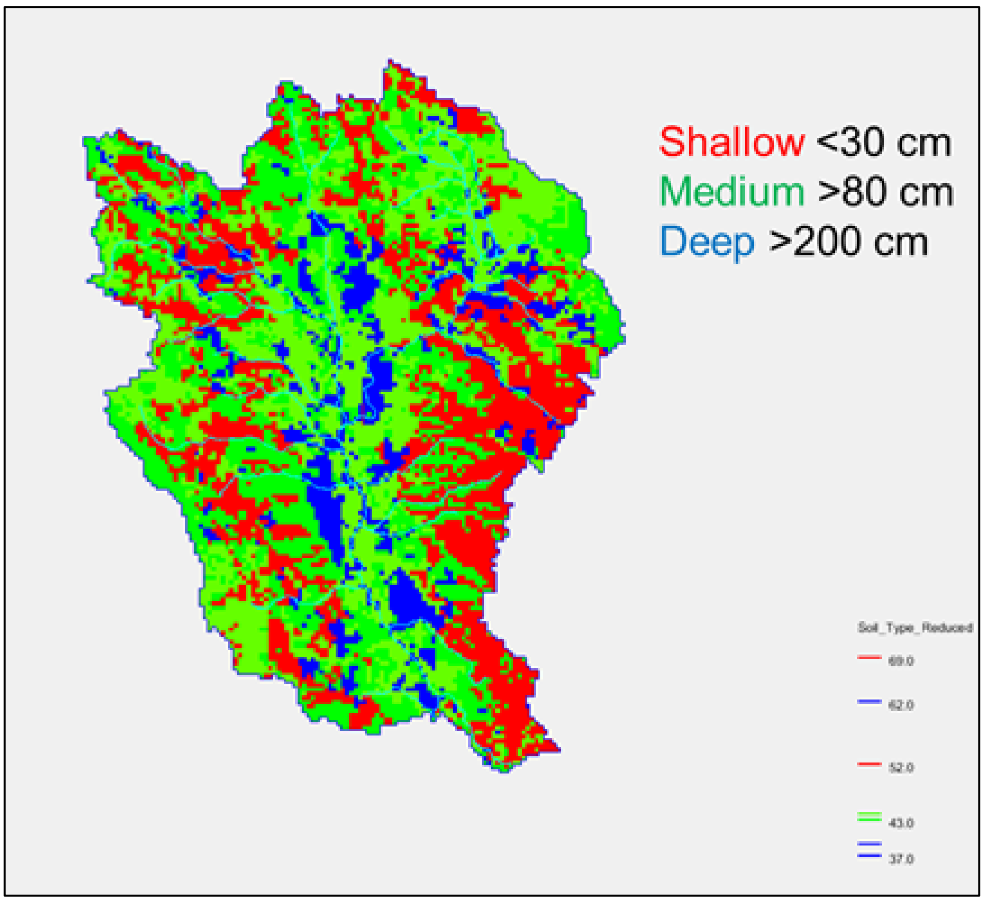

Figure 6. Depth of soils in the upper Russian River watershed.

Soils are underlain by weathered and unweathered bedrock, which prevents, or strongly inhibits vertical flow of water, forcing any water reaching the bedrock layer to flow laterally as saturated groundwater flow. Because soils are typically well drained, consisting of primarily loamy soils (Figure 6) the soils above the bedrock have substantial storage capacity for infiltrated water, especially after an extended dry period, such as the long 6-8 month dry season. And, as discussed by Flint et. al. (2013) even the bedrock has significant water holding capacity. Soil moisture data collected in the basin indicates soil moistures near residual at the beginning of the wet season. Thus, a significant amount of rainfall may be required to initiate runoff, but once the system is saturated, as in during the rainy period, the watershed can be expected to generate substantial runoff.

Anderson (1997) describes geology and hydrology in the region as a combination of overland and groundwater flow intermixing as it moves downslope. His research indicates that the groundwater contribution to runoff in the beginning of events is very low, on the order of 10%, but increases to greater than 50% toward the tail end of the hydrograph. In utilizing chloride, ^{18}O and ^{2}H (D) as tracers, Ellis et. al. (2019) used hydrograph separation techniques to determine that in the main fork of the East Russian River the pattern was somewhat different, but that the total contribution from surface and groundwater was fairly evenly split during the event they sampled. In Cold Creek, a tributary to the East Fork of the Russian River, the distribution was more similar to that described by Anderson, yet the contribution of surface water flows remained high, from 35 to 85% of the total at any given time, with the groundwater dominating only toward the very tail end of the hydrographs.

The watershed has substantial relief; elevations on the ridges are greater than 1000m, dropping to about 180m at the outlet. Steep slopes result in rapid overland flow, given the right conditions.

Observed hydrographs indicate little to no flow in the upper Russian River watershed, other than prescribed discharges, for much of the year. Early in the rainy season flows are peaky, likely surface water dominated, but as the season progresses base flow increases, with surface water flow peaks occurring on top of the base flow. Flows, including the apparent amount of base flow, increase in the downstream direction. Figure 7 shows observed flows at Ukiah (top panel), and Hopland (bottom panel) for the 2004/2005 water year. Calpella is on the East fork of the upper Russian River watershed, above Lake Mendocino. Ukiah is located on the West fork roughly at the watershed midpoint whereas Hopland is the defined domain outlet (Figure 4). As seen in Figure 7, the observed flows match the description above.

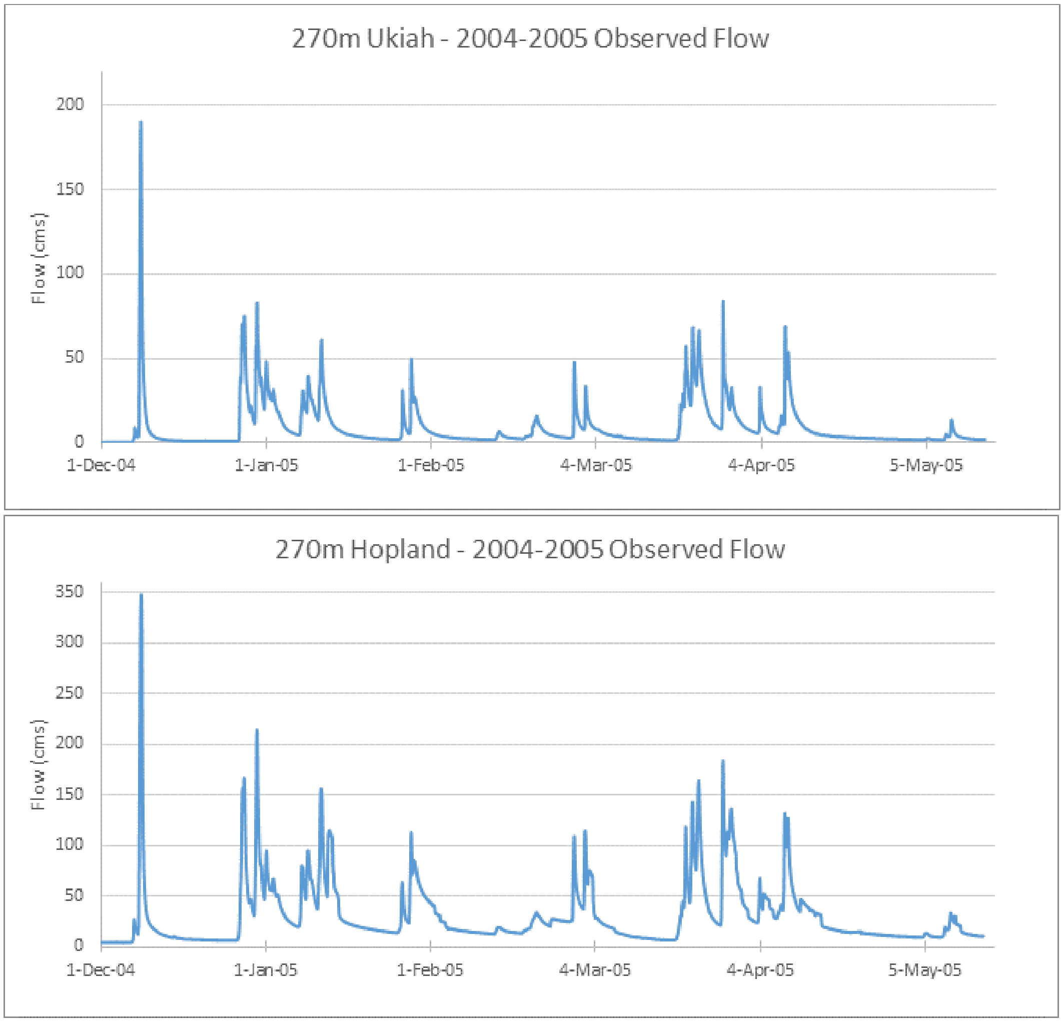

Figure 7. Observed discharge on the Russian River at Ukiah (Top Panel) and Hopland (Bottom Panel). See Figure 4 for locations.

Observations, field studies, and previous simulation efforts point to a complex watershed where pervious soils are underlain by an impervious bedrock layer, with shallow soils in the uplands, and deeper soils in valleys. Rainfall patterns result in an extended rain-free period where soils become desiccated and have substantial storage capacity that must be satisfied before runoff can begin. As such, early precipitation events may produce no runoff. Early runoff producing events produce peaky surface water dominated runoff, where later events produce more groundwater streamflow. As mentioned, this effect is exaggerated in the downstream direction.

3.2 Model Processes Simulated

GSSHA is a process-based and option-driven model. It is up to the user to configure the model such that it includes the important processes that control streamflow in the watershed. The only process that is mandated is that the model must include overland flow. For the upper Russian River watershed, the model was configured to simulate the processes as described in Section 3.1. Table 1 describes the processes simulated, the methods employed, and the rationale for including that process.

Table 1. Processes and representation of the GSSHA models for the upper Russian River watershed.

Process	Representation	Description	Rationale
Rainfall Distribution	Thiessen Polygons	Rainfall is uniform in polygons defined by equal distance between gauges	Conforms exactly to gridded precipitation products, such as West-WRF grid, without interpolation
Infiltration	Multi-layer Green and Ampt	Water infiltrates as sharp front and is impacted by soil layering	Strongly layered soils with impervious layer
Surface retention	Specified by land use	Water is retained in the cell until the retention depth is exceeded	Accounts for micro-topography, leaf litter, etc.
Overland flow	Diffusive wave Roughness related to land use	2D flow that accounts for backwater effects	
Stream flow	Diffusive wave	1D flow that accounts for backwater effects	
Reservoir	Dynamic stream and overland feature	Reservoir expands and contracts due to	Dynamic reservoir better represents stream/overland/groundwater interaction

		inflows and releases	
Groundwater	2D free surface equation	Simulates lateral groundwater flow	Groundwater contribution to stream flow is substantial
Groundwater Stream Interaction	Flux boundary	Water flows between groundwater and stream according to head difference	Groundwater/stream interaction is substantial
Evapo-transporation	Penman-Montieth	ET based on physical forcings (atmospheric, radiative, convective), and vegetative state	State of the art method for vegetated areas
Soil moisture	2 layer continuous soil moisture calculations	Includes infiltration, downward flux between layers, and interaction with groundwater table	Overlaps with MLGA soil profile definition

3.3 Model Boundary

The overall model boundary is the watershed boundary, defined by the overland flow divides above the Hopland gage on the Russian River. The boundary encompasses approximately 938 Km^2 (Figure 8).

3.4 Model Resolution

As the name implies, GSSHA is grid-based model with uniform grid elements. The grid cells are used by GSSHA to make several different calculations of modeled processes during a computer simulation, including overland flow, channel flow, infiltration, surface moisture, groundwater levels, etc. As such, the larger the number of grid cells, the more computationally intensive the model becomes, and therefore the more time required for the simulation to complete, but also the more potentially accurate the solution may be. So a compromise must be made between computational efficiency and the amount of physical details the model can capture.

One research objective of this study was to look at the effect of model resolution on simulations of the Russian River. To test this effect, a range of models were developed of the upper Russian River watershed or portions thereof. The range of model resolutions was chosen to test the limits of what the data and watershed features would support, with grid resolutions between 30m and 270m. As the land use data are at 30m resolution, no finer grid resolution was possible without creating data. The 270m resolution was chosen as an upper bound partially because the Basin Characterization Model (BCM) (Flint et al., 2013), a volumetric USGS hydrologic model of the Russian River, utilized this resolution. Moreover, the larger the grid size becomes, the less detail that can be captured in the model grid, resulting in flatted hills and/or elevated low areas, for example.

The number of computational elements rapidly increases with increasing model resolution, given the same domain. Models of 270m, 100m, and 50m resolution were developed for the entire, upper Russian River watershed, while a smaller domain, focusing on the Lake Mendocino sub-watershed was simulated at 30m resolution (Figure 10). The number of elements in each model is shown in Table 2.

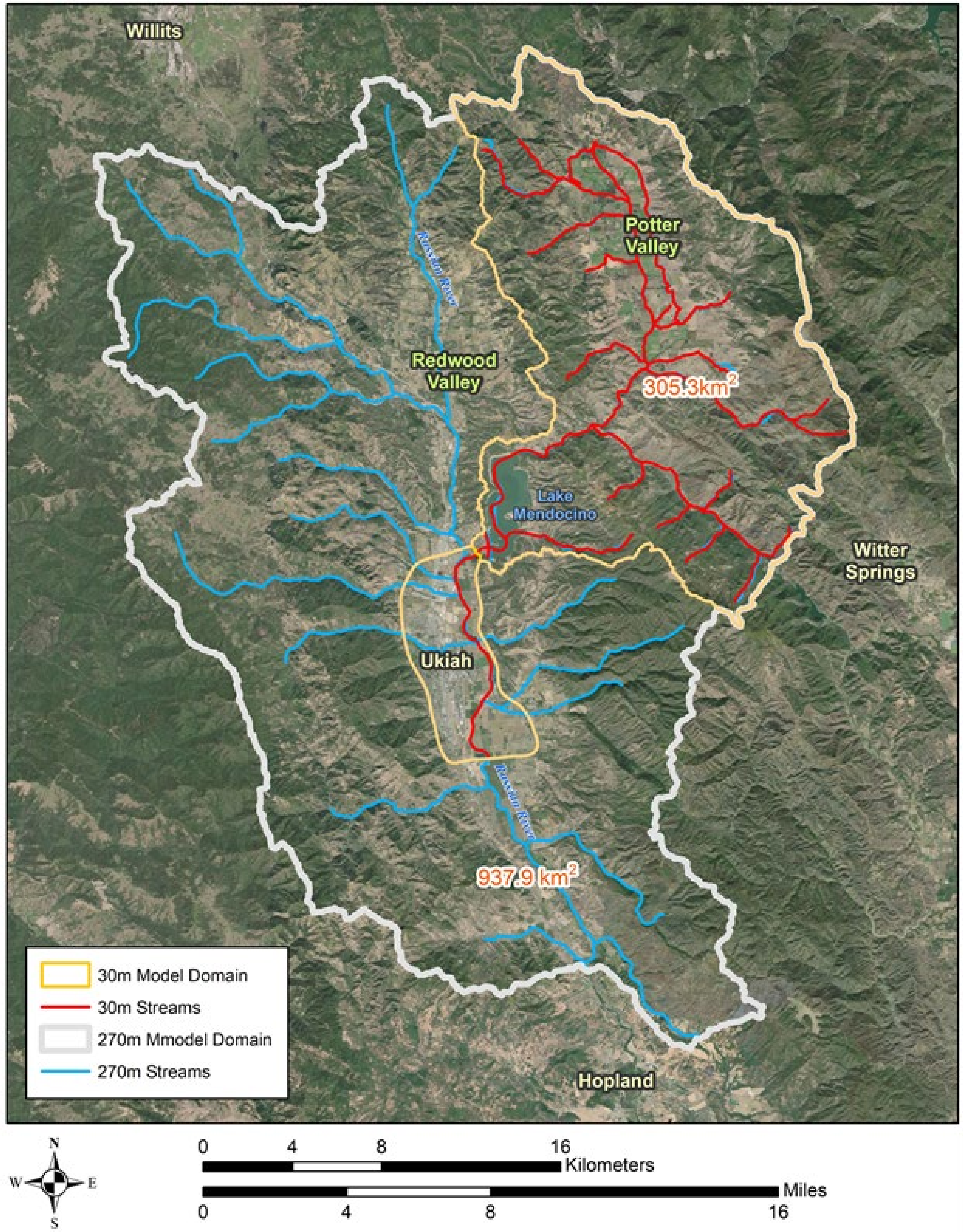

Figure 8. Mendocino model domains.

Table 2. GSSHA models grid cell sizes and number of grid cells.

Cell Size (m)	# Grid Cells
270	12,867
100	93,780
50	374,874
30*	338,286

** 30 meter model covers a smaller domain.*

An idea about the effect of resolution can be gained from Figure 9, which depicts a portion of the model at 270 m resolution.

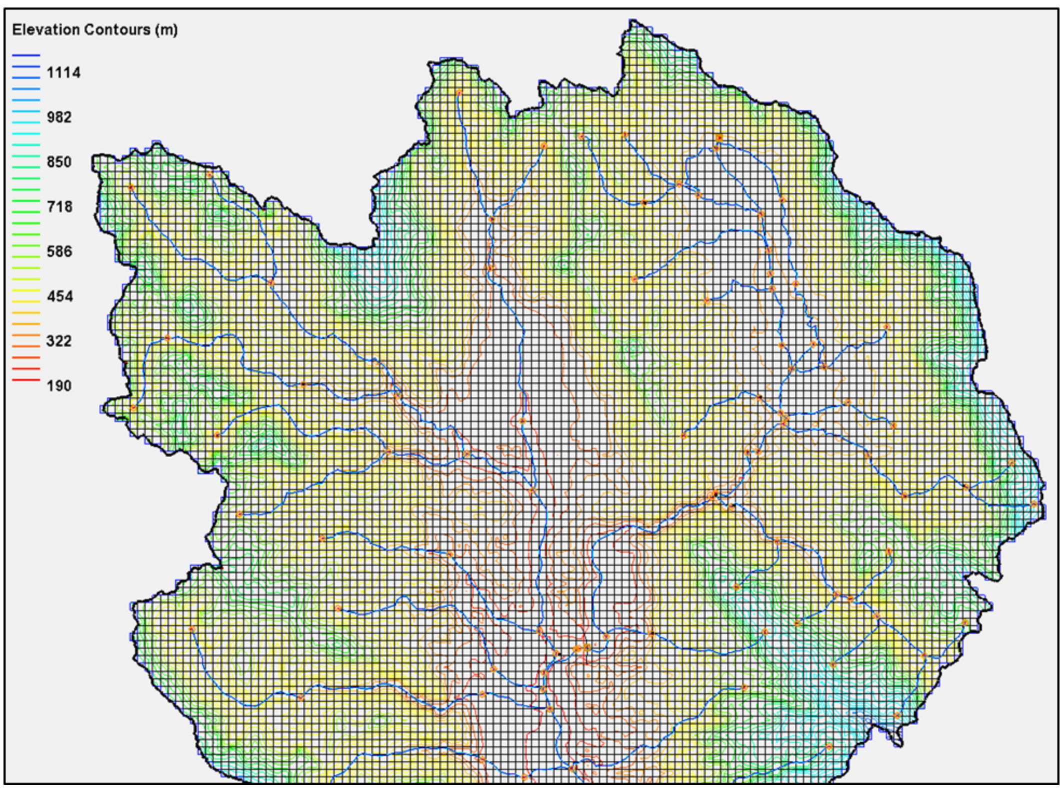

Figure 9. Portion of the upper Russian River watershed model at 270m resolution.

Figure 10 depicts how the resolution affects the representation of Lake Mendocino in the model domain.

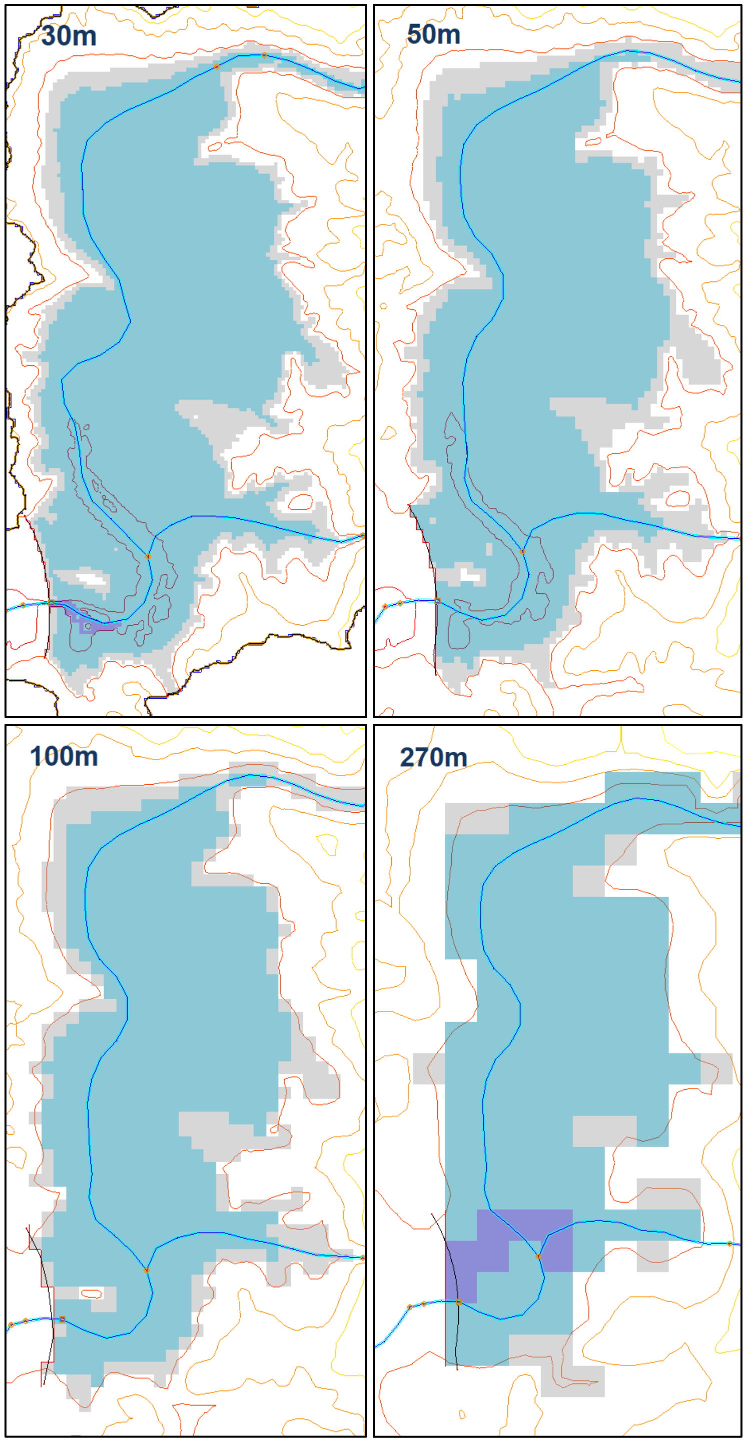

Figure 10. Representation of Lake Mendocino on the overland flow plane at varying grid cell resolutions.

3.5 Spatial Data

Spatial components of the models were developed using the Watershed Management System (WMS) software developed by Aquaveo. WMS is a graphical user interface that has tools with algorithms that have been used for more than 15 years to create physics-based watershed models. The WMS assisted with delineation of the basins and creation of the stream networks, and for generation of soil type and land cover maps. Additionally, Environmental Systems Research Institute's (ESRI) ArcMap™ Graphical Information Systems (GIS) software was used to combine the soil and land cover maps, as well as to create the water table and impermeable bedrock boundary layer for the groundwater component of the models.

3.5.1 Elevations

When a digital elevation dataset is created via satellite scanning, water bodies are recorded as a single elevation, which is the elevation of the water surface at the time of the scan. The actual bathymetry of the underlying terrain is not detected with those scans. This flat surface is not useful when it is necessary to model a lake response to hydro-meteorological forcings such as precipitation, evaporation, as well as dam operations.

The 10m terrain elevation dataset from which the Mendocino model grids were derived is no exception. In order to simulate the lake in the models, the bathymetry of the lake must first be inserted into the terrain elevation dataset. ArcMap™ was used to merge bathymetric survey data with the terrain elevation dataset.

The left side of Figure 11, shows a satellite image of Lake Mendocino and the right side shows the lake bathymetry after merging the LiDAR survey data (Figure 5), terrain elevation data, and bathymetric survey data.

ArcMap was used to convert these data points to a spatial raster, and to merge them with the 10m DEM of the terrain in the Lake Mendocino study area. This final DEM, which included the bathymetry for Lake Mendocino, was used to generate the 30, 50, 100, and 270-meter GSSHA model grids.

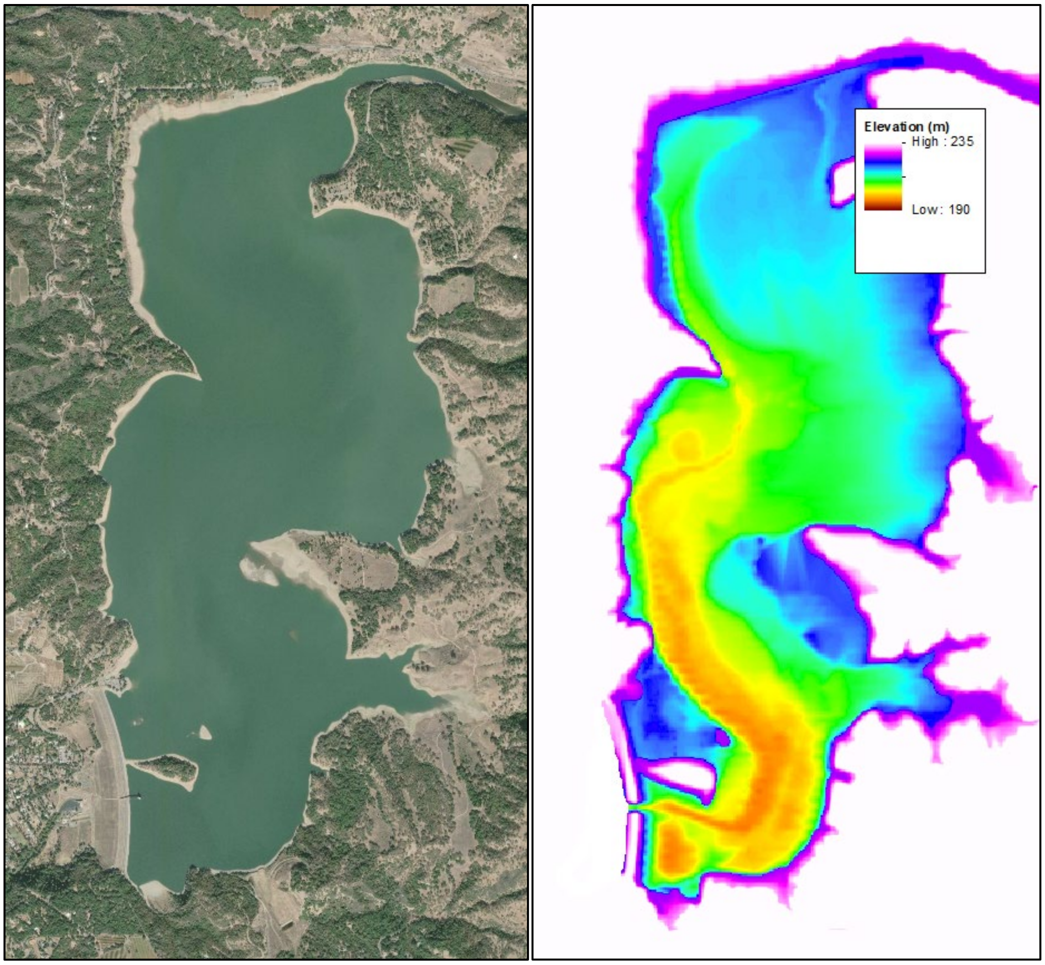

Figure 11. Lake Mendocino: (Left) Satellite image. (Right) Elevation contours after inserting the lake bottom bathymetry into the 10 meter resolution DEM.

3.5.2 Lake Mendocino Domain

The lake was defined in the GSSHA models via the Watershed Modeling System (WMS) by specifying a detention basin created behind an embankment structure (Coyote Dam) which has a crest elevation of 239.8 meters. Using the information about the dam crest elevation, and the maximum lake surface elevation, the WMS selects the overland cells in the model grid that are below the crest elevation and that reside immediately above the embankment, and designates those as lake cells for the initial state of a model run. Lake cells are added and removed during a model run as the lake level rises and falls. The lake representation in each model is shown in
Figure 10.

In addition to specifying the dam elevation and determining the possible reservoir cells, the minimum, maximum, and initial lake stages are specified. The maximum lake level for all models is the dam height, 239.8 m. The minimum lake level is determined by the lowest elevation cell within the reservoir (basically an empty reservoir). The minimum cell elevations in each model are shown in Table 3.

Table 3. Minimum Lake Mendocino elevations for the GSSHA models.

Model Resolution (m)	Minimum Lake Elevation (m, NAVD88)
30	194.812
50	196.082
100	196.491
270	195.64

The description above is how the lake interacts with the overland grid. Within the stream network, the lake is input a boundary condition with a stage/area/volume relationship and an outlet structure. The capacity curve for Lake Mendocino is shown in Figure 12. The information in the figure is used to develop a lookup table that is input to GSSHA at 0.001-m intervals. The model engine interpolates between values in the lookup table. The outlet structure in these GSSHA models are the specified measured flows.

Inflows to the lake include flows from any streams entering the lake, from the overland flow plane where it intersects the lake, or from groundwater exchange, which can be positive or negative. In the reservoir, a hydraulic conductivity of the bed material is specified, and the flux between the reservoir and the groundwater depends on the head difference between the two, along with the area of the lake.

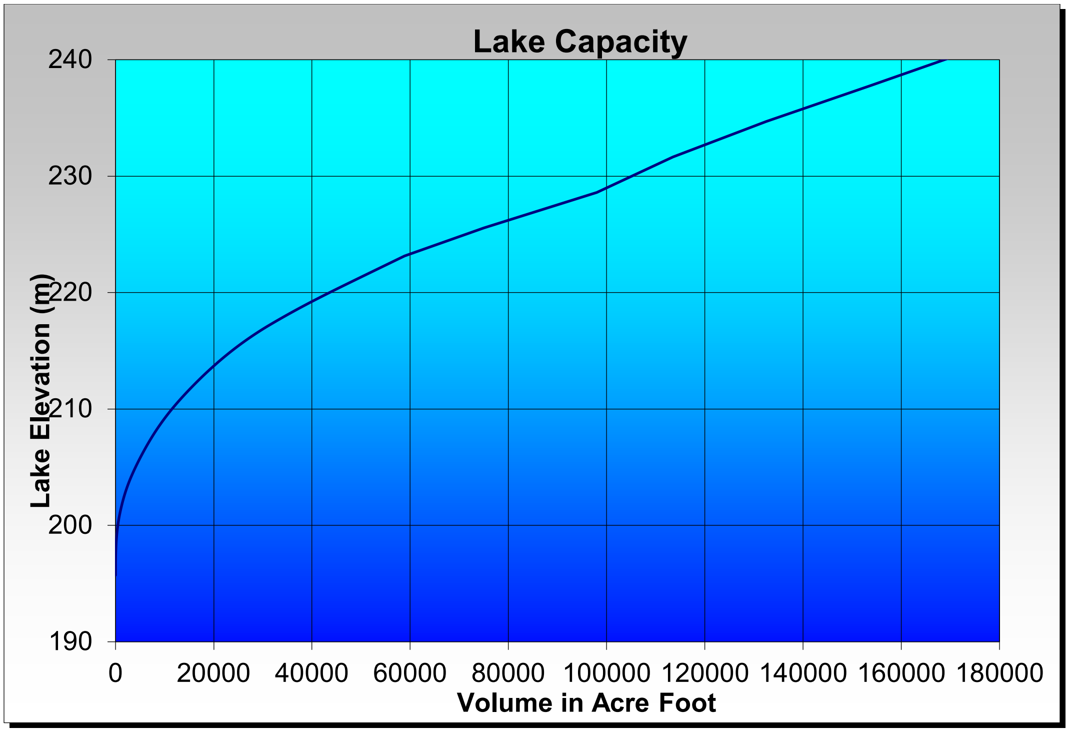

Figure 12. Stage/capacity curve for Lake Mendocino.

3.5.3 Bedrock Elevations

For groundwater simulations, the bedrock is an impervious boundary layer that constrains the 2-D groundwater numerical simulation above it. Conceptually, however, while building the groundwater processes, a model user may define a constant rate of seepage through this confining bedrock.

A map of bedrock elevations dataset was derived from the USGS ground penetrating radar and field-measured depth-to-impervious-layer combined with NRCS soil profile data. This data was used to develop a continuous bedrock map in ArcMap for depth-to-bedrock specifically for Potter Valley and Redwood Valley. Information outside these valleys was not complete enough to be very useful. Site observations and NRCS soil profile data showed that the bedrock depth in most of hill slopes around the watershed was shallow (at 1.0-meter minimum). In the models, depth to bedrock along the streams gradually increased to 8 meters according to the order of stream with the greatest depths occurring near the domain outlet, except in the Potter and Redwood valleys where the USGS survey was used. Figure 13 shows the resulting depth-to-bedrock layer which was used to generate the gridded maps for the models.

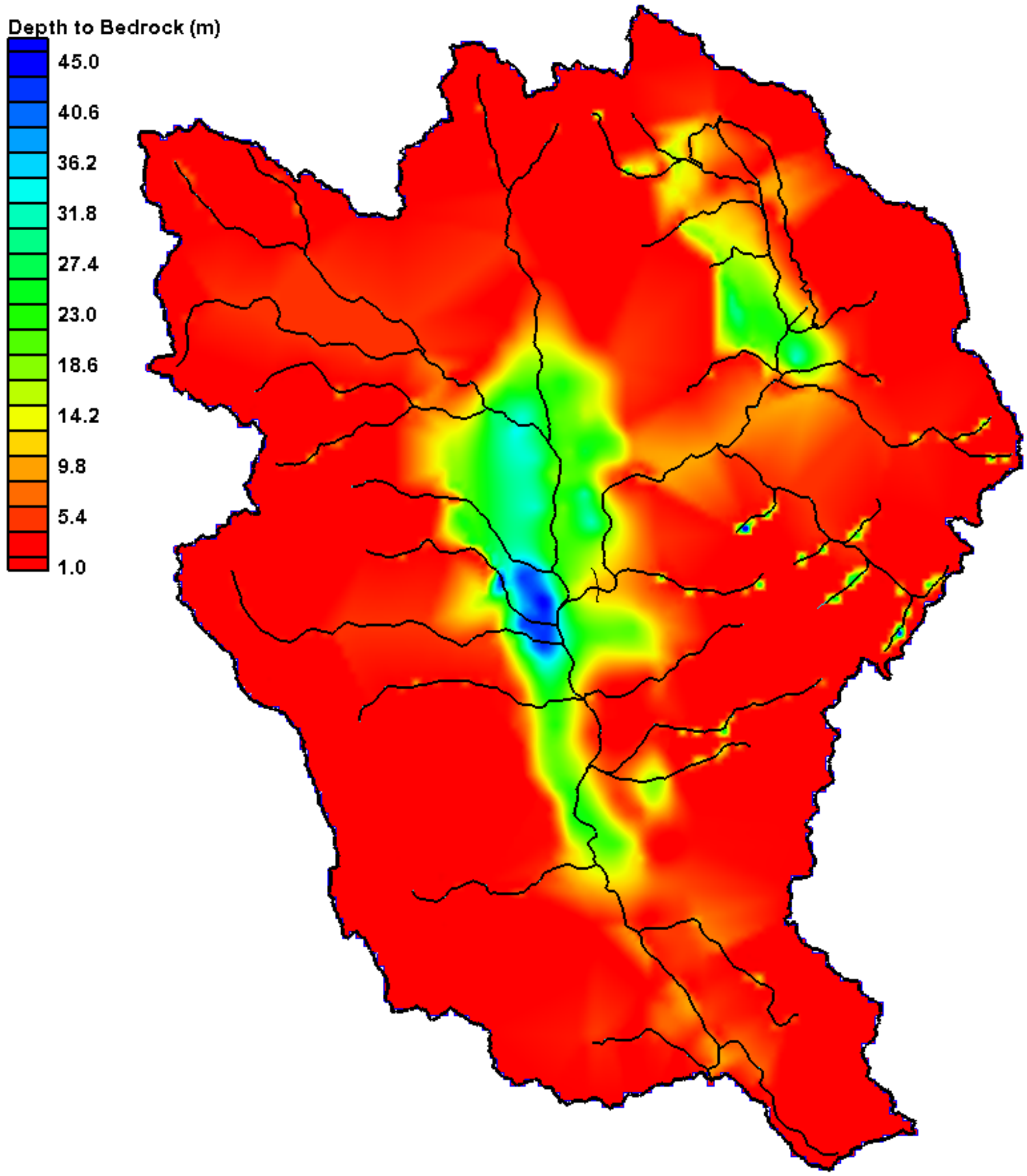

Figure 13. Depth to bedrock from the land surface.

3.6 Index Maps

Physical parameters may be assigned in GSSHA using either a single uniform (global) value, or values specified for every GSSHA grid cell. Typically, index maps related to some physically measureable quantity are used to assign the spatial distribution of parameters. Most common are soil type and land use, or a combination of these two. These map types are used to assign most spatial parameters needed in the model.

For this study the soil type index map (ST) is combined with the land use map (LU), resulting in a soil type land use (STLU) map which was used to assign the infiltration properties.

3.6.1 Soils

The NRCS Soil Survey Geographic Database (SSURGO) soil data were used to derive soil textures for the models. Two types of quantities were taken from the soils SSURGO maps and related text – soil textures and soil profiles. The model domain included 13 soil SSURGO derived textures:

- Sand (S)
- Very gravelly sandy loam (VGSL)
- Gravelly sandy loam (GSL)
- Sandy loam (SL)
- Loam (L)
- Gravely clay loam (GCL)
- Sandy clay loam (SCL)
- Clay loam (CL)
- Sandy clay (SC)
- Clay (C)
- Loam (L)
- Weathered bedrock (WBR)
- Unweathered bedrock (UBR)

From these, eight soil profiles were derived comprised of these 13 textural classes (Table 4). The distribution of these soil profiles is shown in Figure 14. Note, however, that this figure does not include a soil with an ID of 2 because the occurrence of this type is infrequent and not the dominant type within the grid cell.

Table 4. Soil profiles used in the upper Russian River watershed GSSHA models.

Soil ID	Description	Profile Texture	Layer depth (cm)	Incidence (%)	Color in Figure 14
2	Gravely Sandy Loam	GSL SL SL	23 84	<1	none
37	Water	CL CL CL	25 100	3	blue
39	Sandy Clay Loam	SCL CL C	20 36	8	orange
43	Clay Loam	CL C	20 104	30	red

		SCL			
44	Loam	C L WB	30 80	29	green
52	Sandy Loam	SL UBR UBR	28 38	14	yellow
62	Very Gravely Sandy Loam	VGSL SL SL	20 83	1	yellow
69	Loam	GSL SL SL	30 100	14	green

As seen in the table, the soils are generally loamy. In the figure less permeable soils, such as clay loams, are darker, blues, oranges, and reds; with more permeable soils, such as sandy loam, being lighter, greens and yellow. A combined soil type (ST) and land use (LU) map (STLU), was used to assign infiltration properties in these models (Section 3.6.3).

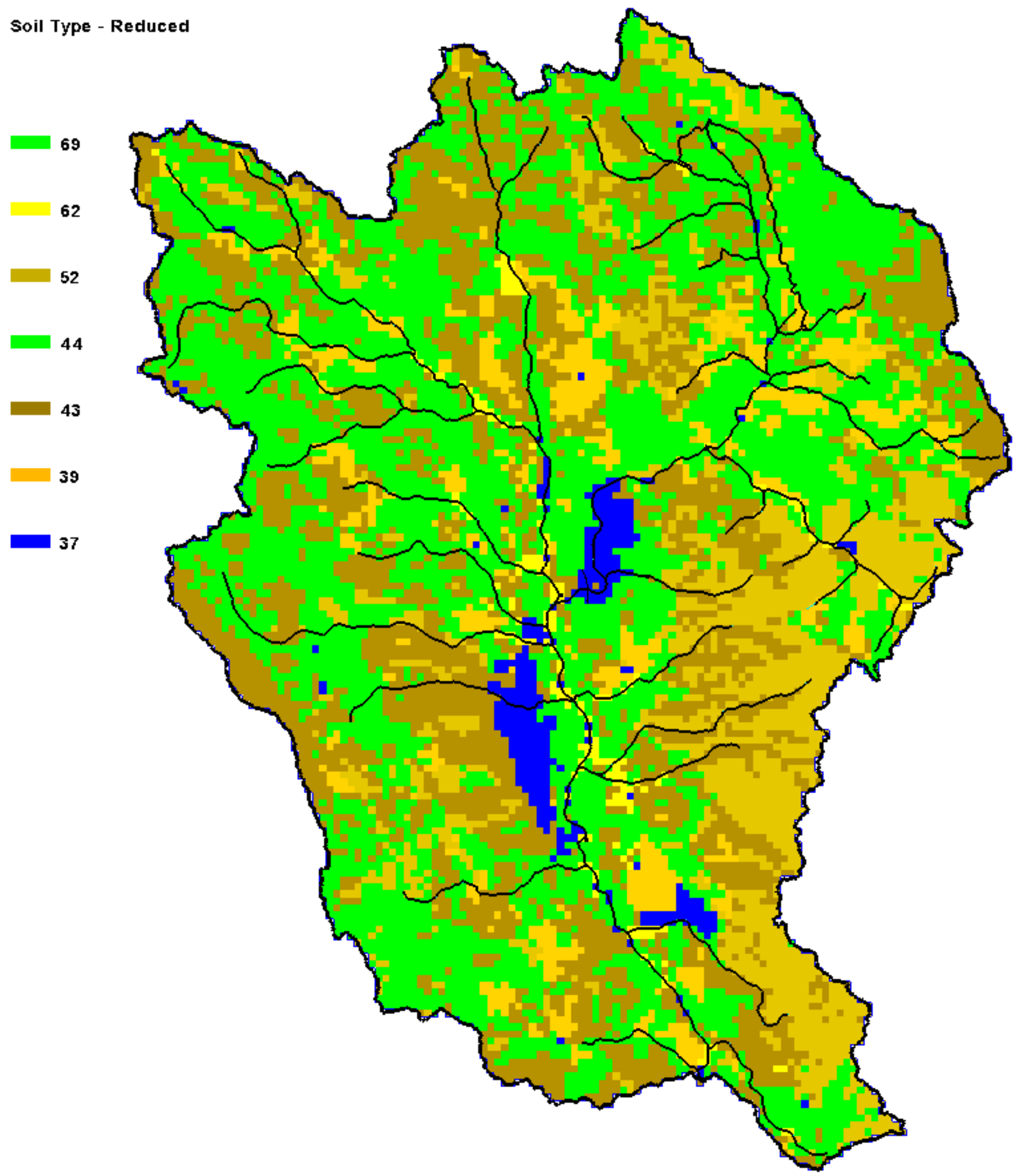

Figure 14. Distribution of soil profiles used in the upper Russian River watershed GSSHA models.

3.6.2 Landuse

The land use index map was derived from the 30m NLCD land use data. Fifteen different land use types were used in the models (Table 5). Dominant land uses are forest (32%) and shrub (38%) with 14% grasslands and 9% of developed areas to varying degree. The land use maps are used to assign overland roughness and evapotranspiration values. A combined soil type (ST) and land use (LU) map, (STLU), was used to assign infiltration properties in these models (Section 3.6.3).

Table 5. Land uses used in the upper Russian River watershed GSSHA models.

ID	Land Use	Incidence (%)	Color in Figure 15
11	Water	1	Blue
21	Developed open space	6	Light gray
22	Developed low intensity	1	Gray
23	Developed medium intensity	1	Dark Gray
24	Developed high intensity	<1	Black
31	Barren land	<1	Brown
41	Deciduous forest	2	Dark green
42	Evergreen forest	19	Light green
43	Mixed forest	11	Green
52	Shrub	38	Olive
71	Grassland	14	Light yellow
81	Pasture	<1	Yellow
82	Crops	6	Orange
90	Woody wetlands	<1	Green/blue
95	Emergent herbaceous wetlands	<1	Blue/green

Generally, upland areas are forested or shrub (Green), larger valleys are agricultural (orange) and pasture/grassland (yellows), with limited development (grays), mostly along the main river stem. Small wetland areas (green/blue) occur alongside streams and lakes. The distribution of these land uses is shown in Figure 15.

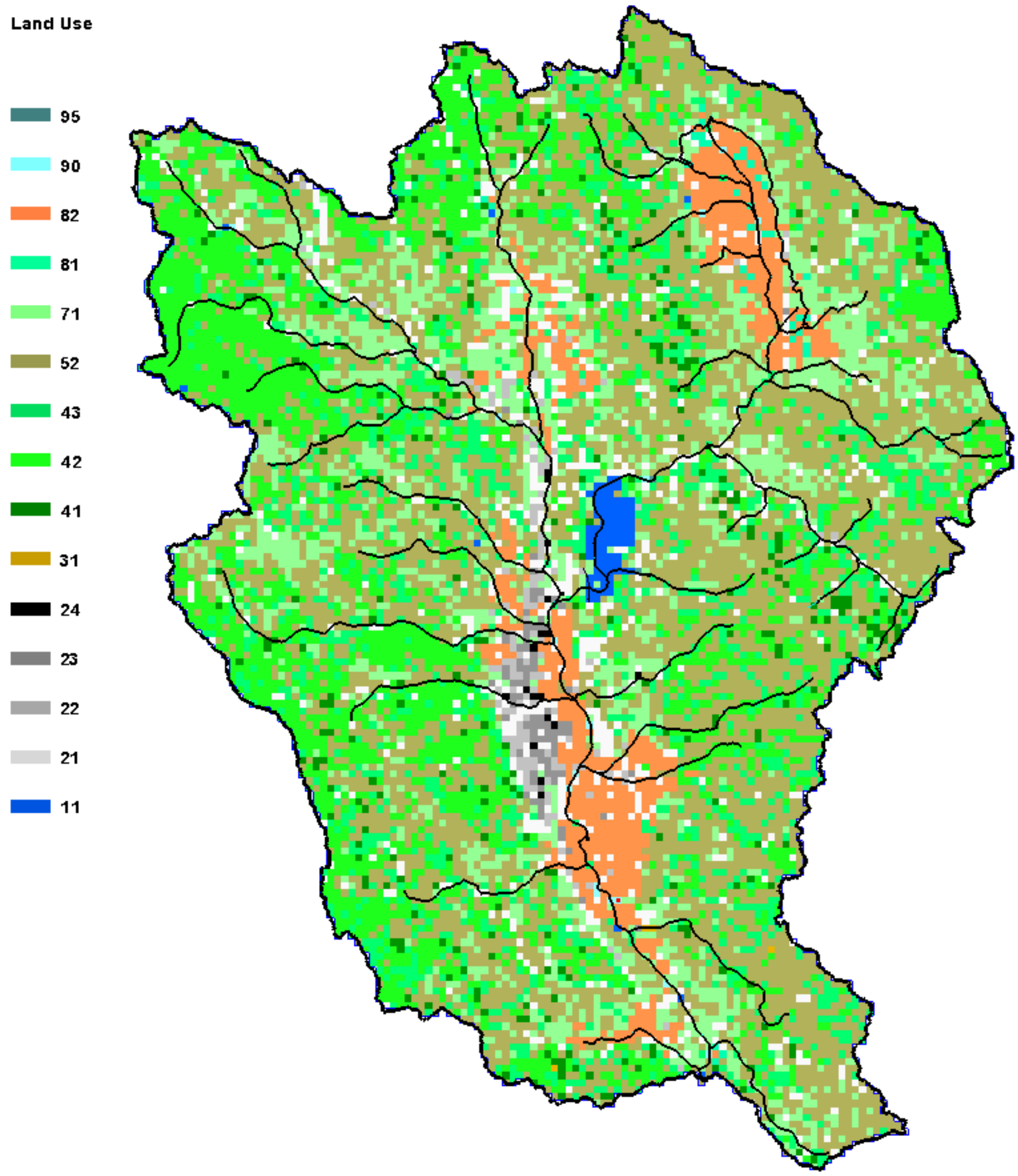

Figure 15. Distribution of land uses in the URRW GSSHA models.

3.6.3 Soil Type and Land Use (STLU)

A combined soil type and land use (STLU) index map was created by reducing the number of land uses from 15 to 9 (water, open/low intensity development, med/high intensity development, barren, forest, shrub, grass/pasture, crops, and wetland), assigning the land use values ranging from 1000 to 9000, and finally adding the soil type to the land use. This resulted in 72 unique STLU categories, which were used to specify soil hydraulic properties for the multi-layer Green and Ampt infiltration method (Downer, 2002)

3.6.4 Subsurface properties

Limited information exists about the subsurface properties within the watershed. In order to perform groundwater simulation GSSHA requires information for subsurface soil porosity and lateral hydraulic conductivity. Due to the paucity of data, uniform values were used and treated as calibration parameters.

3.7 Stream Network

Although 2D overland flow can be used in GSSHA to simulate flow in the watershed, the 1D stream network allows for a better representation of stream flow, independent of the overland flow grid. The density of the stream network included depends on both the location and purpose of the study. In this study, the focus is on flows in the Russian River and into Lake Mendocino. The proper stream network allows this to be accomplished without undue stream density, as stream flow calculations can be time consuming and very small streams may behave more like overland flow in extreme events. As described below, the stream network was developed using multiple sources of data.

3.7.1 Stream Network Generation

For the models, streams were delineated from the 10m land surface DEM using the TOPAZ model (Garbrecht and Martz, 1999). This stream delineation was then compared to the NLI stream network (Nagel et al., 2017). Additionally, a field survey of the watershed was conducted to determine the size and importance of streams in the basin. This field information, combined with satellite imagery of the basin, allowed the inclusion of important streams and the exclusion of streams not thought to significantly contribute to total stream flow. Care was taken to include all significant stream links that include either a specified inflow or a gaging station. This led to the inclusion of some relatively small streams in the model that may be extraneous in adequately capturing main stem Russian River flows. The final stream network, shown in Figure 4, was comprised of 101 stream links with individually specified cross sections. Computational nodes were distributed roughly every 200 m along the stream reaches.

3.7.2 Stream Cross Sections

Stream cross section information was available for all the gaged locations (Figure 4). Additional stream cross sections were measured during a field visit. Cross section field measurement locations are shown in Figure 16. Stream cross sections were measured only in the East Fork of the Russian River. The cross sections measured in the East Fork were also assigned to the streams in the West Fork that were assumed to be of similar size and shape, related to order of the stream. Satellite imagery was used to confirm this assumption.

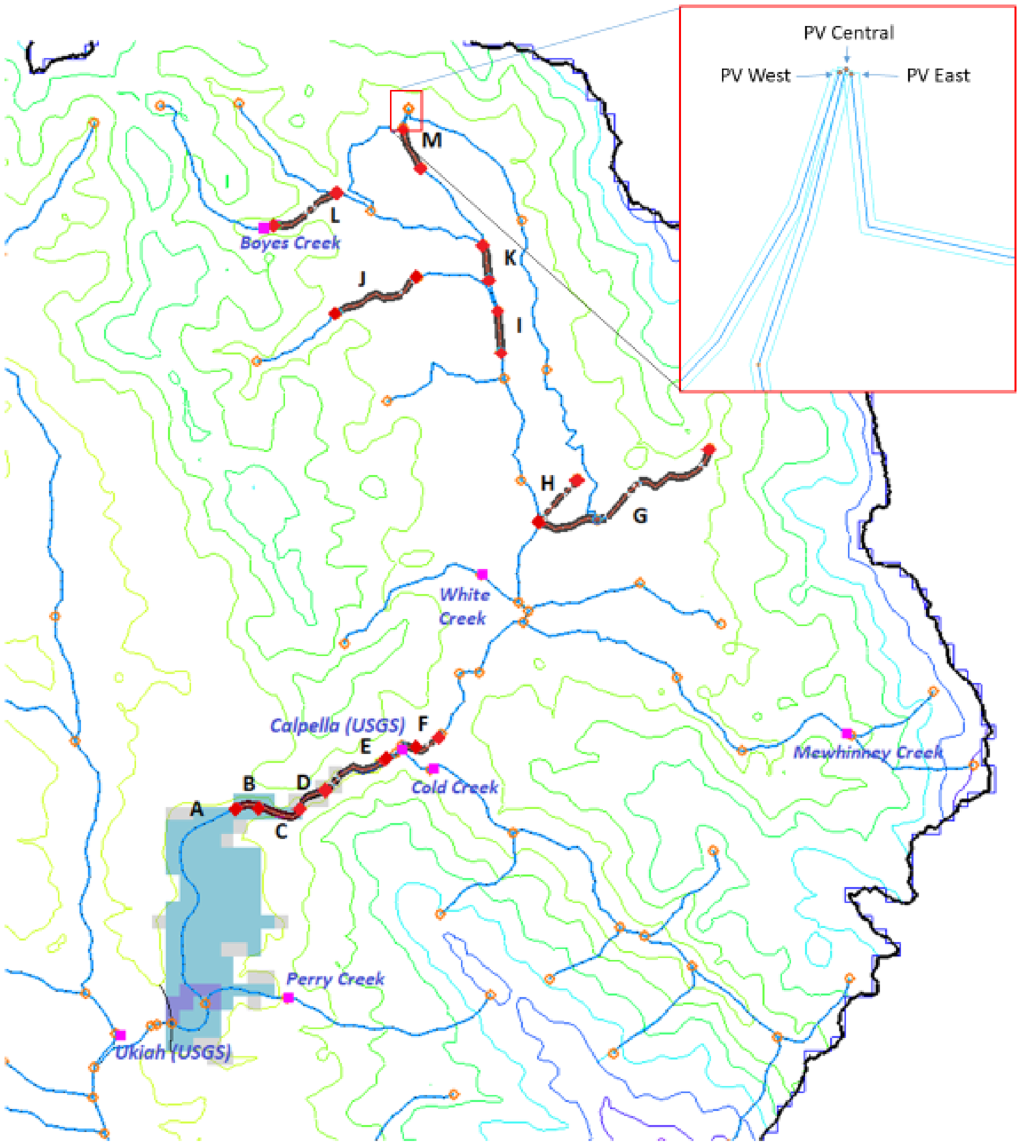

Figure 16. Locations of measured cross sections during field visit.

3.7.3 Stream to Groundwater Interaction

All stream sections were defined as “river flux” stream types, meaning the streams interact with the groundwater according to specified bed thickness and hydraulic conductivity, and the head difference between the stream and the groundwater.

3.8 Forcing Data

3.8.1 Precipitation

The main forcing in GSSHA is the precipitation. Precipitation from 4 sources was used to drive the model:

1. Historical rainfall gauge network in and around the basin.

2. The gauges in (1) plus the newer CW3E network.

3. West-WRF forecast beginning at, say, West-WRF forecast hour 36 for “1 day lead” (i.e., 12 hours of forecast “spinup”, then 1 day lead; spinup being necessary for WRF at resolution to develop its own weather from the initial relatively coarse GFS weather of each forecast).

4. CNRFC gridded gage derived data.

3.8.1.1 Historical Measured Rainfall

The gauge networks for precipitation (1) and (2) are described in Section 2.1. These gages were used to create an observed record from 1971 through 2019. Precipitation data were applied over the GSSHA grids using Thiessen polygons. Use of Thiessen polygons result in rainfall distributions in each area covered by the polygons to be equal in each of the models, regardless of resolution.

3.8.1.2 Historical Plus CW3E

The historical gage network plus the 15 precipitation gages as described in Section 1.1.6.

3.8.1.3 West-WRF

The West-WRF model (Section 1.1.4) was used to produce a 10-day forecast every day during the rainy seasons of 2017/2018 and 2018/2019, roughly, from January to April. West-WRF precipitation rates are produced every 3 hours at 3 km resolution, and then downscaled to 1 hourly hydro-meteorological input for each GSSHA model on its spatial resolution. Precipitation data from the West-WRF model was applied to the GSSHA model using Thiessen polygons, resulting in a similar aerial rainfall distribution in the modeled sub-watersheds, regardless of resolution. Continuous GSSHA input files were developed for a forecast lead time, i.e. 1 day (beginning at West-WRF forecast hour 36), by taking the consecutive 1-day precipitation forecast from daily 10-day forecast and stringing them together to produce a seasonal 1-day precipitation forecast. One-day forecasts were used when calibrating the models that run with West-WRF data, while 1, 3, and 7-day forecasts were used to validate these models.

3.8.2 CNRFC

Two datasets are generated as a forcing based on California Nevada River Forecast Center (CNRFC) precipitation using a multi-gauge precipitation network and a single meteorological station for required meteorological forcing (temperature, humidity e.g.), otherwise. The precipitation estimate (QPE) is generated through the following basic process including a quality control (QC) process that is driven with 6-hr and 24-hr precipitation totals that are computed from the raw gauge reporting. An automated basic screening removes obvious errors. The other data are visualized in a geographical editor and compared to their neighbors.

The QPE is assessed across the entire CNRFC area regardless of the basin boundaries. On the order of 750 precipitation gages are considered. There are more than 2,000 in the CNRFC database, but some are considered unreliable while others are considered redundant, primarily in areas where gauges are clustered (i.e., Southern California). Some basins have few gages while others have a significant number of them. Each observation is topographically and orographically "normalized" using the Parameter Regression against Independent Slopes Model (PRISM) so that location observations are comparable (Daly et al., 1994).

Sites are subjectively judged as "bad" when they do not fit with their neighbors and a good reason cannot be identified for discrepancies (e.g. radar imagery indicating localized heavy rain). Most commonly, gage reports of zero precipitation in areas where close-by stations record non-zero amounts are eliminated (under colder conditions more generally, this can also occur when the precipitation is snow and gages are capped). Once the bad observations are removed, the gridded field is estimated through a distance weighting of PRISM normalized deviates and then transformed back into precipitation via the PRISM normal field for that month or season.

The basin estimates extracted from the grids within the basin boundaries and subareas. Because the watersheds were calibrated with long period of record Cooperative Observer Program (COOP) data, a correction factor is applied to each subarea QPE estimate to account for the difference between the real time network and the COOP network (a 10-year overlap is used to define correction factors). Additionally, CNRFC precipitation products are disaggregated into hourly temporal resolution (at 4-km spatial resolution) using North American Land Data Assimilation System (NLDAS) hourly precipitation analyses (themselves a blend of products; NLDAS precipitation products are considered a standard in performance more generally over the continent across various measures). This precipitation is incorporated into a modified forcing dataset (with the same meteorology otherwise as the CNRFC Ukiah gauge -based weather fields) referred to as CNRFC-mod.

The NLDAS hourly precipitation is re-gridded into a CNRFC 4km grid using an inverse distance interpolation based on 10 nearest neighbors. The interpolated hourly product is then used to disaggregate 6-hourly CNRFC precipitation accumulations into hourly totals by multiplying the fraction of 6-hr total precipitation occurring within each hourly bin.

3.8.3 Inflows and Outflows

Outflows originating from the PG&E power plant at Potter Valley are split into three discharge canals -- one central primary channel, which feeds directly into the main channel running through Potter Valley, and two smaller channels used for irrigation purposes (Figure 16).

For these three small streams, the daily measured flows were input into the GSSHA models via discharge hydrographs as the inflow boundary conditions.

Measured daily outflows from Lake Mendocino (Coyote Dam) were specified as the lake outlet boundary condition.

3.8.4 HMET

Hourly values of barometric pressure, temperature, relative humidity, total sky cover, direct radiation and global radiation are required for continuous (long-term) simulations in GSSHA.

There are two sources of HMET used in this study – measured HMET for the period of record obtained from the Ukiah Airport (used for the gauged network and the CNRFC runs), and generated HMET via the West-WRF model. When using the measured data, the values are uniform across the watershed. Elevation adjustments are made for computing snowfall and melt. When using West-WRF forecast data, gridded forecast HMET variable from West-WRF are used in lieu of the measured data.

3.9 Model Initialization

3.9.1 Groundwater Table Initialization

The initial elevation of the groundwater table is significant for long-term groundwater, surface-water, and stream flow integrated simulation. Since no groundwater table level data were available to determine a starting groundwater elevation, the model itself was used to develop the initial conditions in a two-step process. First, the groundwater leakage capability of GSSHA was disabled in the models so that no water could leave the system through the aquifer bottom. Next, an initial groundwater condition was established by setting the water table at the topographic surface. Then the model was run for one simulated year, without rainfall. This procedure was run iteratively until the change in groundwater elevation between successive simulations was minimal and the base flow at the watershed outlet was within an order of magnitude of the observed low flow values, around $5m^3\ s^{-1}$. For each successive simulation, the final water table from the previous simulation was used as the initial condition for the next simulation. The new equilibrated water table was then used to establish the initial conditions in the model, which would be used as the starting point for the long-term calibration and verification simulations to come.

3.9.2 Final Model Initialization

The initial conditions to be used when running the models in production mode were obtained by simulating the system (spin up) for an extended period of 3 to 12 months, depending on the availability of forcing data, with this spin up simulation ending just prior to the period of interest. The final conditions from these simulations were then used as the initial conditions in the calibration and validation simulations.

After the model initialization (spin up) period, the models were then deployed with these new starting conditions to run the long-term simulations henceforth.

4 Model Calibration

4.1 Calibration Strategy

The GSSHA models of the upper Russian River watershed are complex models of variable resolution. Simulation run times are dependent on model complexity, resolution, and simulation period. Automated calibration methods require hundreds, if not thousands, of simulations to converge on an optimal parameter set. The approach to calibration of the models was to start with calibrating the lowest resolution (270m) surface water model for a single isolated event (December 2004) and then increase model resolution, then the simulation period, and finally the model complexity. Additionally, additional parameters obtained using the information from the previous calibration efforts were added to minimize the number of parameters and the range of those parameters, to minimize calibration convergence times.

Selected models were calibrated for both surface water and groundwater, as well as with multiple precipitation and hydro-meteorological (HMET) data sets. Table 6 list all the calibration efforts, including model resolution, calibration period, precipitation inputs, hydro-meteorological inputs, and whether or not the models were surface water only, or included subsurface flow simulations.

Table 6. Calibration Overview.

Resolution	Calibration Period	SW/GW	Precipitation Data	HMET Source
270m	Dec 2004	SW	Observed	Ukiah
50m	Dec 2004	SW	Observed	Ukiah
270m	Dec 2004-May 2005	SW	Observed	Ukiah
50m	Dec 2004-May 2005	SW	Observed	Ukiah
270m	Dec 2004-May 2005	SW/GW	Observed	Ukiah
270m	Jan 18 – April 2018	SW/GW	Observed + CW3E network	Ukiah
270m	Jan 18 – April 2018	SW/GW	West-WRF	Ukiah

270m	Jan 18 – April 2018	SW/GW	West-WRF	West-WRF
100m	Dec 2004- May 2005	SW/GW	Observed	Ukiah
100m	Jan 18 – April 2018	SW/GW	Observed + CW3E network	Ukiah
100m	Jan 18 – April 2018	SW/GW	West-WRF	West-WRF

4.2 Historical Data Sets

For the GSSHA Mendocino watershed model, daily flow volumes, event discharges, and peak flow rates were compared against historical observations for single events in Dec 2004 and two periods of record from 01Dec2004 – 15May2005, and 01Jan2018 – 15Apr2015. Table 7 shows the selected USGS gauging stations for the GSSHA Mendocino watershed model calibration and the available period of records.

Table 7. Selected USGS stream flow gauging stations used in the GSSHA Mendocino watershed model calibration.

Period of Simulation	USGS Station No.	USGS Station Description	Available Period of Record
01Dec2004-15May2005; 01Jan2018-15Apr2018	11461000	Russian River near Ukiah	01Oct1911 – pres.
01Dec2004-15May2005; 01Jan2018-15Apr2018	11462500	Russian River near Hopland	01Oct1939 – 30Oct2019
01Dec2004-15May2005; 01Jan2018-15Apr2018	11461500	Russian River near Calpella	01Oct1941 – pres.
01Jan2018-15Apr2018	11462080	Russian River near Talmage	06Aug2009 – pres.

Historical flow data at 15 minute interval were obtained from the USGS National Water Information System (USGS, 2019). The data sets for the periods of 01Dec2004 through 15May2004 and 01Jan2018 through 15Apr2018 were plotted as flow hydrographs and the results are shown in Figure 17 and Figure 18. Maximum peak flow rates during the 01Dec2004-15May2005 period were 342.3, 185.6, and 184.2m^3/s for Hopland, Ukiah, and Calpella, respectively. Maximum peak flow rates for the 01Jan2018-15Apr2018 period were 259.4, 227.4, 156.9, and 213.2m^3/s for Hopland, Ukiah, Calpella, and Talmage, respectively.

In addition to the USGS gauging stations, historical data collected at CW3E stations were used. Table 8 shows a description of these stations and their location within the Russian river tributaries in the Lake Mendocino watershed.

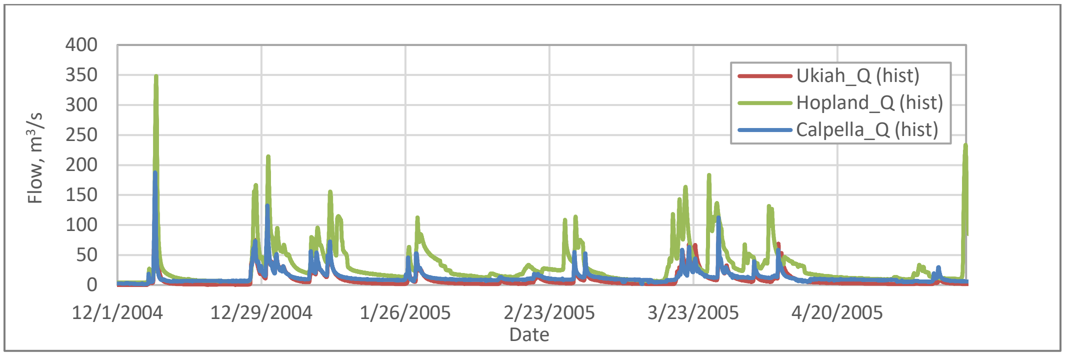

Figure 17. Flow hydrographs for USGS gauging stations in the Russian River for the 01Dec2004 – 15May2015 period of record.

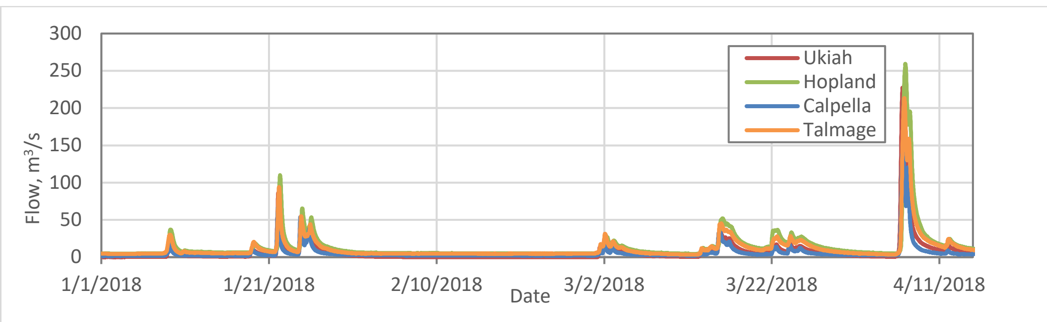

Figure 18. Flow hydrographs for USGS gauging stations in the Russian River for the 01Jan2018 – 15Apr2018 period of record.

Table 8. CW3E flow gauging stations in tributaries of the Russian river.

Station Name	Location
BYS	Boys Creek
CLD	Cold Creek
MEW	Mewhinney Creek
MLL	Mill Creek
DRW (PRY)	Perry Creek
WHT	White Creek

Similar to the USGS gauging stations, flow hydrographs for the CW3E stations were plotted and these are shown in Figure 19. Maximum peak flow rates at these locations occurred around 06Apr2018 with magnitudes of 2.1, 3.3, 0.3, 10.1, 3.2, and 17.2 m^3/s at BYS, CLD, MEW, MLL, DRW (PRY), and WHT, respectively.

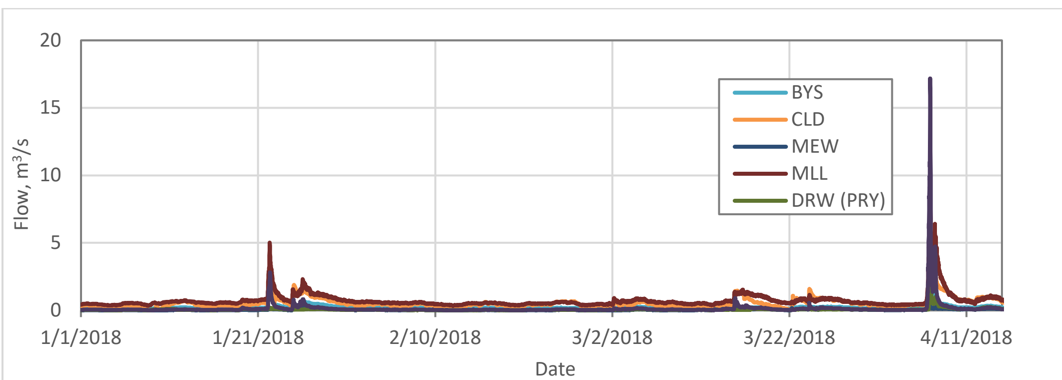

Figure 19. Flow hydrographs for the CW3E gauging stations in tributaries of the Russian River.

Daily total volumes, event based volumes, and event peak flow rates were used as the observed (i.e, historical) data sets during the calibration process. Event-based peak and flow rates were determined by inspection of the flow hydrographs and selecting a corresponding start and end date for a particular event. Figure 20 shows an example of how an event was identified from a given hydrograph. The figure depicts the event start date (06Dec2004), end date (16Dec2004), and peak flow rate (342.4 $m^3\ s^{-1}$). The area under the curve between the start and end dates is representative of the volume for that particular event.

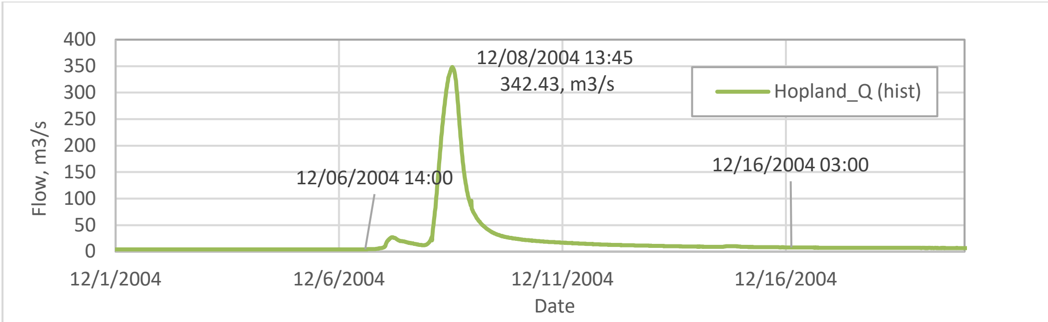

Figure 20. Event based determination from the flow hydrographs. Start date, end date, and peak flow rates were used as part of the observed data set during the calibration process.

Table 9 summarizes the selected events used in the calibration process for the 01Dec2004-15May2004 for the USGS gauging stations; and Table 10 and Table 11 provide similar information for all the stations for the 01Jan2018-15Apr2018 period of record.

Table 9. Event volumes and peaks for the USGS gauging stations for the 01Dec2004-15May2005 period.

Event No.	Start Date/Time	End Date/Time	Event Volumes, m^3			Event Peaks, m^3/s		
			Hopland	Ukiah	Calpella	Hopland	Ukiah	Calpella
1	12/4/2004 5:45	12/17/2004 18:00	30031844	10217917	13754421	348.30	190.29	187.74
2	12/17/2004 17:45	12/20/2004 15:00	1742826	203193	1726591	7.25	0.99	7.05
3	12/20/2004 15:00	12/24/2004 9:00	2098803	287319	2138889	6.82	0.99	6.88
4	12/25/2004 0:45	1/24/2005 12:00	123021627	41002500	53169710	214.36	82.97	132.24
5	1/24/2005 11:45	1/31/2005 10:00	26919932	7266871	9876223	112.70	49.55	52.95
6	1/31/2005 9:45	2/5/2005 20:00	13212709	1881057	4658757	46.72	6.88	11.81
7	2/5/2005 19:30	2/9/2005 14:00	4964366	730709	2836392	16.71	2.61	9.03
8	2/9/2005 13:45	2/11/2005 13:00	2316986	305567	1418629	14.03	1.93	9.32
9	2/11/2005 13:00	2/23/2005 14:00	19175846	4948701	11231039	33.70	15.97	18.58
10	2/23/2005 13:15	3/5/2005 23:00	36377129	7823983	13148004	114.40	47.86	54.93
11	3/5/2005 23:00	3/9/2005 11:00	4900942	1163268	2986220	21.12	5.13	11.04
12	3/16/2005 15:00	3/26/2005 9:00	41434396	18678911	16112891	163.95	68.24	63.43
13	3/26/2005 8:30	3/31/2005 15:00	36174471	9271436	10666542	183.78	83.82	112.42
14	3/31/2005 15:00	4/2/2005 7:00	5242391	1179987	1882203	46.44	10.28	14.10
15	4/2/2005 6:45	4/16/2005 14:00	52935623	15028754	16987872	131.96	68.81	58.62
16	4/16/2005 13:45	4/21/2005 11:00	6682375	1430761	3919561	18.75	4.11	10.22
17	4/21/2005 10:45	5/3/2005 12:00	12066237	2263258	8531808	14.78	2.94	9.49
18	5/3/2005 11:45	5/14/2005 14:00	13794382	2815622	7786214	33.41	13.45	30.02
19	5/14/2005 13:45	5/15/2005 23:45	1309731	219452	749262	11.30	1.87	6.14

Table 10. Event volumes (in m^3) for the gauging stations used for the 01Jan2018-15Apr2018 calibration period.

Event #	Start Date/Time	End Date/Time	Hopland	Talmage	Ukiah	Calpella	DRW	CLD	MLL	MEW	WHT	BYS
1	1/3/2018 13:00	2/5/2018 18:00	34152920	28504567	13957392	14335350	173926	1505003	2197603	109384	357007	679653
2	2/6/2018 19:30	2/9/2018 19:00	1381602	1216738	23523	571818	6777	110958	141640	6239	15518	50031
3	2/11/2018 15:00	2/12/2018 10:00	365049	327357	2195	145857	1021	14849	26554	-1943	1359	8090
4	2/13/2018 18:45	2/13/2018 19:00	9226	8257	36	3726	48	756	951	24	83	288
5	2/18/2018 3:00	2/20/2018 10:00	989181	906584	2583	390252	4541	50485	83945	-2909	5096	27578
6	2/21/2018 17:00	3/30/2018 3:00	42644274	35688478	18984167	16443562	176737	1581025	2126616	149236	316677	561089
7	3/31/2018 14:00	3/31/2018 15:00	33360	24491	8724	12867	246	1941	2267	196	264	653
8	4/2/2018 10:00	4/2/2018 20:00	223760	163793	40065	99277	1535	9200	15476	562	1333	3915
9	4/3/2018 23:30	4/15/2018 23:45	38740020	31664014	24150749	15996743	207805	998900	1310282	101464	545391	338407

Table 11. Event peak flow rates (in m^3/s) for the gauging stations used for the 01Jan2018-15Apr2018 calibration period.

Event #	Start Date/Time	End Date/Time	Hopland	Talmage	Ukiah	Calpella	DRW	CLD	MLL	MEW	WHT	BYS
1	1/3/2018 13:00	2/5/2018 18:00	109.87	94.30	85.80	69.09	0.20	1.89	5.01	0.21	2.82	2.08
2	2/6/2018 19:30	2/9/2018 19:00	5.49	4.90	0.15	2.32	0.03	0.53	0.62	0.04	0.08	0.23
3	2/11/2018 15:00	2/12/2018 10:00	5.38	4.79	0.04	2.14	0.02	0.31	0.42	-0.01	0.02	0.13
4	2/13/2018 18:45	2/13/2018 19:00	5.15	4.62	0.02	2.08	0.03	0.42	0.53	0.01	0.05	0.16
5	2/18/2018 3:00	2/20/2018 10:00	5.10	4.90	0.07	2.03	0.04	0.47	0.52	0.01	0.05	0.18
6	2/21/2018 17:00	3/30/2018 3:00	52.10	45.31	33.41	32.85	0.13	1.57	1.54	0.21	0.91	0.32
7	3/31/2018 14:00	3/31/2018 15:00	7.45	5.47	1.96	2.89	0.05	0.44	0.51	0.04	0.06	0.15
8	4/2/2018 10:00	4/2/2018 20:00	6.23	4.56	1.12	2.76	0.04	0.27	0.44	0.02	0.04	0.11
9	4/3/2018 23:30	4/15/2018 23:45	259.38	213.23	227.38	156.88	3.15	3.34	10.08	0.31	17.18	2.11

4.3 Calibration Methods

4.3.1 PEST

This section provides basic information of PEST as it pertains to the calibration of the GSSHA Lake Mendocino watershed models. Additional information of the software can be found in the online PEST documentation available at PEST (2020).

Although the PEST software serves several functions in support of numerical modeling, its primary role is to assist in model calibration, sensitivity analysis, and predictive uncertainty analysis. The software is basically a model-independent parameter optimizer which uses a nonlinear parameter estimation technique known as the Gauss-Marquardt-Levenberg method. Other important features of PEST include the user intervention functionality, predictive/uncertainty analysis due to parameter non-uniqueness, and regularization. Most of these features of PEST are used to enhance the efficiency of the calibration process of models.

With regard to its calibration functionality, PEST wraps itself around a numerical model and independently runs it. It adapts to and takes full control of the model, and during the calibration process, it compares model output with observed (historical) data. PEST constantly analyzes the relation between parameters and the comparison between output and observed data. Based on the differences in simulated outcomes and observations, and other predetermined criteria, PEST automatically adjusts model parameters until the fit between these is "optimal" from a weighted least square residuals perspective.

As for the parameter optimization process, the user must supply a set of initial parameter values. These can either remain fixed or change during a run. Parameters that remain fixed are generally more certain, and are usually used in the derivation of other less certain parameters that may change, within a predefined range of values, during the optimization process.

During the optimization process, several options are available which can be used to steer PEST through a run. A PEST run can be initiated and run to completion without user interruption. Also, at any stage of the PEST run, a user can request that certain troublesome parameters be held at their current values. Because of PEST's predictive analysis capability, at any stage of the optimization process, sensitive and insensitive parameters can be distinguished. Insensitive parameters cause the most problems. PEST no longer ceases execution with an error message if a parameter has no effect on observations; rather it simply holds the parameter at its initial value.

To apply PEST to a model such as the GSSHA Mendocino watershed model, a series of “template” files were created from relevant GSSHA model input files in which calibration parameters were defined, and using “replacement” variables in place of specific hard coded parameter values for parameters that are desired to be calibrated. PEST uses these template files to “replace” values for the calibration parameters prior to a model run. It then launches GSSHA to run with that series of updated parameter values. Once a model run is complete, PEST uses the GSSHA results to compare against a set of “observations”. This process continues and the results compared to the observed data. The comparison between “simulated” and “observed” outcomes is made through a user defined objective function of the following form:

$$\Phi = (\mathbf{c} - \mathbf{Xb})^T \mathbf{Q}(\mathbf{c} - \mathbf{Xb})$$

where:

Φ = objective function
c = vector of system response
X = model excitations
b = vector of system parameters
Q = observation weights

This function is minimized through a series of parallel optimization iterations until the difference in the several consecutive objective function values falls within a user defined threshold. The process is conceptually illustrated in Figure 21.

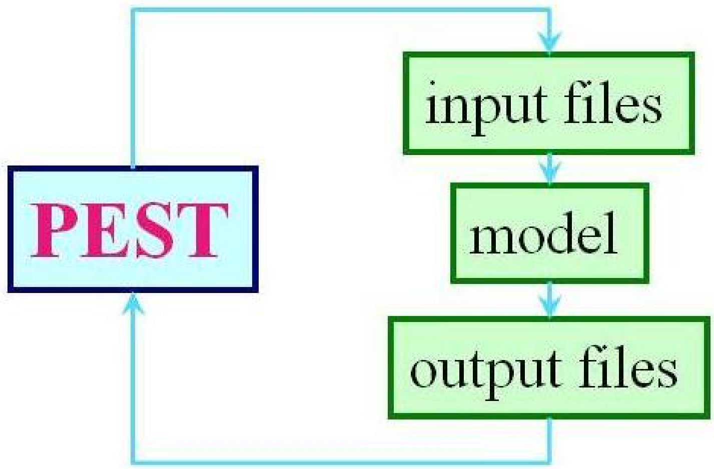

Figure 21. Conceptual flowchart diagram of the PEST parameter estimation process.

4.3.2 BeoPEST (parallel)

BeoPEST is a special version of Parallel PEST inspired by computer clusters that is suitable to be run in highly parallelized environments such as the ERDC High Performance Computer systems. BeoPEST differs from the traditional Parallel PEST only in how it communicates with “slave processes” and how these slave processes know what to do. In the traditional Parallel PEST, a master process creates files using a template and reads the results using the instruction file, in addition to performing the actual parameter estimation calculations. The slave simply executes the model runs. In BeoPEST, the master process still performs the parameter estimation calculations exactly as before, but instead of writing and reading files, it sends the set of parameters to be run to the slave, and receives observations from the slave in binary form over a network connection. The BeoPEST slave is smart and creates the model input files from the parameters as instructed by the master, runs the model, extracts the observations from the model output files, and sends the resulting observations back to the master.

Therefore as much of the work as is possible is offloaded to the slave, and the master only deals with the parameter estimation proper.

4.4 Calibration Parameters

For the GSSHA Mendocino watershed model, a series of parameters were defined as variable parameters during the PEST parameter estimation process. These are listed in Table 12. Template files were created from the channel input (*.cif), project (*.prj), and mapping table (*.cmt) GSSHA model input files. Likewise, a PEST control file was developed where inputs, outputs, and configuration control variables to the PEST process were defined.

Initial parameter values were populated based on literature values. Calibration ranges for these were set based on literature values, a physical understanding of the system from observations, or a combination of the two. In some cases parameter ranges were expanded to allow a better fit to observed data when the automated calibration was reaching the upper or lower range values in a search for the best fit.

Table 12. Parameters in the GSSHA Mendocino watershed models.

Parameter	Description	Initial Value(s)	Range
ch_rough1	Manning's roughness coefficients for the Russian River (main channel)	0.028	0.025-0.15
ch_rough2	Manning's roughness coefficients for the Russian River (1st order tributaries)	0.126	0.025-0.15
ch_rough3	Manning's roughness coefficients for the Russian River (2nd or more order tributaries)	0.126	0.025-0.15
gwkriv1	Leakance coefficient Russian River main channel	0.3	0.00001-1
gwkriv2	Leakance coefficient Russian River 1st order tributaries	0.1	0.00001-1
gwkriv3	Leakance coefficient Russian River 2nd or greater order tributaries	0.1	0.00001-1
rov1	Overland roughness coefficient "Water", "Open Space" or "Barren" land uses	0.011	0.01-0.3
rov2	Overland roughness coefficient for "Evergreen Forest" land use	0.862	0.15-1.5
rov3	Overland roughness coefficient for "Shrub" land use	0.555	0.11-1
rov4	Overland roughness coefficient for "Grassland" and "Pasture" land use	0.123	0.05-0.4
rov5	Overland roughness coefficient for "Crops" land use	0.301	0.1-0.4
rov6	"Overland roughness coefficient for "Deciduous Forest" land use	0.724	0.11-1
retn1	Retention depth for "Deciduous Forest" land use	17.03	0.00001-25
retn2	Retention depth for "Shrub" land use	2.15	0.00001-25
retn3	Retention depth for "Grassland" and "Pasture" land use	1.95	0.00001-25
retn4	Retention depth for "Crops" land use	13.3	0.00001-25
canr1	Canopy resistance factor for "Deciduous Forest" land use	101	50-150
canr2	Canopy resistance factor for "Evergreen Forest" land use	140	50-150
canr3	Canopy resistance factor for "Mixed Forest" land use	98	50-150

canr4	Canopy resistance factor for "Shrub" land use	179	50-200
prsty1	Porosity for "UBR" soil type	0.078	0.07-0.4
prsty2	Porosity for "WB" soil type	0.102	0.07-0.4
hdrc1	Hydraulic conductivities for sediments	0.02	0.015-0.15
hdrc2	Hydraulic conductivities for sediments	0.231	0.05-0.3
hdrc3	Hydraulic conductivities for sediments	0.759	0.33-2.2
hdrc6	Hydraulic conductivities for sediments	0.432	0.1-0.7
hdrc7	Hydraulic conductivities for sediments	1.742	0.3-3
hdrc10	Hydraulic conductivities for sediments	0.006	0.001-0.01
hdrc11	Hydraulic conductivities for sediments	0.017	0.001-0.025
hdrc20	Hydraulic conductivities for sediments	0.436	0.22-1
hdrc21	Hydraulic conductivities for sediments	0.42	0.18-3.5
hdrc30	Hydraulic conductivities for sediments	0.286	0.02-1
hdrc31	Hydraulic conductivities for sediments	0.182	0.15-0.8
hdrc32	Hydraulic conductivities for sediments	0.838	0.35-2.1
hdrc40	Hydraulic conductivities for sediments	0.64	0.1-1
gwhyd	Hydraulic conductivity for the surficial aquifer system	1.0	0.1-100
gwporos	Porosity for the surficial aquifer system	0.35	0.05-0.5
sgl_uns_sat	Parameter for the soil infiltration model	0.75	0.01-0.9
gw_lkg_rt	Groundwater leakance rate	0.00001	0.00001-0.1

4.5 Calibration Metrics

Model parameters were calibrated to match, as closely as possible, measured flows in three USGS flow gauging stations in the 2004 calibration period, or a combination of four USGS with six CW3E gauging stations in the 2018 period. Each period of record calibration was focused on minimizing an objective function composed of daily flows, event based volumes, and event based peaks components at each gauging stations. The event based volumes and peaks are defined in Table 9, Table 10, and Table 11.

The objective function was specified as:

$$\varphi = \sum_{p=1}^{p=P} \left\{ W_p^Q \overbrace{\sum_{i=1}^{i=T} (Q_i^o - Q_i^s)_p^2}^{Daily\ Flows\ at\ p} + W_p^V \overbrace{\sum_{m=1}^{m=M} (EV_m^o - EV_m^s)_p^2}^{Event\ Vols\ at\ p} + W_p^K \overbrace{\sum_{m=1}^{m=M} (EP_m^o - EP_m^s)_p^2}^{Event\ peaks\ at\ p} \right\}_p$$

where:

Q_i^o = is the i^{th} observed daily flow at station p

Q_i^s = is the i^{th} simulated daily flow at station p

T = total number simulated and observed daily flows at station p

W_p^Q = weight assigned to the daily flows at station p

EV_m^o = is the m^{th} observed flood event volume at station p

EV_m^s = is the m^{th} simulated flood event volume at station p

W_p^V = weight assigned to the event volumes at station p

EP_m^o = is the m^{th} event observed peak flow rate at station p

EP_m^s = is the m^{th} event simulated peak flow rate at station p

W_p^K = weight assigned to the event peak flow rates at station p

M = total number simulated and observed flood event volumes and peak flow rates at station p

In this function, the first term represents the sum of the square residuals between observed and simulated daily flows at any given flow gauging station. The second and third terms, represent the sum of the square residuals between the observed and simulated event volumes and peaks, respectively, at the same station. The overall sum (from $p=1$ to P), is the aggregation of the terms for all gauging stations.

Goodness of fit metrics used to assess the calibration outcome included the Nash-Sutcliffe Efficiency (*NSE*) coefficient, the Correlation Coefficient

(*R*), the Root Mean Square Errors (*RMSE*), and the Mean Absolute Error (*MAE*). Math formulas to calculate these metrics are given by:

$$NSE = 1 - \frac{\sum_{i=1}^{T}\left(Q_s^i - Q_o^i\right)^2}{\sum_{i=1}^{T}\left(Q_o^i - \bar{Q}_o\right)^2} \tag{3}$$

$$R = \frac{\sum_{i=1}^{T}\left(Q_o^i - \bar{Q}_o\right)\left(Q_s^i - \bar{Q}_s\right)}{\sqrt{\sum_{i=1}^{T}\left(Q_o^i - \bar{Q}_o\right)^2}\sqrt{\sum_{i=1}^{T}\left(Q_s^i - \bar{Q}_s\right)^2}} \tag{4}$$

$$RMSE = \sqrt{\frac{\sum_{i=1}^{T}\left(Q_s^i - Q_o^i\right)^2}{T}} \tag{4}$$

$$MAE = \frac{\sum_{i=1}^{T} ABS\left(Q_s^i - Q_o^i\right)}{T} \tag{5}$$

where:

Q_s^i= is the i^th model outcome (i.e., stage, flow, depth, etc).

Q_o^i = is the i^th observed outcome

$\bar{Q}_o$ = is the mean of the observed outcomes

$\bar{Q}_s$ = is the mean of the simulated outcomes

T = is the total number of outcomes considered.

4.6 Calibration Results

4.6.1 Surface Water Only Models (No Groundwater)

4.6.1.1 Surface Water Calibration Parameter Values

The calibration values for this model were derived from a combination of the initial single event calibration and the extended calibration period, through one wet season. In general, hydraulic parameters could be determined during the single event calibration whereas the long term period is required to determine evapotranspiration parameters (canopy resistance). All parameter values were allowed to float in both periods, such that hydraulic parameters were further adjusted during the seasonal calibration effort. Experience shows that having multiple events results in an improved calibration parameter set. Final calibration values for the models are shown in Table 13.

In general, the final values from the two models do not differ dramatically and parameter values are well within physical limits for the parameters. Substantially different values are shown in bold. As seen in the table there are only three parameters that are substantially different. There are no obvious reasons for the large differences.

Table 13. Calibrated parameters SW model only

Parameter Type	Class	Initial Value	Final 270m Value	Final 50m Value
channel roughness	Main channel	0.030	0.028	0.0254
channel roughness	Secondary channel	0.035	0.126	0.114
Overland roughness 1	Open, barren	**0.1**	**0.011**	**0.112**
Overland roughness 2	Evergreen forest	0.3	0.862	0.702
Overland roughness 3	shrub	0.3	0.555	0.895
Overland roughness 4	Grassland, pasture	0.2	0.123	0.145
Overland roughness 5	crops	0.15	0.301	0.261
Overland roughness 6	Deciduous & mixed forest	0.3	0.724	0.903
Retention depth 1	forest	0	17.03	15.8
Retention depth 2	shrub	0	2.15	2.59
Retention depth 3	Grass and pasture	0	**1.95**	**15.8**
Retention depth 4	crops	0	13.30	19.3
Canopy resistance 1	Deciduous forest	120	101.4	132.0
Canopy resistance 2	Evergreen forest	140	140.4	138.0
Canopy resistance 3	Mixed forest	130	98.0	50.1
Canopy resistance 4	shrub	150	179.9	179.0
Porosity 1	Unweathered bedrock	0.085	0.078	0.1
Porosity 2	Weathered bedrock	0.2	0.102	0.1
Soil hydraulic conductivity 1	clay	0.03	0.02	0.0338
Soil hydraulic conductivity 2	Clay loam	0.1	0.231	0.15
Soil hydraulic conductivity 3	Sandy loam	0.66	0.759	0.857
Soil hydraulic conductivity 6	Sandy clay loam	0.15	0.431	0.226
Soil hydraulic conductivity 7	Sandy loam	1.09	**1.742**	**0.26**
Soil hydraulic conductivity 10	Un-weathered bedrock	0.002	0.006	0.00185
Soil hydraulic conductivity 11	Weathered bedrock	0.02	0.017	0.0148
Soil hydraulic conductivity 20	Clay loam/forest	0.1	0.436	0.99
Soil hydraulic conductivity 21	Loam/forest	0.66	0.42	0.902
Soil hydraulic conductivity 30	Clay loam/shrub	0.1	0.286	0.159
Soil hydraulic conductivity 31	Loam/shrub	0.66	0.182	0.273
Soil hydraulic conductivity 32	Sandy loam/shrub	1.09	0.838	1.06
Soil hydraulic conductivity 40	Loam/grassland, pasture	0.66	0.64	0.55

4.6.1.2 Surface Water Calibration Results – Flows and Reservoir Levels

The 270 meter and 50 meter models covering the December 2004 – April 2005 period were initially calibrated with no groundwater processing to help obtain initial parameter values for the surface water process components. Flows from the 270m model are shown in Figure 22. Flows from the 50m model are shown in Figure 23. As seen in these figures, the models at both resolutions reasonably simulate the flows during the first events, which was specifically chosen as an event with only surface water contributions. However, as the season progresses and the source of stream flow presumably becomes more groundwater (base flow), the surface water model is not capable of accurately representing the flows and begins to significantly under predict the streams flows. As shown in Figure 22 and Figure 23; and Table 13, neither increasing the resolution of the surface water model, nor adjusting surface water parameter values can result in an adequate simulation of the observed flows. A decision was made to explicitly simulate the groundwater in GSSHA, in addition to the surface water component.

Simulated versus observed reservoir levels are shown in Figure 24 for the 270m and 50m models in panels 1 and 2, respectively. The models initially simulates the lake levels relatively well. However, as the rainy season advances, the simulated lake level begins to depart from the observed and by May, is several meters below the observed level. Although still inaccurate, the 50m model is closer to the actual level for most of the simulation period, indicating there is an advantage to the increased resolution in the 50m model. However, when the decision to go to a fully coupled surface water/groundwater modelling effort was made, another decision was to develop a 100m for use as the “fine resolution” model for the coupled model as the coupled model takes significantly more computational resources and even with only surface water modeling, the 50m model already had significant computational burden.

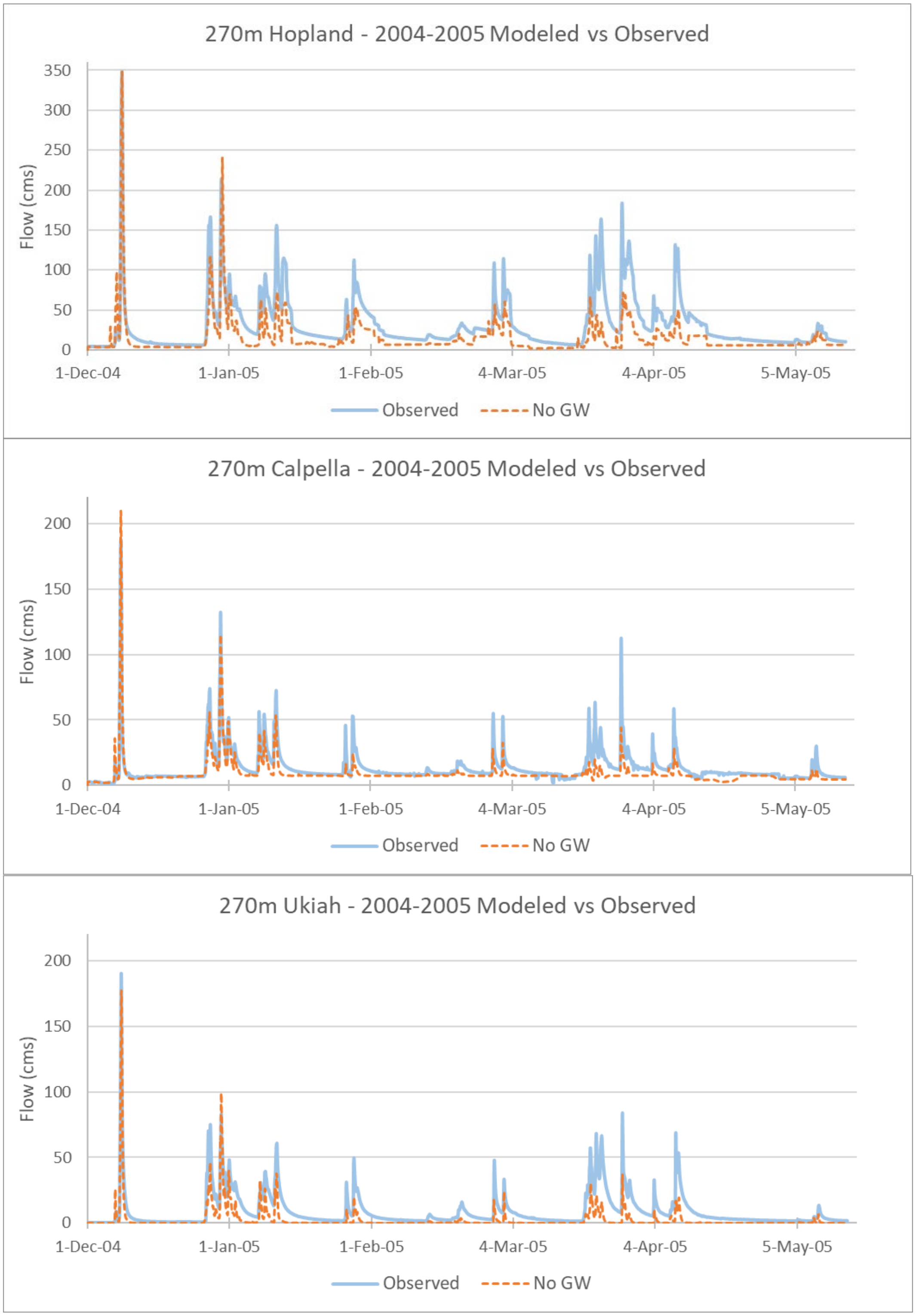

Figure 22. Observed versus the 270m surface water model simulated flows for the flow gauge locations at Hopland, Calpella, and Ukiah.

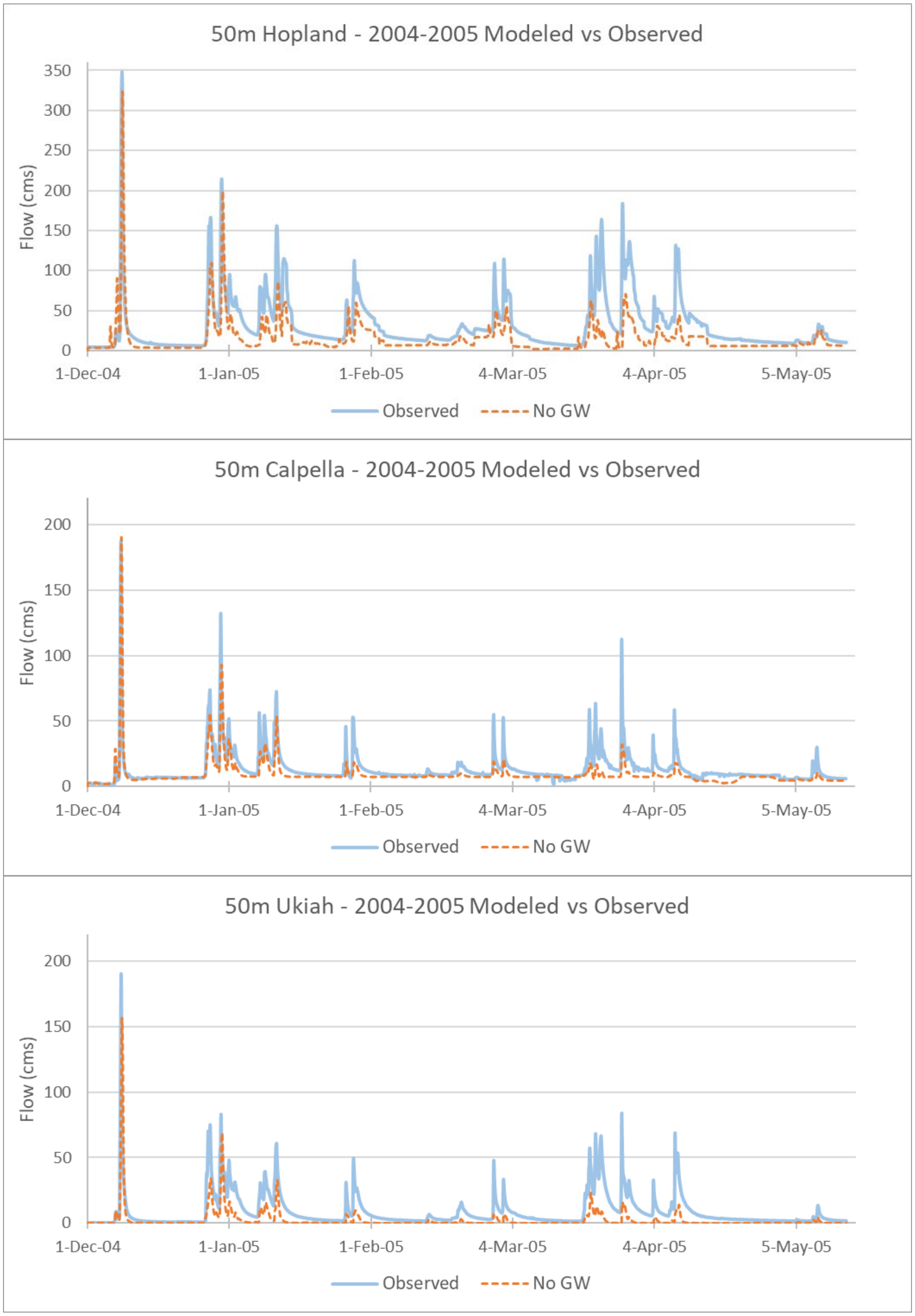

Figure 23. Observed versus the 50m surface water model simulated flows for the flow gauge locations at Hopland, Calpella, and Ukiah.

The difference in reservoir level between observed and simulated is due almost exclusively to the difference in inflows, with other differences attributed to differences in computed and actual lake evaporation and seepage possibly contributing. As with the flows, this analysis indicates the need for a coupled surface-water/groundwater model to adequately simulate the Lake Mendocino Reservoir levels.

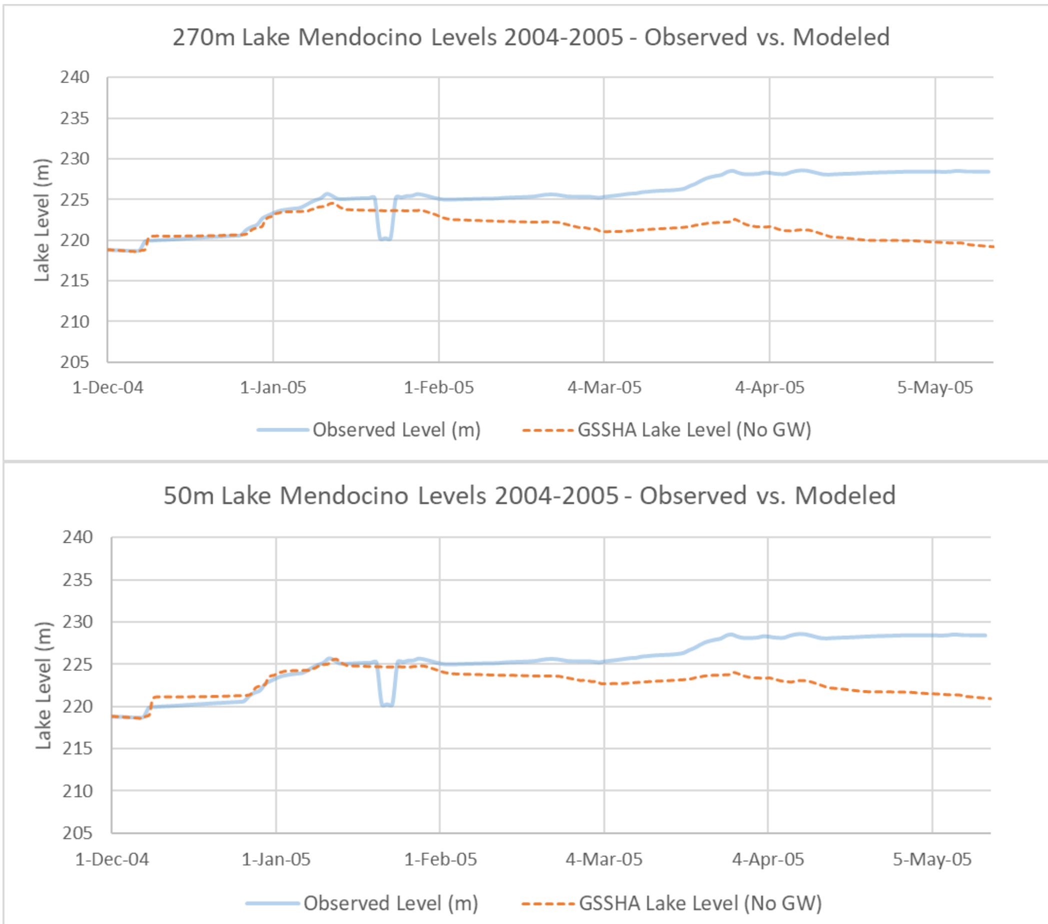

Figure 24. Observed versus simulated flow for the 270m (Panel 1) and the 50m (Panel 2) SW only resolution models.

4.6.2 Reservoir Leakance Calibration

In GSSHA, leakage from the bottom of the reservoir can be computed by specifying the M_LAKE card for each reservoir in the model. M_LAKE represents the reservoir bottom layer depth to compute seepage across. Seepage is computed in each inundated GSSHA overland grid cell using a Darcy flux equation:

$$Q = \frac{K_{bed}}{M\_LAKE} D_{cell} A_{cell}$$

where:

K_{bed} = hydraulic conductivity of the reservoir bed material (cm hr^{-1})

M_LAKE = thickness of the reservoir bed material (cm)

D_{cell} = depth of water in the cell (cm)

A_{cell} = area of the grid cell (cm^2)

Q = flow across the sediment bed (cm^3/s)

Cells identified with the land use type of "water" were given vertical soil hydraulic conductivities of 0.1cm/hr, assuming that the clay loam present in the watershed would cover the bottom of the reservoir, ponds, or other water bodies, as it settles. Clay loam was assigned a *K* of 0.1cm/hr. While the reservoir can cover cells that are not defined as the land use water, and these cells would have different values of *K*, most the cells in the lake have these values.

The value of *M_LAKE* was used as a calibration parameter. The dry season of 2004, April 1 – Dec 01, was used for the calibration period. During this period, the only flows into the lake are the measured flows from Potter Valley and the only outflows are the flows from Lake Mendocino. Changes in lake level are primarily due to the measured inflows and outflows, evaporation from the lake surface (computed in GSSHA), and leakage, also computed in GSSHA. In conducting the calibration we focused on the slope of the lake recession curve and varied the value of M_LAKE until the observed and simulated lake level slopes were as close as possible (Figure 25). The final value of M_LAKE 12 cm, was used in all successive modeling efforts.

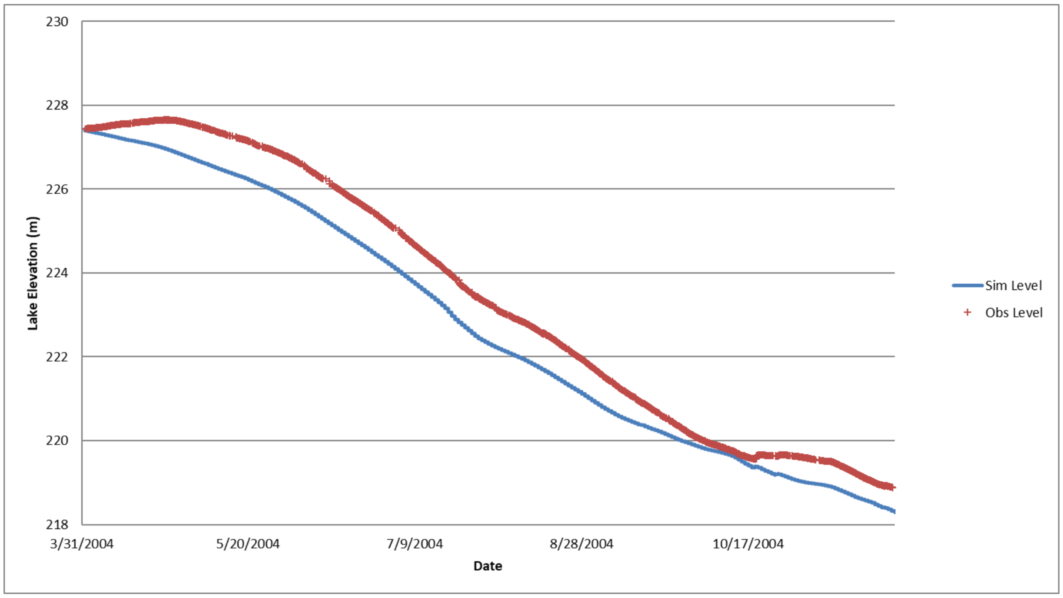

Figure 25. Simulated vs. Observed Lake Mendocino water levels for calibration of lake seepage.

4.6.3 Surface Water with Groundwater Calibration

4.6.3.1 Calibration periods, model resolutions, and precipitation data sets

Two calibration periods and two model resolutions were used for calibrating the coupled surface-groundwater GSSHA Mendocino models. These were:

- 01Dec2004-15Apr2005: 270m; historical gage data
- 01Jan2018-15May2018: 270m; expanded gauge data; 270m West-WRF data
- 01Dec2004-25Dec2004: 100m; historical gage data
- 27Feb2018-20Mar2018: 100m; expanded gauge data; 100m West-WRF data

The reasons for a reduced calibration period for the 100m model is due to long (greater than 1 day for 1 event) model runtimes at these resolutions. The time allotted for these "jobs" in the ERDC's HPC systems were not long enough to complete one full optimization round if longer calibration periods were used. As discussed in Section 4.6.1, for coupled surface water/groundwater modeling, a decision to develop a 100m surface water/groundwater model to represent the "fine resolution" model was made to ease computational burden and facilitate the automated calibration process.

4.6.3.2 Groundwater parameter values

As there was very little supporting information about the subsurface materials within the model domain. The hydraulic conductivity of the groundwater was set to a range of 0.10 to 100.0 cm hr-1 and the soils porosity was set to a range of 0.05 to 0.6 for the auto-calibration process. Final values, shown in Table 14, varied significantly among the model types.

In order to model groundwater interaction with the GSSHA channel network, sub-surface discharge losses/gains were allowed from a defined bed layer thickness of 1.0 m at a rate of $1x10^{-5}$ to 1.0cm hr^{-1} for primary, secondary, and tertiary channels. Calibrated values for these parameters for the 2004, 2018, and 2018WRF model set ups for the 270 and 100m resolutions are included in Section 4.6.4. River flux was the type of boundary condition used to define the sub-surface losses/gains.

Final calibration values for the models are shown in Table 14. In general, some parameters vary significantly from one period to another and from one resolution to another, while others are closer to one another. All parameter values are within "physically" possible values. Variability is due to differences in resolution, rainfall distribution and volume, as well as the result of the solver itself. When using an automated calibration process, such as BeoPest, there are many possible parameter sets that will produce equivalent results, therefore there is no "best" parameter set for any one model.

As part of the calibration output, BeoPEST also computes the relative parameter sensitivity and these results are shown in Table 15. Green colors in the table indicate a low sensitivity and red colors indicate higher sensitivity. From this table, it can be seen that some parameters are equally sensitive irrespective of the calibration period or the model resolution. For example, the sensitivity of the surficial aquifer porosity (gw_poros) is medium to high sensitive in all models considered. Likewise, the canopy resistance for some vegetation types (e.g. canr3) is a low sensitive parameter for most calibration models.

Table 14. Final calibrated parameters for the SW-GW models

Parameter	270m Model			100m Model		
	2004	2018	2018WRF	2004	2018	2018WRF
canr1	200.000	193.008	50.000	200.000	50.000	50.000
canr2	200.000	200.000	200.000	200.000	101.161	150.000
canr3	136.283	141.660	162.893	136.283	50.000	50.000
canr4	107.661	300.000	300.000	107.661	50.000	50.000
ch_rough1	0.025	0.025	0.075	0.025	0.030	0.032
ch_rough2	0.025	0.025	0.025	0.025	0.150	0.150
ch_rough3	0.066	0.025	0.025	0.066	0.150	0.150
gw_lkg_rt	0.02107	0.04649	0.03468	0.02107	0.00001	0.00029
gwhyd	12.684	2.037	15.444	12.684	22.041	2.449
gwkriv1	0.060	0.008	0.000	0.060	1.000	0.359
gwkriv2	0.012	0.217	0.097	0.012	0.010	0.005
gwkriv3	0.018	0.013	0.027	0.018	0.528	0.726
gwporos	0.600	0.050	0.600	0.600	0.181	0.050
hdrc1	0.015	0.015	0.060	0.015	0.150	0.025
hdrc10	0.001	0.001	0.010	0.001	0.001	0.001
hdrc11	0.004	0.001	0.006	0.004	0.025	0.025
hdrc2	0.300	0.050	0.095	0.300	0.050	0.050
hdrc20	0.220	0.220	0.220	0.220	0.220	1.000
hdrc21	0.800	0.204	0.180	0.800	0.180	0.771
hdrc3	1.733	0.330	0.330	1.733	0.330	2.200
hdrc30	0.500	0.050	0.542	0.500	0.066	0.059
hdrc31	0.216	0.383	0.150	0.216	0.150	0.150
hdrc32	2.100	0.350	1.319	2.100	0.350	2.100
hdrc40	1.200	0.707	0.100	1.200	1.000	1.000
hdrc6	0.517	0.700	0.700	0.517	0.700	0.700
hdrc7	3.000	2.852	2.080	3.000	1.498	3.000
prsty1	0.321	0.062	0.070	0.321	0.087	0.076
prsty2	0.500	0.259	0.115	0.500	0.070	0.259
retn1	25.000	3.142	25.000	25.000	25.000	25.000

retn2	1.462	0.374	5.100	1.462	0.634	0.111
retn3	1.000	0.023	1.505	1.000	25.000	25.000
retn4	4.000	25.000	22.989	4.000	14.159	0.783
rov1	0.0100	0.3000	0.0050	0.0100	0.3000	0.2700
rov2	0.3940	1.5000	1.2464	0.3940	0.9691	1.5000
rov3	1.0000	0.8172	0.1403	1.0000	1.0000	1.0000
rov4	0.1768	0.1008	0.5000	0.1768	0.4000	0.4000
rov5	0.1268	0.1000	0.4448	0.1268	0.1000	0.1000
rov6	1.5000	1.0000	0.1100	1.5000	1.0000	1.0000
sgl_uns_sat	0.534	0.900	0.244	0.534	0.196	0.392

Table 15. Parameter sensitivities for all calibrated models. Green is least sensitive and red is most sensitive.

Parameter	270m Model			100m Model		
	2004	2018	2018WRF	2004	2018	2018WRF
canr1	316.237	193.541	0.000	316.237	908.472	0.000
canr2	318.752	152.520	0.000	318.752	72.522	0.000
canr3	89.385	57.616	0.000	89.385	203.935	0.000
canr4	107.071	331.529	0.000	107.071	593.698	0.000
ch_rough1	490.858	260.352	480.706	490.858	678.996	96.601
ch_rough2	437.212	366.005	348.492	437.212	260.474	199.229
ch_rough3	128.001	279.260	1155.270	128.001	1414.980	969.053
gw_lkg_rt	475.879	619.313	1110.580	475.879	206.720	196.899
gwhyd	137.672	89.774	558.766	137.672	2318.720	874.266
gwkriv1	107.410	103.354	196.512	107.410	199.135	80.963
gwkriv2	153.581	185.579	109.213	153.581	390.223	69.345
gwkriv3	96.186	63.150	188.736	96.186	2698.400	3181.350
gwporos	257.866	286.363	1194.790	257.866	694.990	1225.910
hdrc1	802.936	738.641	358.533	802.936	392.173	553.560
hdrc10	120.642	282.140	1154.900	120.642	387.104	1089.370
hdrc11	310.098	149.089	396.957	310.098	214.370	249.240
hdrc2	468.331	219.681	229.660	468.331	831.331	95.274
hdrc20	571.680	176.611	1368.820	571.680	186.870	129.425
hdrc21	385.354	48.418	1233.420	385.354	327.307	47.470
hdrc3	175.708	401.632	1189.120	175.708	224.353	291.797
hdrc30	339.320	34.615	155.829	339.320	166.668	63.533
hdrc31	151.479	56.202	478.284	151.479	288.626	203.935
hdrc32	510.553	228.330	204.099	510.553	159.584	134.298
hdrc40	305.769	52.678	505.150	305.769	202.885	167.957
hdrc6	219.481	206.999	1660.490	219.481	134.089	169.311
hdrc7	516.195	108.834	161.461	516.195	229.633	216.568
prsty1	236.532	872.518	1323.050	236.532	18682.100	911.988
prsty2	652.007	91.667	263.105	652.007	48.227	73.706
retn1	551.208	142.045	908.965	551.208	85.282	926.406
retn2	121.850	70.630	135.830	121.850	242.168	21.631

retn3	433.442	41.540	117.168	433.442	174.452	251.425
retn4	385.455	223.356	959.479	385.455	158.847	99.849
rov1	349.041	266.568	820.800	349.041	149.543	22.304
rov2	131.827	190.142	82.315	131.827	156.496	142.559
rov3	372.888	159.845	229.814	372.888	374.412	365.758
rov4	98.462	72.756	431.657	98.462	110.893	34.565
rov5	80.616	162.227	155.429	80.616	67.267	112.297
rov6	533.286	144.992	558.803	533.286	91.224	91.961
sgl_uns_sat	103.954	1359.450	143.130	103.954	783.204	725.625

4.6.3.3 SW/GW Calibration Results

Daily flow hydrographs for the 2004 270m models with gauge forcing data for the USGS stations at Hopland, Ukiah, and Calpella are shown in Figure 26. These plots show that the model reasonably matches the observed flow values for this period of record. The events occurring in the period from 01Dec2004 to about December 2004 are comparatively matched closer than those occurring at later dates in the same period of calibration. This can be seen in the three gauging stations used in this period.

Table 18 and Table 19 show the event based volumes and peaks, respectively, for the same stations. From these tables, it can be seen that event nos. 1 through 8, and 16 through 19, are reasonably well matched in this period, both, from a volume and peak flow perspective. Events 9, 10, 12, 13, and 15, are all under predicted in this period. One possible reason is that the magnitude and geospatial pattern (including of weights and hydro-meteorology/runoff) of the former are much larger and different, geospatially, from the other events and could bias the calculation of the objective function within the PEST process towards matching those higher events.

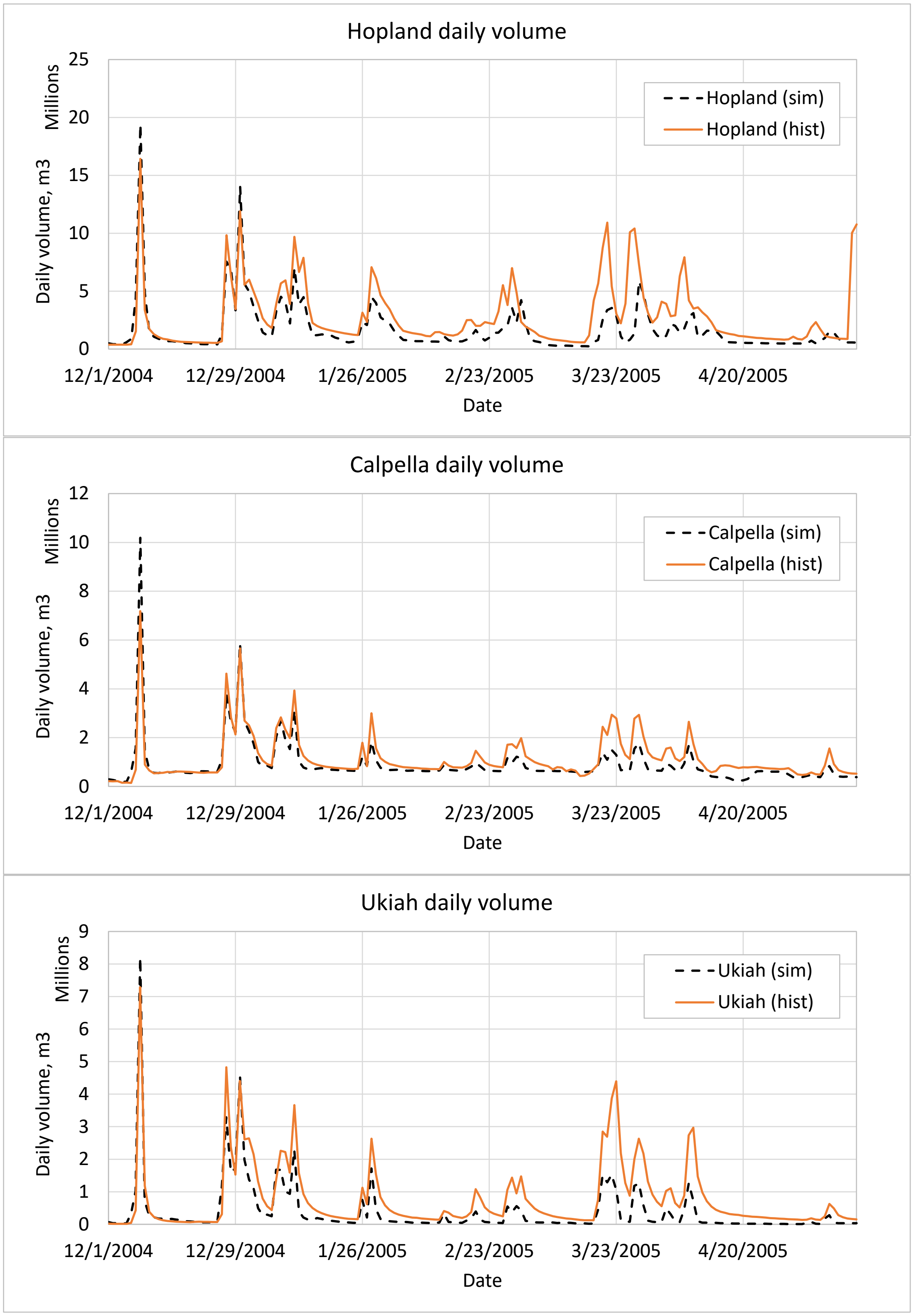

Figure 26. Daily flow hydrographs for the USGS stations for the 270m resolution, 2004 calibration period with gauge forcing data.

Table 16. Simulated and observed event volumes for the USGS stations for the 270m 2004 calibration model with gauge forcing data.

			Hopland	Ukiah	Calpella
Event #	**Start Date/Time**	**End Date/Time**	**Simulated Event Volumes, 10^6 m^3**		
1	12/4/2004 5:45	12/17/2004 18:00	37.05	11.71	18.76
2	12/17/2004 17:45	12/20/2004 15:00	1.46	0.27	1.62
3	12/20/2004 15:00	12/24/2004 9:00	1.60	0.23	2.32
4	12/25/2004 0:45	1/24/2005 12:00	95.12	27.61	46.72
5	1/24/2005 11:45	1/31/2005 10:00	17.95	3.43	6.98
6	1/31/2005 9:45	2/5/2005 20:00	7.77	0.45	3.67
7	2/5/2005 19:30	2/9/2005 14:00	2.58	0.19	2.43
8	2/9/2005 13:45	2/11/2005 13:00	1.28	0.08	1.24
9	2/11/2005 13:00	2/23/2005 14:00	10.62	1.58	8.83
10	2/23/2005 13:15	3/5/2005 23:00	21.10	2.32	8.78
11	3/5/2005 23:00	3/9/2005 11:00	1.63	0.21	2.24
12	3/16/2005 15:00	3/26/2005 9:00	15.87	6.14	9.19
13	3/26/2005 8:30	3/31/2005 15:00	16.80	3.24	6.02
14	3/31/2005 15:00	4/2/2005 7:00	1.96	0.11	1.10
15	4/2/2005 6:45	4/16/2005 14:00	23.55	3.81	10.54
16	4/16/2005 13:45	4/21/2005 11:00	2.75	0.12	1.37
17	4/21/2005 10:45	5/3/2005 12:00	5.99	0.16	6.39
18	5/3/2005 11:45	5/14/2005 14:00	8.93	0.79	5.36
19	5/14/2005 13:45	5/15/2005 23:45	0.81	0.05	0.55
Event #	**Start Date/Time**	**End Date/Time**	**Observed Event Volumes, 10^6 m^3**		
1	12/4/2004 5:45	12/17/2004 18:00	30.03	10.22	13.75
2	12/17/2004 17:45	12/20/2004 15:00	1.74	0.20	1.73
3	12/20/2004 15:00	12/24/2004 9:00	2.10	0.29	2.14
4	12/25/2004 0:45	1/24/2005 12:00	123.02	41.00	53.17
5	1/24/2005 11:45	1/31/2005 10:00	26.92	7.27	9.88
6	1/31/2005 9:45	2/5/2005 20:00	13.21	1.88	4.66
7	2/5/2005 19:30	2/9/2005 14:00	4.96	0.73	2.84
8	2/9/2005 13:45	2/11/2005 13:00	2.32	0.31	1.42
9	2/11/2005 13:00	2/23/2005 14:00	19.18	4.95	11.23
10	2/23/2005 13:15	3/5/2005 23:00	36.38	7.82	13.15
11	3/5/2005 23:00	3/9/2005 11:00	4.90	1.16	2.99
12	3/16/2005 15:00	3/26/2005 9:00	41.43	18.68	16.11
13	3/26/2005 8:30	3/31/2005 15:00	36.17	9.27	10.67
14	3/31/2005 15:00	4/2/2005 7:00	5.24	1.18	1.88
15	4/2/2005 6:45	4/16/2005 14:00	52.94	15.03	16.99
16	4/16/2005 13:45	4/21/2005 11:00	6.68	1.43	3.92
17	4/21/2005 10:45	5/3/2005 12:00	12.07	2.26	8.53
18	5/3/2005 11:45	5/14/2005 14:00	13.79	2.82	7.79
19	5/14/2005 13:45	5/15/2005 23:45	1.31	0.22	0.75

Table 17. Simulated and observed event peak flow rates for the USGS stations for the 270m 2004 calibration model with gauge forcing data.

			Hopland	Ukiah	Calpella
Event #	Start Date/Time	End Date/Time	Simulated Event Peaks, m³/s		
1	12/4/2004 5:45	12/17/2004 18:00	351.62	203.24	231.14
2	12/17/2004 17:45	12/20/2004 15:00	6.91	1.57	6.77
3	12/20/2004 15:00	12/24/2004 9:00	5.51	0.98	7.26
4	12/25/2004 0:45	1/24/2005 12:00	257.36	116.58	119.57
5	1/24/2005 11:45	1/31/2005 10:00	67.65	35.86	32.69
6	1/31/2005 9:45	2/5/2005 20:00	28.74	1.50	8.43
7	2/5/2005 19:30	2/9/2005 14:00	8.51	1.00	7.93
8	2/9/2005 13:45	2/11/2005 13:00	7.69	0.55	7.28
9	2/11/2005 13:00	2/23/2005 14:00	25.44	8.84	14.34
10	2/23/2005 13:15	3/5/2005 23:00	74.38	37.78	42.02
11	3/5/2005 23:00	3/9/2005 11:00	7.38	0.81	7.50
12	3/16/2005 15:00	3/26/2005 9:00	71.02	50.08	32.68
13	3/26/2005 8:30	3/31/2005 15:00	94.90	62.04	55.56
14	3/31/2005 15:00	4/2/2005 7:00	17.77	0.95	7.73
15	4/2/2005 6:45	4/16/2005 14:00	59.28	33.05	44.39
16	4/16/2005 13:45	4/21/2005 11:00	7.19	0.43	7.11
17	4/21/2005 10:45	5/3/2005 12:00	6.28	0.43	7.67
18	5/3/2005 11:45	5/14/2005 14:00	24.84	10.37	18.36
19	5/14/2005 13:45	5/15/2005 23:45	6.68	0.59	4.55
Event #	Start Date/Time	End Date/Time	Observed Event Peaks, m3/s		
1	12/4/2004 5:45	12/17/2004 18:00	348.30	190.29	187.74
2	12/17/2004 17:45	12/20/2004 15:00	7.25	0.99	7.05
3	12/20/2004 15:00	12/24/2004 9:00	6.82	0.99	6.88
4	12/25/2004 0:45	1/24/2005 12:00	214.36	82.97	132.24
5	1/24/2005 11:45	1/31/2005 10:00	112.70	49.55	52.95
6	1/31/2005 9:45	2/5/2005 20:00	46.72	6.88	11.81
7	2/5/2005 19:30	2/9/2005 14:00	16.71	2.61	9.03
8	2/9/2005 13:45	2/11/2005 13:00	14.03	1.93	9.32
9	2/11/2005 13:00	2/23/2005 14:00	33.70	15.97	18.58
10	2/23/2005 13:15	3/5/2005 23:00	114.40	47.86	54.93
11	3/5/2005 23:00	3/9/2005 11:00	21.12	5.13	11.04
12	3/16/2005 15:00	3/26/2005 9:00	163.95	68.24	63.43
13	3/26/2005 8:30	3/31/2005 15:00	183.78	83.82	112.42
14	3/31/2005 15:00	4/2/2005 7:00	46.44	10.28	14.10
15	4/2/2005 6:45	4/16/2005 14:00	131.96	68.81	58.62
16	4/16/2005 13:45	4/21/2005 11:00	18.75	4.11	10.22
17	4/21/2005 10:45	5/3/2005 12:00	14.78	2.94	9.49
18	5/3/2005 11:45	5/14/2005 14:00	33.41	13.45	30.02
19	5/14/2005 13:45	5/15/2005 23:45	11.30	1.87	6.14

Flow hydrographs for the 2018 270m models with precipitation gauge data that included the additional CW3E stations forcing for the USGS stations at Hopland, Ukiah, and Calpella, and Talmage are shown in Figure 27. These plots show that the model does a good job of matching the observed flow values for this period of record at the USGS stations. The match at flow gauging stations located in secondary and tertiary tributaries (i.e., other CW3E stations) are not matched that well. These figures are included in Appendix A. However, a lower weight was assigned to these stations in the calibration weighting scheme because these are located in smaller streams in the watershed.

Table 18 and Table 19 show the event based volumes and peaks, respectively, for the USGS gauging stations in the 2018 calibration period with gauge forcing data. In general, event volumes and peaks at these stations located in the main channel of the river are all better predicted than stations located in secondary and tertiary tributaries. There are some stations in smaller creeks where the event discharge volume and peaks matched reasonably well with the historical observations (Appendix A). This is the case of stations WHT, MLL, and BYS.

Daily flow hydrographs for the 2018 calibration period with West-WRF forcing data are shown in Figure 28. In general, the calibration with this data set shows an improved match between the historical and simulated daily flows for the USGS and the CW3E stations than the calibration for the 2004 and the 2018 periods with gauge forcing data, perhaps attributable to more realistic hydro-meteorological patterns afforded by the WRF model. A similar observation can be made by inspecting the event based volumes (Table 20) and the event peak flow rate discharge (Table 21). USGS gauging stations Ukiah, Hopland, Calpella, and Talmage all showed a very close agreement between the observed and simulated outcomes during this period.

Similar outcomes that those for the 270m resolution models for the three calibration scenarios and their associated forcing data were obtained when the model resolution was increase to a cell size of 100m by 100m. Figure 29 shows the comparison of daily flow hydrographs for the 100m resolution models for the 2004 calibration period at the USGS stations with gauge forcing data. As stated elsewhere, the matching period of record for this model was limited to the events occurring between 01Dec2004 and 25Dec2005 due excessively long model run times.

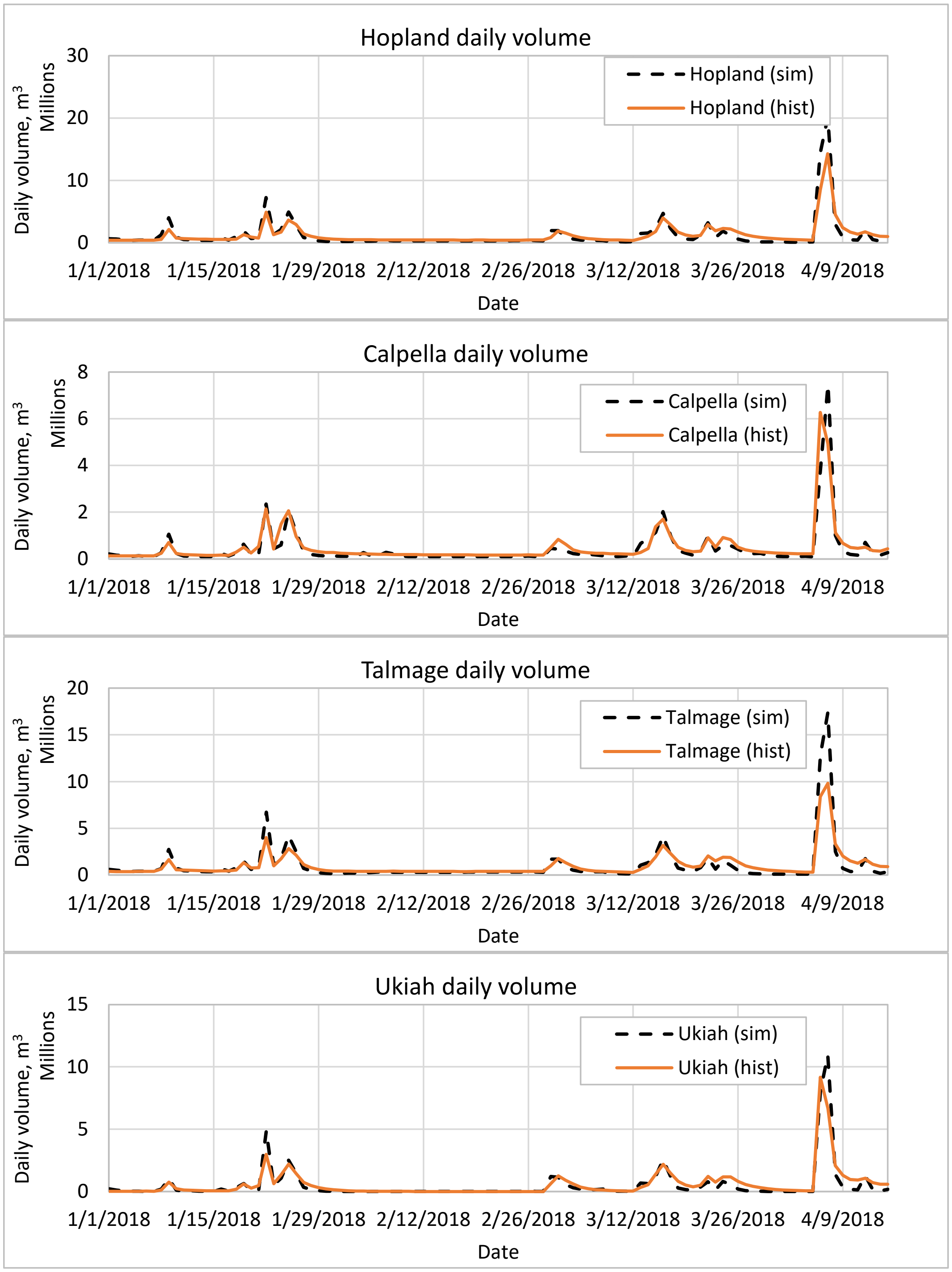

Figure 27. Daily flow hydrographs for the USGS stations for the 270m resolution, 2018 calibration period with gauge forcing data.

Table 18. Simulated and observed event volumes for the USGS stations for the 270m 2018 calibration model with gauge forcing data.

			Hopland	Talmage	Ukiah	Calpella
Event #	**Start Date/Time**	**End Date/Time**	**Simulated Event Volumes, 10^6 m^3**			
1	1/3/2018 13:00	2/5/2018 18:00	37.22	31.87	14.02	12.38
2	2/6/2018 19:30	2/9/2018 19:00	1.01	0.98	0.03	0.64
3	2/11/2018 15:00	2/12/2018 10:00	0.24	0.24	0.01	0.08
4	2/13/2018 18:45	2/13/2018 19:00	0.01	0.01	0.00	0.00
5	2/18/2018 3:00	2/20/2018 10:00	0.73	0.73	0.02	0.23
6	2/21/2018 17:00	3/30/2018 3:00	34.00	28.56	13.79	13.71
7	3/31/2018 14:00	3/31/2018 15:00	0.01	0.01	0.00	0.01
8	4/2/2018 10:00	4/2/2018 20:00	0.05	0.04	0.00	0.04
9	4/3/2018 23:30	4/8/2018 23:45	42.87	37.08	22.65	14.49
Event #	**Start Date/Time**	**End Date/Time**	**Observed Event Volumes, 10^6 m^3**			
1	1/3/2018 13:00	2/5/2018 18:00	34.15	28.50	13.96	14.34
2	2/6/2018 19:30	2/9/2018 19:00	1.38	1.22	0.02	0.57
3	2/11/2018 15:00	2/12/2018 10:00	0.37	0.33	0.00	0.15
4	2/13/2018 18:45	2/13/2018 19:00	0.01	0.01	0.00	0.00
5	2/18/2018 3:00	2/20/2018 10:00	0.99	0.91	0.00	0.39
6	2/21/2018 17:00	3/30/2018 3:00	42.64	35.69	18.98	16.44
7	3/31/2018 14:00	3/31/2018 15:00	0.03	0.02	0.01	0.01
8	4/2/2018 10:00	4/2/2018 20:00	0.22	0.16	0.04	0.10
9	4/3/2018 23:30	4/8/2018 23:45	28.16	22.21	18.02	12.76

Table 19. Simulated and observed event peak discharge for the USGS stations for the 270m 2018 calibration model with gauge forcing data.

			Hopland	Talmage	Ukiah	Calpella
Event #	**Start Date/Time**	**End Date/Time**	**Simulated Event Peaks, m3/s**			
1	1/3/2018 13:00	2/5/2018 18:00	152.31	148.82	123.24	50.10
2	2/6/2018 19:30	2/9/2018 19:00	4.90	4.85	0.27	6.11
3	2/11/2018 15:00	2/12/2018 10:00	3.74	3.77	0.28	1.18
4	2/13/2018 18:45	2/13/2018 19:00	3.86	3.61	0.09	1.14
5	2/18/2018 3:00	2/20/2018 10:00	3.88	3.91	0.25	1.16
6	2/21/2018 17:00	3/30/2018 3:00	77.91	73.32	53.49	36.81
7	3/31/2018 14:00	3/31/2018 15:00	1.51	1.26	0.19	1.26
8	4/2/2018 10:00	4/2/2018 20:00	1.36	1.18	0.03	1.21
9	4/3/2018 23:30	4/8/2018 23:45	412.96	384.19	275.93	148.19
Event #	**Start Date/Time**	**End Date/Time**	**Observed Event Peaks, m3/s**			
1	1/3/2018 13:00	2/5/2018 18:00	109.87	94.30	85.80	69.09
2	2/6/2018 19:30	2/9/2018 19:00	5.49	4.90	0.15	2.32
3	2/11/2018 15:00	2/12/2018 10:00	5.38	4.79	0.04	2.14
4	2/13/2018 18:45	2/13/2018 19:00	5.15	4.62	0.02	2.08
5	2/18/2018 3:00	2/20/2018 10:00	5.10	4.90	0.07	2.03
6	2/21/2018 17:00	3/30/2018 3:00	52.10	45.31	33.41	32.85
7	3/31/2018 14:00	3/31/2018 15:00	7.45	5.47	1.96	2.89
8	4/2/2018 10:00	4/2/2018 20:00	6.23	4.56	1.12	2.76
9	4/3/2018 23:30	4/8/2018 23:45	259.38	213.23	227.38	156.88

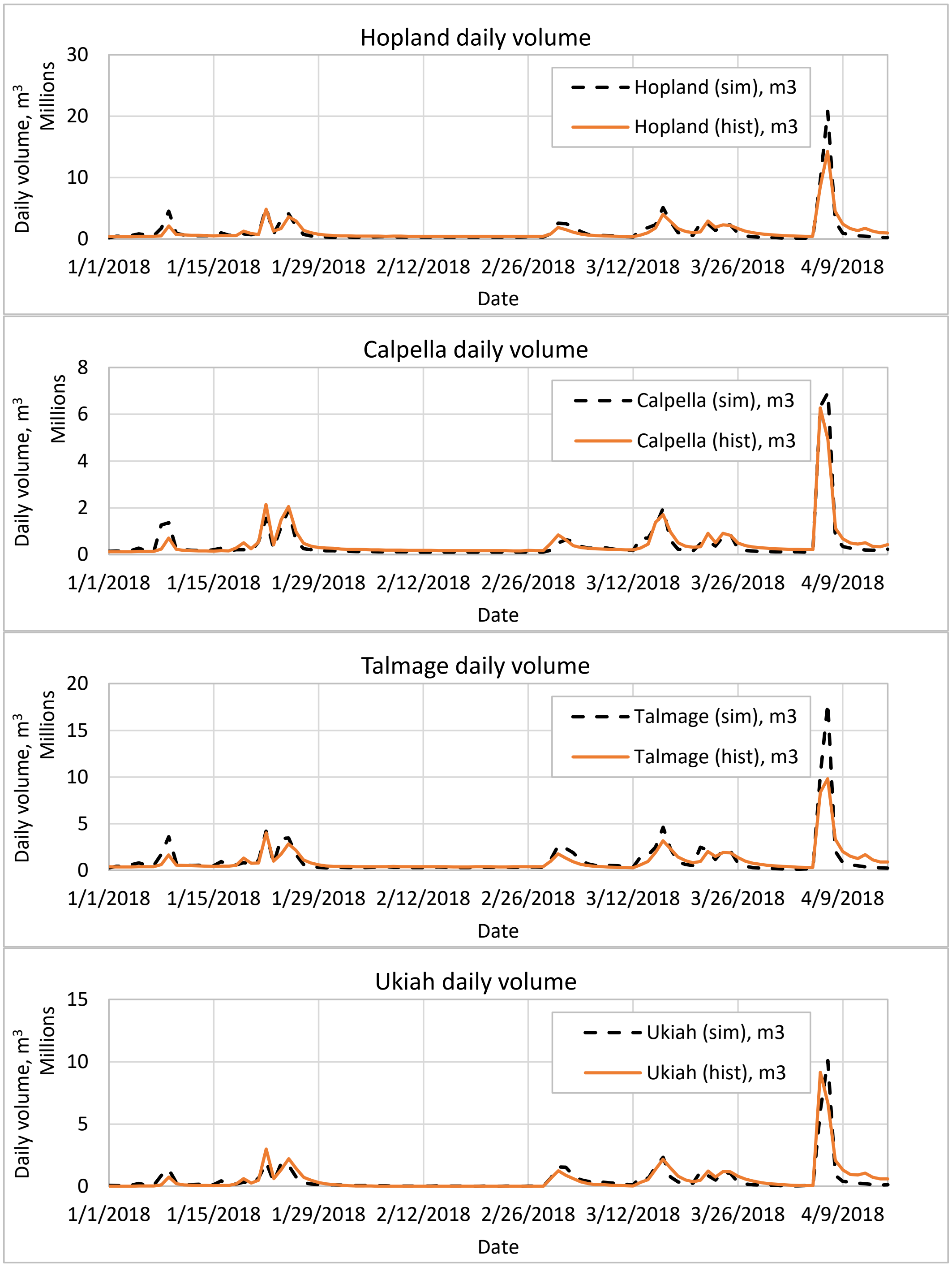

Figure 28. Daily flow hydrographs for the USGS and CW3E stations for the 270m resolution, 2018 calibration period with West-WRF forcing data.

Table 20. Simulated and observed event volumes for the USGS stations for the 270m 2018 calibration model with West-WRF forcing data.

			Hopland	Talmage	Ukiah	Calpella
Event #	Start Date/Time	End Date/Time	Simulated Event Volumes, 10^6 m^3			
1	1/3/2018 13:00	2/5/2018 18:00	36.61	33.15	13.52	13.30
2	2/6/2018 19:30	2/9/2018 19:00	1.12	1.08	0.08	0.36
3	2/11/2018 15:00	2/12/2018 10:00	0.26	0.25	0.01	0.09
4	2/13/2018 18:45	2/13/2018 19:00	0.01	0.01	0.00	0.00
5	2/18/2018 3:00	2/20/2018 10:00	0.76	0.76	0.02	0.25
6	2/21/2018 17:00	3/30/2018 3:00	44.67	41.68	19.43	14.26
7	3/31/2018 14:00	3/31/2018 15:00	0.01	0.01	0.00	0.01
8	4/2/2018 10:00	4/2/2018 20:00	0.07	0.07	0.02	0.05
9	4/3/2018 23:30	4/8/2018 23:45	36.74	33.56	18.79	15.91
Event #	Start Date/Time	End Date/Time	Observed Event Volumes, 10^6 m^3			
1	1/3/2018 13:00	2/5/2018 18:00	34.15	28.50	13.96	14.34
2	2/6/2018 19:30	2/9/2018 19:00	1.38	1.22	0.02	0.57
3	2/11/2018 15:00	2/12/2018 10:00	0.37	0.33	0.00	0.15
4	2/13/2018 18:45	2/13/2018 19:00	0.01	0.01	0.00	0.00
5	2/18/2018 3:00	2/20/2018 10:00	0.99	0.91	0.00	0.39
6	2/21/2018 17:00	3/30/2018 3:00	42.64	35.69	18.98	16.44
7	3/31/2018 14:00	3/31/2018 15:00	0.03	0.02	0.01	0.01
8	4/2/2018 10:00	4/2/2018 20:00	0.22	0.16	0.04	0.10
9	4/3/2018 23:30	4/8/2018 23:45	28.16	22.21	18.02	12.76

Table 21. Simulated and observed event peak discharge for the USGS stations for the 270m 2018 calibration model with West-WRF forcing data.

			Hopland	Talmage	Ukiah	Calpella
Event #	Start Date/Time	End Date/Time	Simulated Event peaks, m³/s			
1	1/3/2018 13:00	2/5/2018 18:00	103.62	94.31	55.42	47.71
2	2/6/2018 19:30	2/9/2018 19:00	5.29	5.26	0.47	1.44
3	2/11/2018 15:00	2/12/2018 10:00	3.70	3.66	0.20	1.32
4	2/13/2018 18:45	2/13/2018 19:00	3.71	3.68	0.68	1.28
5	2/18/2018 3:00	2/20/2018 10:00	4.29	4.32	0.09	1.25
6	2/21/2018 17:00	3/30/2018 3:00	67.97	64.67	38.20	32.28
7	3/31/2018 14:00	3/31/2018 15:00	2.55	2.37	0.94	1.43
8	4/2/2018 10:00	4/2/2018 20:00	1.82	2.18	0.48	1.36
9	4/3/2018 23:30	4/8/2018 23:45	342.92	319.05	181.50	170.12
Event #	Start Date/Time	End Date/Time	Observed event peaks, m³/s			
1	1/3/2018 13:00	2/5/2018 18:00	109.87	94.30	85.80	69.09
2	2/6/2018 19:30	2/9/2018 19:00	5.49	4.90	0.15	2.32
3	2/11/2018 15:00	2/12/2018 10:00	5.38	4.79	0.04	2.14
4	2/13/2018 18:45	2/13/2018 19:00	5.15	4.62	0.02	2.08
5	2/18/2018 3:00	2/20/2018 10:00	5.10	4.90	0.07	2.03
6	2/21/2018 17:00	3/30/2018 3:00	52.10	45.31	33.41	32.85
7	3/31/2018 14:00	3/31/2018 15:00	7.45	5.47	1.96	2.89
8	4/2/2018 10:00	4/2/2018 20:00	6.23	4.56	1.12	2.76
9	4/3/2018 23:30	4/8/2018 23:45	259.38	213.23	227.38	156.88

The daily flow hydrographs in this figure (Figure 29) show that the model does a good job of matching observed daily flows for the sub-set of the calibration period used at this resolution.

Likewise, Table 22 and Table 23 show the event based volumes and peaks, respectively, for the USGS stations at 100m resolution for the 2004 calibration period with gauge forcing data. It can be seen that event in the beginning of the period was very well matched with the historical period of record.

Flow hydrographs for the 2018 100m models with gauge forcing data for the USGS stations at Hopland, Ukiah, and Calpella are shown in Figure 30. The calibration effort for this model resolution was focused on the events occurring between 27Feb2018 and 20Mar2018 for model run time purposes. These plots show that the model did not reasonably match the observed flow values for this sub-period at the USGS stations. Other stations in secondary and tertiary tributaries did not match very well the historical flow observations either. Lower weights were assigned to these stations in the calibration weighting scheme because these are located in smaller streams in the watershed. Possible reasons for the poor matches include limited simulation period and a limited number of BeoPest simulations due to computational burden and time constraints.

Table 24 and Table 25 show the event based volumes and peaks, respectively, for the USGS gauging stations in the 100m resolution model for the 2018 calibration period with gauge forcing data. In general, these three events are matched reasonably in this period. Similarly, the peak discharge flow rates for these events are all reasonably matched.

Similar to the outcomes obtained with the 270m 2018 calibration with WRF gauging data, the daily flow hydrographs for the 100m resolution model showed an improved match between historical and simulated daily flows for the USGS stations (Figure 31). The same can be stated about the event volumes and peaks by inspecting Table 26 and Table 27.

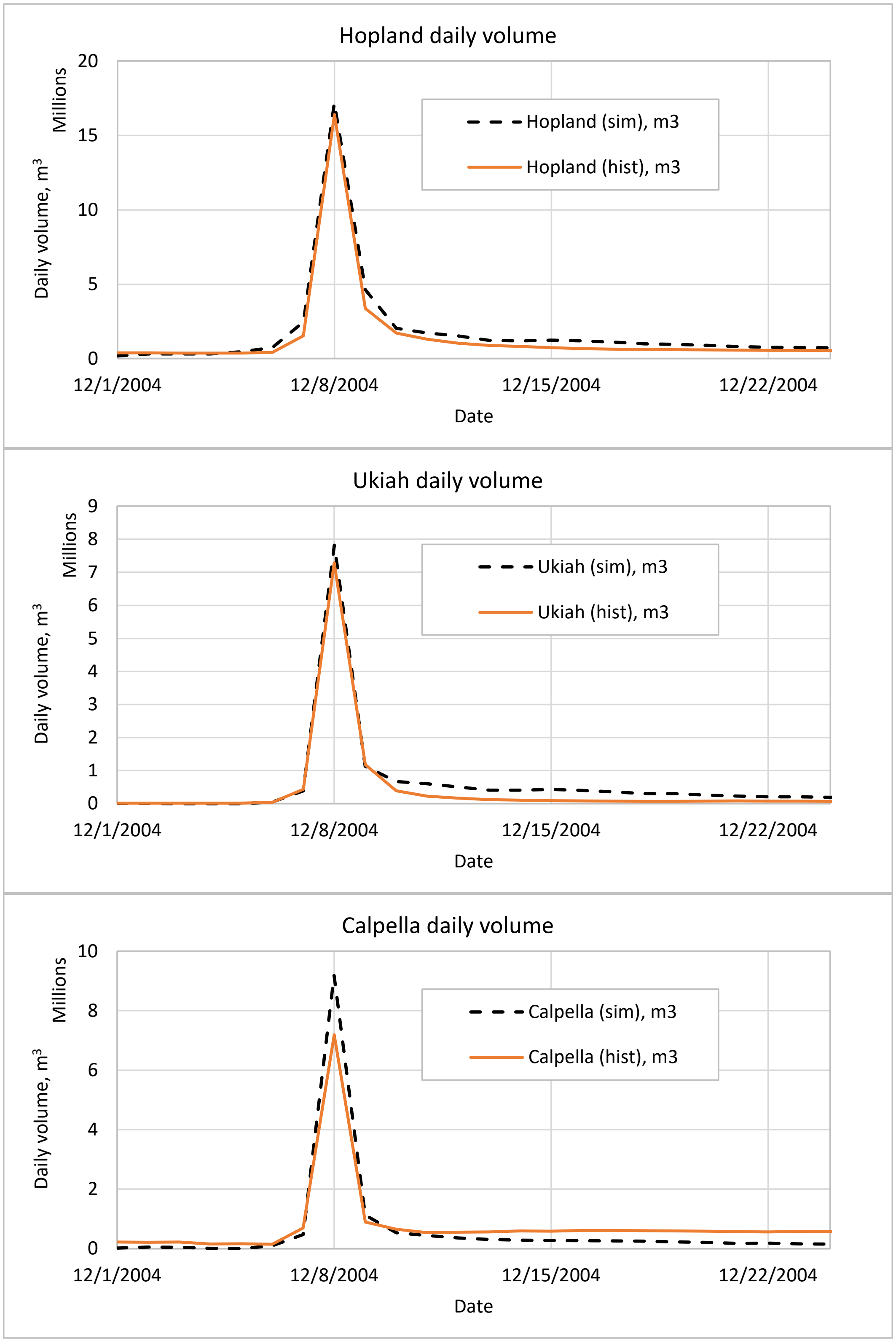

Figure 29. Daily stage hydrographs for the USGS stations for the 100m resolution, 2004 calibration period.

Table 22. Simulated and observed event volume for the 100m 2004 calibration model with gauge forcing data.

			Hopland	Ukiah	Calpella
Event #	Start Date/Time	End Date/Time	Simulated Event Volume, 10^6 m^3		
1	12/4/2004 5:45	12/17/2004 18:00	36.66	13.09	13.55
Event #	Start Date/Time	End Date/Time	Historical Event Volume, 10^6 m^3		
1	12/4/2004 5:45	12/17/2004 18:00	30.03	10.22	13.75

Table 23. Simulated and observed event peak discharge for the 100m 2004 calibration model with gauge forcing data.

			Hopland	Ukiah	Calpella
Event #	Start Date/Time	End Date/Time	Simulated Events Peak flows, m3/s		
1	12/4/2004 5:45	12/17/2004 18:00	346.43	139.36	212.05
Event #	Start Date/Time	End Date/Time	Historical Event Peak flow rate		
1	12/4/2004 5:45	12/17/2004 18:00	348.30	190.29	187.74

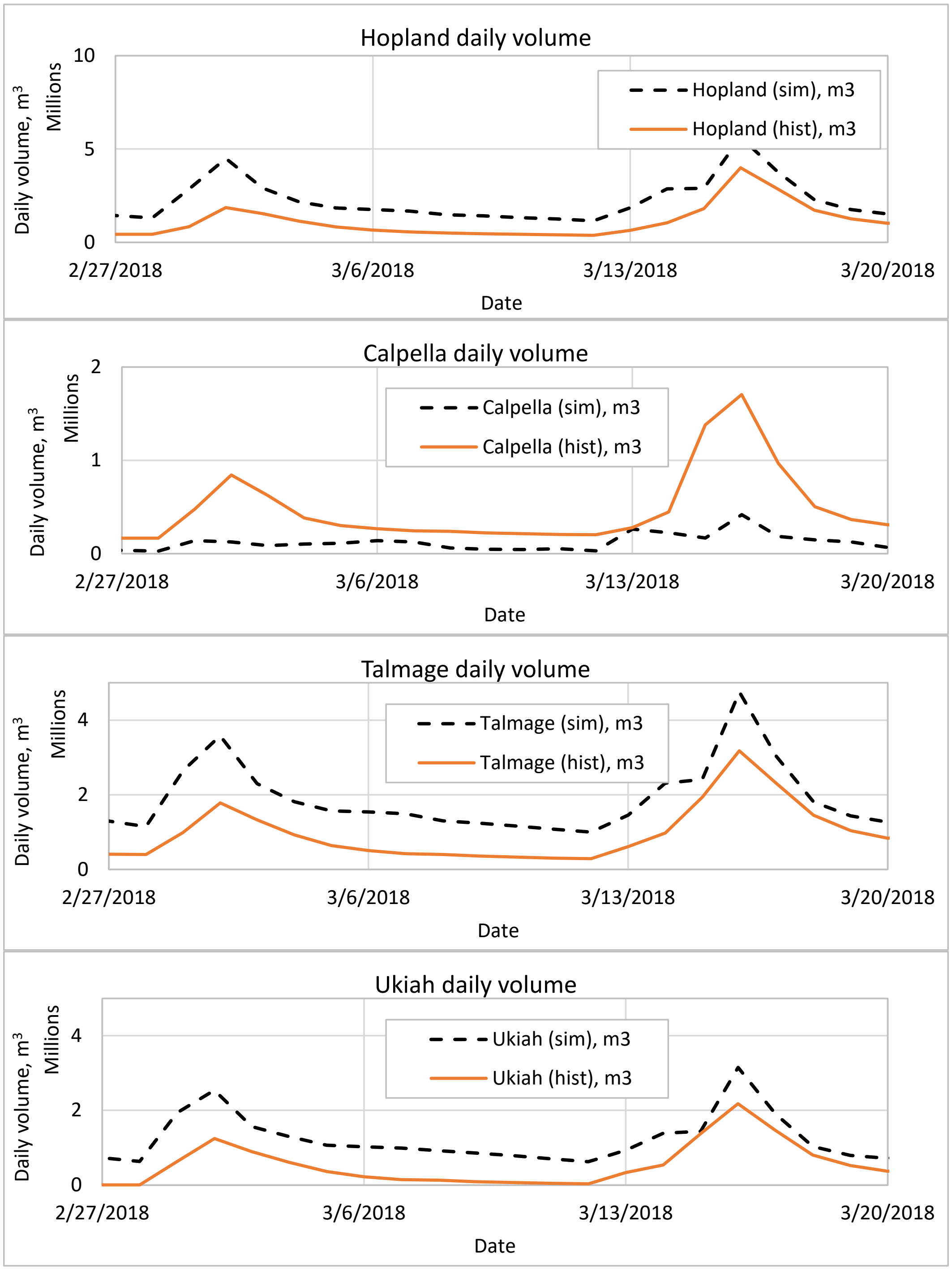

Figure 30. Daily flow hydrographs for the USGS stations for the 100m resolution, 2018 calibration period with gauge forcing data.

Table 24. Simulated and observed event volume for the 100m 2018 calibration model with gauge forcing data.

Event #	Start Date/Time	End Date/Time	Hopland	Talmage	Ukiah	Calpella
			Simulated Events Volumes, 10^6 m^3			
1	2/18/2018 3:00	2/20/2018 10:00	3.00	2.67	1.40	0.07
2	2/21/2018 17:00	3/30/2018 3:00	75.39	62.14	38.78	4.13
3	3/31/2018 14:00	3/31/2018 15:00	0.06	0.05	0.03	0.00
Event #	Start Date/Time	End Date/Time	Historical Events Volumes, 10^6 m^3			
1	2/18/2018 3:00	2/20/2018 10:00	0.99	0.91	0.00	0.39
2	2/21/2018 17:00	3/30/2018 3:00	42.64	35.69	18.98	16.44
3	3/31/2018 14:00	3/31/2018 15:00	0.03	0.02	0.01	0.01

Table 25. Simulated and observed event peak discharge for the 100m 2018 calibration model with gauge forcing data.

Event #	Start Date/Time	End Date/Time	Hopland	Talmage	Ukiah	Calpella
			Simulated Event Peak Flow, m^3/s			
1	2/18/2018 3:00	2/20/2018 10:00	16.49	15.18	8.37	0.56
2	2/21/2018 17:00	3/30/2018 3:00	75.47	67.00	44.61	9.89
3	3/31/2018 14:00	3/31/2018 15:00	12.79	11.08	7.05	0.58
Event #	Start Date/Time	End Date/Time	Observed Event Peak Flow, m^3/s			
1	2/18/2018 3:00	2/20/2018 10:00	5.10	4.90	0.07	2.03
2	2/21/2018 17:00	3/30/2018 3:00	52.10	45.31	33.41	32.85
3	3/31/2018 14:00	3/31/2018 15:00	7.45	5.47	1.96	2.89

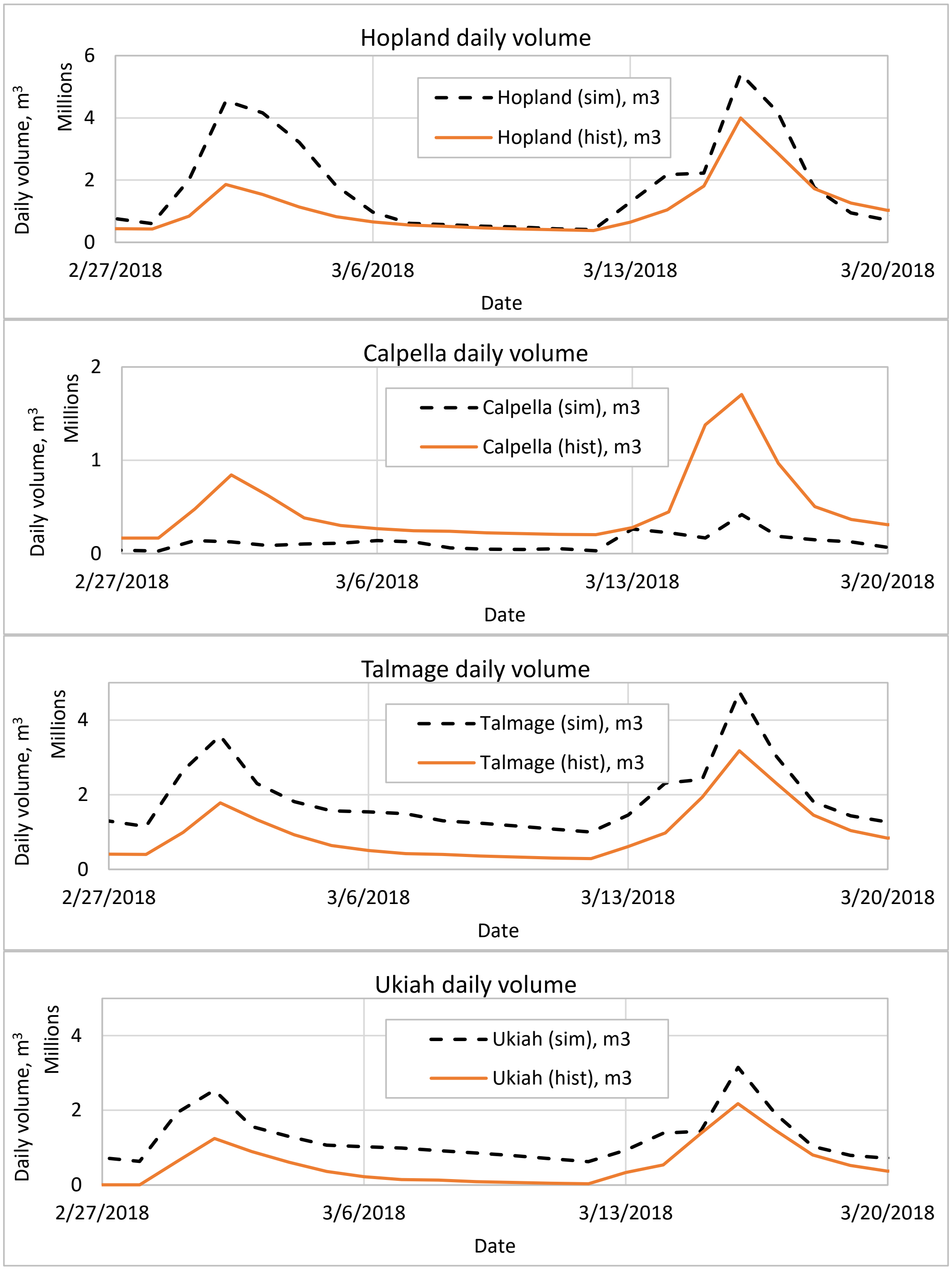

Figure 31. Daily flow hydrographs for the USGS and CW3E stations for the 100m resolution, 2018 calibration period with WRF data

Table 26. Simulated and observed event volumes for the 100m 2018 calibration model with West-WRF forcing data.

			Hopland	Talmage	Ukiah	Calpella
Event #	**Start Date/Time**	**End Date/Time**	**Simulated Event Volumes, 10^6 m^3**			
1	2/18/2018 3:00	2/20/2018 10:00	1.20	1.13	0.25	0.47
2	2/21/2018 17:00	3/30/2018 3:00	58.86	46.95	25.49	19.68
3	3/31/2018 14:00	3/31/2018 15:00	0.02	0.02	0.01	0.02
Event #	**Start Date/Time**	**End Date/Time**	**Simulated Event Peak Volumes, 10^6 m^3**			
1	2/18/2018 3:00	2/20/2018 10:00	0.99	0.91	0.00	0.39
2	2/21/2018 17:00	3/30/2018 3:00	42.64	35.69	18.98	16.44
3	3/31/2018 14:00	3/31/2018 15:00	0.03	0.02	0.01	0.01

Table 27. Simulated and observed event peak discharge for the 100m 2018 calibration model with West-WRF forcing data.

			Hopland	Talmage	Ukiah	Calpella
Event #	**Start Date/Time**	**End Date/Time**	**Simulated Event Peak Flow, m^3/s**			
1	2/18/2018 3:00	2/20/2018 10:00	6.56	6.10	1.37	3.23
2	2/21/2018 17:00	3/30/2018 3:00	70.34	56.93	38.46	18.46
3	3/31/2018 14:00	3/31/2018 15:00	4.42	3.82	1.66	3.50
Event #	**Start Date/Time**	**End Date/Time**	**Simulated Event Peak Flow, m^3/s**			
1	2/18/2018 3:00	2/20/2018 10:00	5.10	4.90	0.07	2.03
2	2/21/2018 17:00	3/30/2018 3:00	52.10	45.31	33.41	32.85
3	3/31/2018 14:00	3/31/2018 15:00	7.45	5.47	1.96	2.89

Table 28, Table 29, and Table 30 include the goodness of fit metrics for all the calibration scenarios at all gauging stations for daily flows, event based volumes, and event based peaks, respectively.

Efficiencies calculated at the USGS gauging stations near Hopland for the daily flow volumes ranged from -0.957 (100m-2018 w/gauge) to 0.978 (100m-2004 w/gauge). In general, the metrics obtained at this station showed that these models, with the exception of the 100m-2018 w/gauge and 100m-2018 w/WRF, are all good predictors of the observed outcomes from a daily flow perspective.

For the event based volumes (Table 29), the NSE obtained at this station were all higher than 0.6, with the exception of the 100m-2018 w/WRF data (0.091), suggesting that these models are reasonable predictors of the event based volumes observed at this location. The same can be said about the event based peaks (Table 30) where all NSE values at this location are greater than 0.490.

Similarly, efficiencies at the Calpella gauging station ranged from -0.522 (100m-2018 w/gauge) to 0.879 (270m-2018 w/ West-WRF). The metrics at this station showed that these models are good predictors of the observed outcomes from a daily flow perspective, with the exception of the 100m-2018 w/gauge model. NSE obtained at this station for the event based volumes were all higher than 0.9, with the exception of the 100m-2018 w/gauge data (0.138), suggesting that these models are also reasonable predictors of this type of events at this location. The same can be said about the event based peaks (Table 30) where all NSE values at this location are greater than 0.600, with the exception of the 100m 2018 w/gauge forcing data. Statistics for all other stations are provided in these tables.

Table 28. Calibration statistics for the daily flows at the stations for all calibration scenarios.

		270m Models			100m Models		
Station	**Statistic**	**2004**	**2018 w/gauge**	**2018 w/WRF**	**2004 Period**	**2018 w/gauge**	**2018 w/WRF**
Hopland	NSE	0.664	0.664	0.748	0.978	-0.957	-0.565
	R^2	0.925	0.925	0.908	0.993	0.821	0.740
	MAE, 10^6 m^3	0.519	0.519	0.455	0.379	1.131	0.739
	RMSE, 10^6 m^3	0.997	0.997	0.864	0.468	1.235	1.105
Ukiah	NSE	0.609	0.790	0.779	0.974	-0.733	0.167
	R^2	0.747	0.869	0.796	0.991	0.788	0.734
	MAE, 10^6 m^3	0.437	0.241	0.269	0.184	0.681	0.357
	RMSE, 10^6 m^3	0.665	0.542	0.556	0.233	0.741	0.514
Calpella	NSE	0.729	0.772	0.879	0.867	-0.522	0.560
	R^2	0.818	0.809	0.921	0.992	0.523	0.650
	MAE, 10^6 m^3	0.315	0.172	0.158	0.334	0.354	0.202
	RMSE, 10^6 m^3	0.483	0.387	0.282	0.493	0.489	0.263
Talmage	NSE	--	0.455	0.483	--	-0.812	-0.138
	R^2	--	0.928	0.876	--	0.841	0.756
	MAE, 10^6 m^3	--	0.425	0.435	--	0.921	0.541
	RMSE, 10^6 m^3	--	0.988	0.962	--	0.996	0.789
WHT	NSE	--	0.868	0.780	--	-4.945	-7.517
	R^2	--	0.880	0.820	--	0.406	0.297
	MAE, 10^6 m^3	--	0.007	0.007	--	0.012	0.012
	RMSE, 10^6 m^3	--	0.011	0.014	--	0.016	0.019
DRW	NSE	--	-21.287	-31.784	--	-178536.280	-507866.982
	R^2	--	0.531	0.448	--	0.007	0.015
	MAE, 10^6 m^3	--	0.013	0.011	--	0.704	1.156
	RMSE, 10^6 m^3	--	0.031	0.037	--	0.844	1.423
CLD	NSE	--	-39.909	-70.341	--	-0.132	-0.444
	R^2	--	0.363	0.214	--	0.311	0.384
	MAE, 10^6 m^3	--	0.079	0.080	--	0.019	0.020
	RMSE, 10^6 m^3	--	0.181	0.239	--	0.022	0.025
MEW	NSE	--	-48.624	-43.454	--	-61.795	-333.302
	R^2	--	0.113	0.163	--	0.431	0.146
	MAE, 10^6 m^3	--	0.010	0.012	--	0.029	0.067
	RMSE, 10^6 m^3	--	0.028	0.026	--	0.032	0.073
MLL	NSE	--	-6.523	-5.819	--	-5.543	-24.468
	R^2	--	0.717	0.564	--	0.303	0.158
	MAE, 10^6 m^3	--	0.064	0.060	--	0.037	0.069
	RMSE, 10^6 m^3	--	0.116	0.110	--	0.055	0.108
BYS	NSE	--	-12.068	-11.253	--	-13.824	-40.675
	R^2	--	0.492	0.235	--	0.191	0.051
	MAE, 10^6 m^3	--	0.020	0.021	--	0.010	0.016
	RMSE, 10^6 m^3	--	0.039	0.037	--	0.016	0.026

Table 29. Calibration statistics for the event volumes for the stations for all calibration scenarios.

		270m Models			100m Models		
Station	**Statistic**	**2004**	**2018 w/gauge**	**2018 w/WRF**	**2004 Period**	**2018 w/gauge**	**2018 w/WRF**
Hopland	NSE	0.784	0.879	0.966	0.993	0.091	0.778
	R^2	0.912	0.899	0.987	0.996	1.000	1.000
	MAE, 10^6 m^3	9.14	3.04	1.54	3.34	11.59	9.36
	RMSE, 10^6 m^3	13.06	5.78	3.05	4.16	18.94	5.48
Ukiah	NSE	0.675	0.918	0.998	0.965	-0.639	0.823
	R^2	0.871	0.922	0.999	0.987	0.999	1.000
	MAE, 10^6 m^3	3.54	1.11	0.20	2.39	7.07	3.76
	RMSE, 10^6 m^3	5.49	2.32	0.33	3.14	11.46	2.25
Calpella	NSE	0.908	0.966	0.962	0.966	0.138	0.940
	R^2	0.948	0.972	0.962	0.979	1.000	1.000
	MAE, 10^6 m^3	2.62	0.75	0.76	0.00	4.21	1.87
	RMSE, 10^6 m^3	3.48	1.26	1.33	0.00	7.11	1.11
Talmage	NSE	--	0.833	0.890	--	0.151	0.847
	R^2	--	0.873	0.982	--	1.000	1.000
	MAE, 10^6 m^3	--	2.89	2.49	--	9.41	6.50
	RMSE, 10^6 m^3	--	5.61	4.55	--	15.31	3.83
WHT	NSE	--	0.976	0.770	--	-0.801	-0.340
	R^2	--	0.991	0.953	--	1.000	1.000
	MAE, 10^6 m^3	--	0.01	0.05	--	0.12	0.17
	RMSE, 10^6 m^3	--	0.03	0.09	--	0.20	0.10
DRW	NSE	--	-5.786	-4.037	--	-25531.280	-67176.786
	R^2	--	0.949	0.810	--	1.000	1.000
	MAE, 10^6 m^3	--	0.11	0.09	--	7.79	21.31
	RMSE, 10^6 m^3	--	0.19	0.17	--	13.14	12.53
CLD	NSE	--	-2.096	-2.583	--	0.716	0.970
	R^2	--	0.832	0.632	--	1.000	1.000
	MAE, 10^6 m^3	--	0.64	0.62	--	0.24	0.13
	RMSE, 10^6 m^3	--	1.09	1.17	--	0.39	0.08
MEW	NSE	--	-9.260	-17.779	--	-68.315	-331.987
	R^2	--	0.782	0.936	--	0.999	0.998
	MAE, 10^6 m^3	--	0.10	0.13	--	0.35	1.30
	RMSE, 10^6 m^3	--	0.17	0.23	--	0.59	0.77
MLL	NSE	--	0.568	0.466	--	0.949	0.361
	R^2	--	0.631	0.509	--	1.000	0.999
	MAE, 10^6 m^3	--	0.32	0.37	--	0.14	0.79
	RMSE, 10^6 m^3	--	0.57	0.64	--	0.22	0.47
BYS	NSE	--	0.621	0.682	--	0.845	0.712
	R^2	--	0.696	0.815	--	1.000	0.999
	MAE, 10^6 m^3	--	0.07	0.08	--	0.06	0.14
	RMSE, 10^6 m^3	--	0.15	0.14	--	0.10	0.09

Table 30. Calibration statistics for the event peak flow rates for the stations for all calibration scenarios.

		270m models			100m models		
Station	**Statistic**	**2004**	**2018 w/gauge**	**2018 w/WRF**	**2004 period**	**2018 w/gauge**	**2018 w/WRF**
Hopland	NSE	0.812	0.558	0.876	0.945	0.498	0.755
	R^2	0.873	0.998	0.987	0.967	0.991	0.995
	MAE, m^3	26.526	26.373	13.233	19.683	13.368	10.704
	RMSE, m^3	39.150	53.870	28.517	34.018	15.323	7.575
Ukiah	NSE	0.908	0.911	0.934	0.892	0.686	0.961
	R^2	0.930	0.994	0.990	0.973	0.993	0.998
	MAE, m^3	9.806	12.172	9.320	14.424	8.196	3.016
	RMSE, m^3	14.309	21.514	18.417	25.546	8.566	2.218
Calpella	NSE	0.845	0.979	0.971	0.966	0.132	0.661
	R^2	0.887	0.986	0.977	0.979	0.999	1.000
	MAE, m^3	12.137	4.599	4.592	11.613	8.913	8.343
	RMSE, m^3	19.524	7.257	8.431	14.545	13.349	5.400
Talmage	NSE	--	0.181	0.713	--	0.434	0.870
	R^2	--	0.998	0.981	--	0.994	0.997
	MAE, m^3	--	29.350	14.851	--	12.530	6.812
	RMSE, m^3	--	60.570	35.888	--	14.234	4.821
WHT	NSE	--	0.521	0.616	--	-0.593	0.767
	R^2	--	0.780	0.988	--	0.998	1.000
	MAE, m^3	--	1.537	1.240	--	0.346	0.195
	RMSE, m^3	--	3.675	3.291	--	0.510	0.117
DRW	NSE	--	-3.674	-7.261	--	-324803.763	-471192.238
	R^2	--	0.742	0.905	--	0.958	0.965
	MAE, m^3	--	1.207	1.441	--	15.119	26.810
	RMSE, m^3	--	2.100	2.791	--	22.259	18.230
CLD	NSE	--	-144.875	-523.915	--	0.529	0.721
	R^2	--	0.993	0.946	--	1.000	1.000
	MAE, m^3	--	6.422	11.335	--	0.359	0.279
	RMSE, m^3	--	11.908	22.588	--	0.363	0.278
MEW	NSE	--	-793.548	-634.661	--	-527.764	-1888.490
	R^2	--	0.954	0.950	--	0.978	0.963
	MAE, m^3	--	1.721	1.591	--	1.299	3.790
	RMSE, m^3	--	3.133	2.802	--	2.005	2.509
MLL	NSE	--	-6.472	-4.445	--	-14.532	-21.583
	R^2	--	0.977	0.952	--	1.000	1.000
	MAE, m^3	--	4.688	3.353	--	1.185	2.297
	RMSE, m^3	--	8.530	7.282	--	1.905	1.511
BYS	NSE	--	-18.632	-11.715	--	-64.266	-64.323
	R^2	--	0.931	0.863	--	0.978	0.969
	MAE, m^3	--	1.937	1.523	--	0.375	0.597
	RMSE, m^3	--	3.529	2.840	--	0.597	0.414

5 Verification and Assessment

5.1 Model Verification

The two resolution models were run over the period of 05Dec2018 – 15Apr2019 for verification of the calibrated parameters. Several different types of input forcing data were modeled. These are:

- Measured precipitation utilizing the expanded rainfall data set used in the 2017/2018 calibration period and hydro-meteorological data at Ukiah Airport station, using parameter set of the corresponding calibrated model
- West-WRF precipitation and hydro-meteorological data, using parameter set from the corresponding resolution for the calibrated West-WRF model

As the precipitation gage network had been expanded significantly between 2004 and 2017, and the models calibrated to this gage network were inferior to the models calibrated with the expanded precipitation network, the 2004 gage network parameter sets were not included in the verification period.

5.1.1 Verification Results

5.1.1.1 Flow Hydrograph comparisons

5.1.1.1.1 Gauge forcing data models

The forcing inputs to the GSSHA model used in the verification period were from rain gauges located throughout the basin area (Figure 3), and hydro-meteorological data from the Ukiah Airport. The flow hydrographs for the USGS gauging stations in Figure 32 show that the model validated very well to the observed data at these locations at the 270m resolution during this period. Also, when the model resolution was increased to 100m, the model still validated the observed flow rate magnitudes for different events at these locations (Figure 33).

From the Lake Mendocino water level perspective, both models do a very good job of simulating the Lake Mendocino levels, with the 270m resolution model doing better in the beginning of the simulation and the 100m resolution model doing better at the end. These results are graphically depicted in Figure 34 where Lake Mendocino levels at both resolutions are compared.

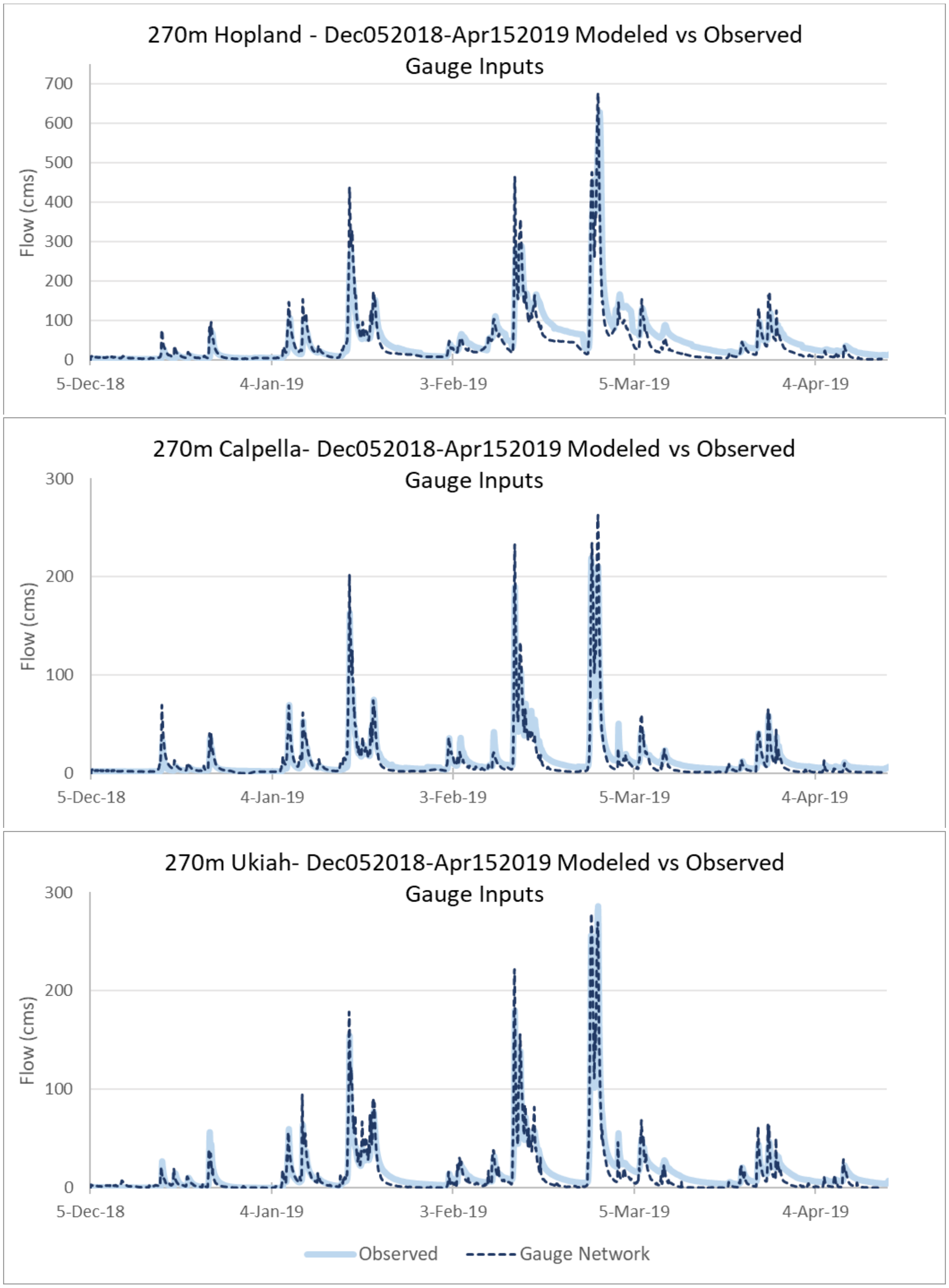

Figure 32. Simulated vs. Observed flow hydrographs for the 270m model resolution with gauged forcing data for the verification period.

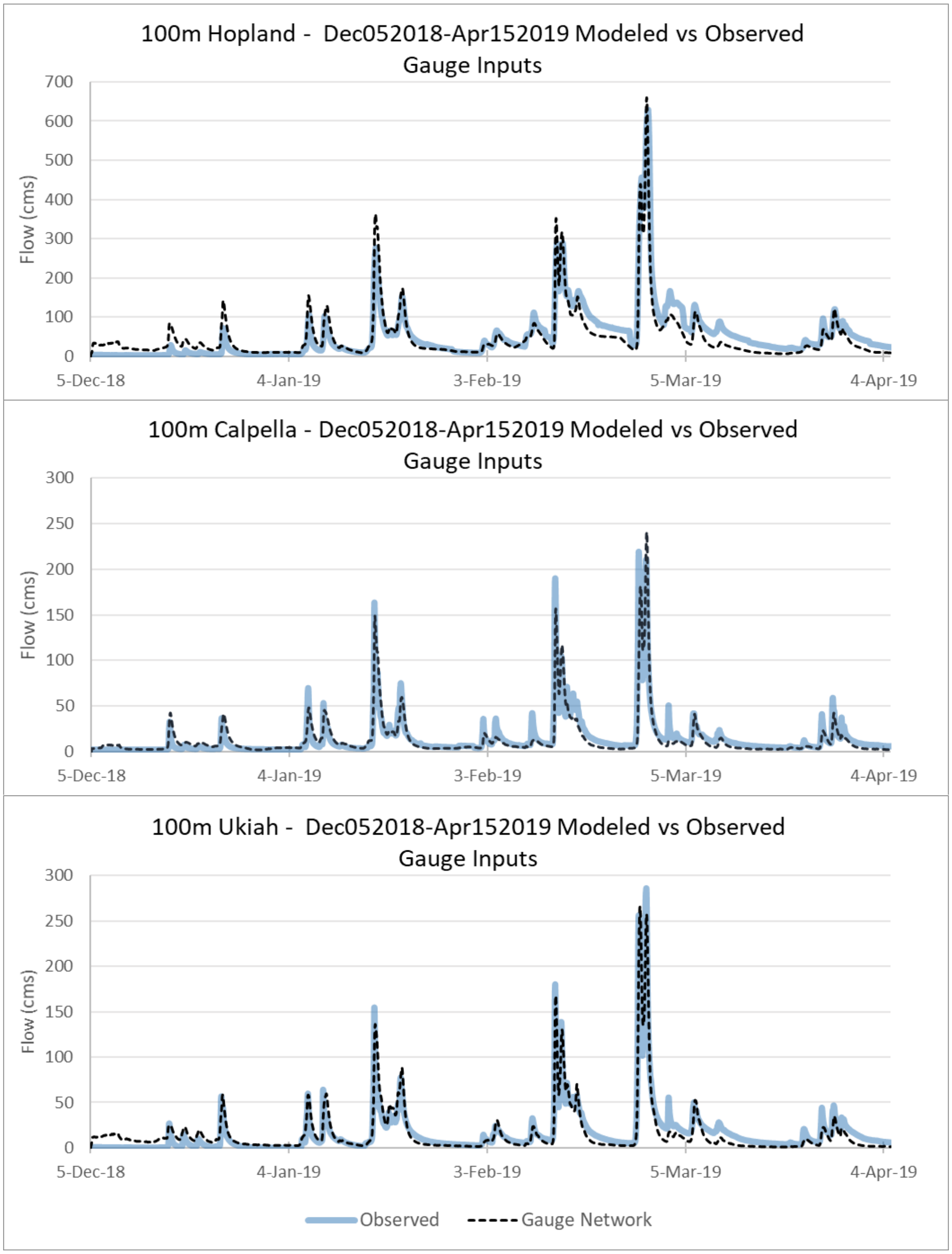

Figure 33. Simulated vs. Observed flow hydrographs for the 100m model resolution with gauge forcing data for the verification period.

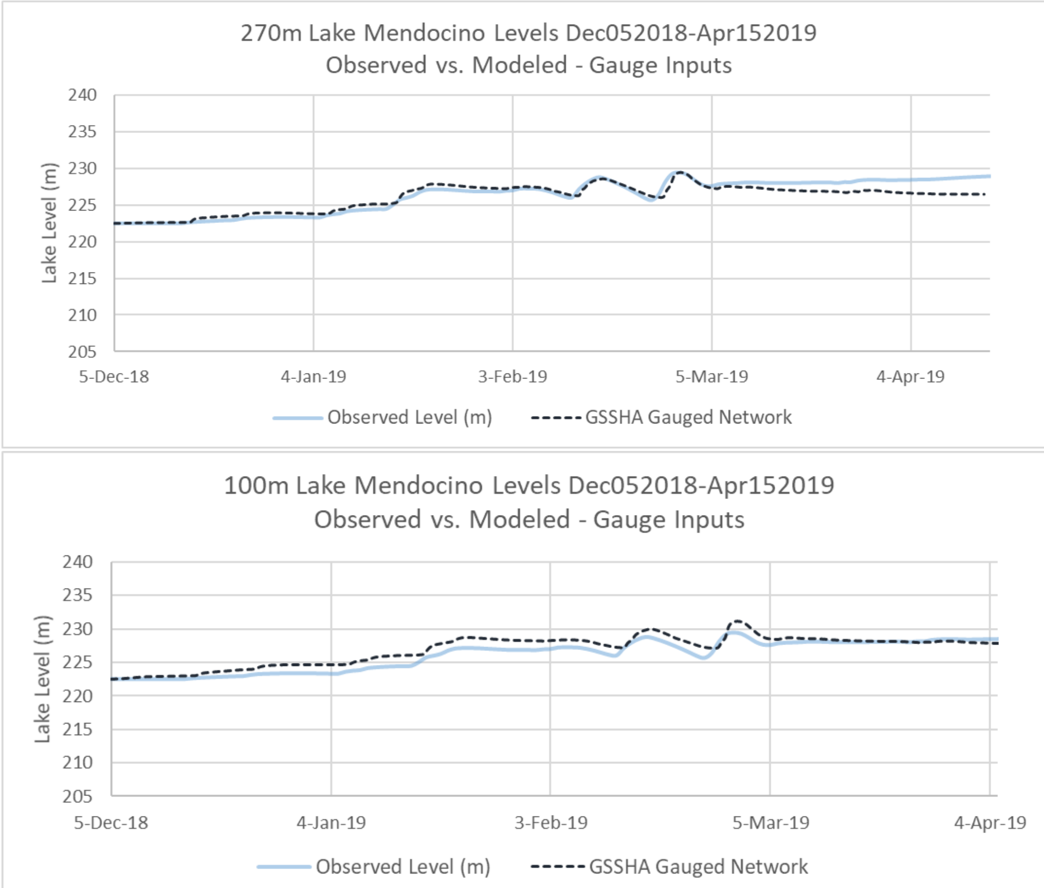

Figure 34. Simulated vs. Observed Lake Mendocino levels for the 270m and 100m resolution models with gauge forcing data for the verification period.

5.1.1.1.2 West-WRF Forecasting forcing data models

A 1-day forecast dataset was used as the West-WRF forcing inputs to the GSSHA models to validate the corresponding calibration parameters for the 05Dec2018 – 15Apr2019 period. The parameter set used for these models was from the corresponding 2018 calibration with West-WRF forcing.

Figure 35 and Figure 36 show the comparison between the observed and simulated flow rates via West-WRF 1 day inputs for the Hopland, Ukiah, and Calpella gauging stations at 270, and 100m resolutions, respectively. As shown in the Figure, the West-WRF 1d forecast driven models did not verify as well as the rain gage driven models, with the West-WRF driven models generally under predicting the flows, with the finer resolution model appearing to do a better job of predicting flows.

Figure 37 shows the simulated and observed Lake Mendocino water levels for the West-WRF models for 270 and 100m resolutions for three different forecasts. Similar to the outcomes of the flow hydrographs, the 1-day West-WRF forecast model at 100m resolution seems to predict better the water levels for the lake. As the forecast period is extended, the coarser model tends to under predict both the flows and lake levels.

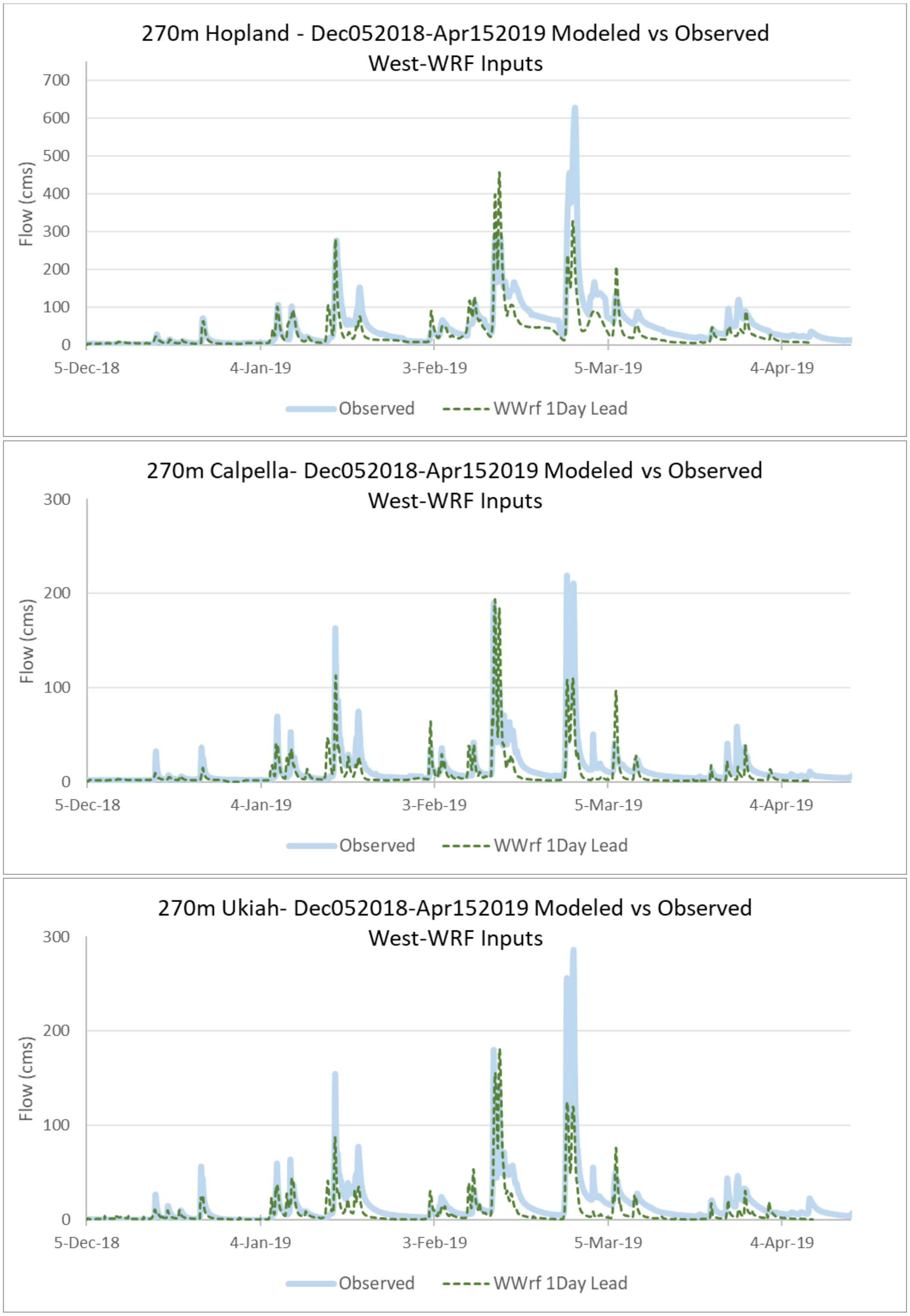

Figure 35. Simulated vs. Observed flow hydrographs for the 270m model resolution with West-WRF forecasted forcing data at Calpella, Ukiah, and Hopland for the 1-day forecast.

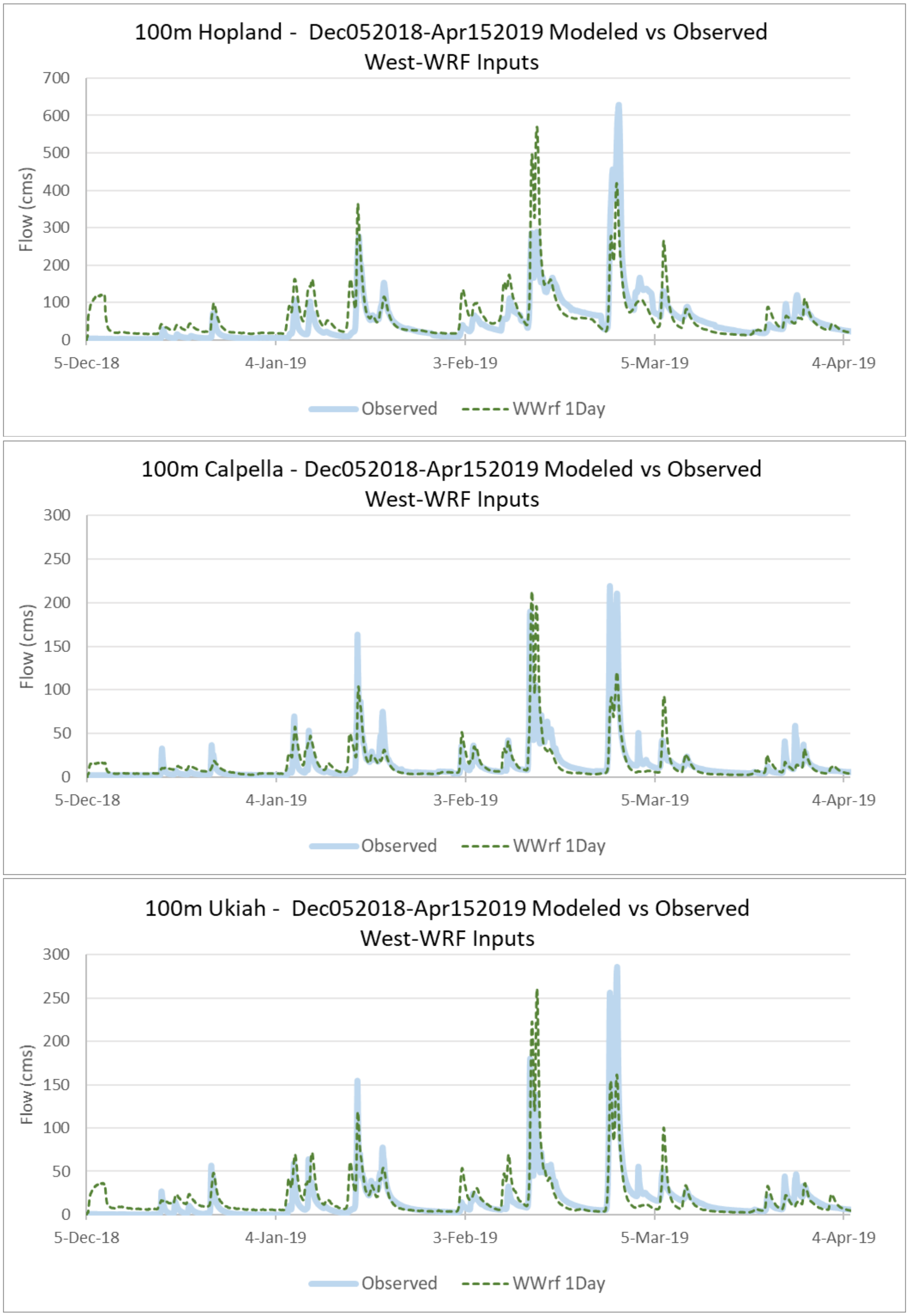

Figure 36. Simulated vs. Observed flow hydrographs for the 100m model resolution with West-WRF forecasted forcing data at Calpella, Ukiah, and Hopland for 1-day forecast.

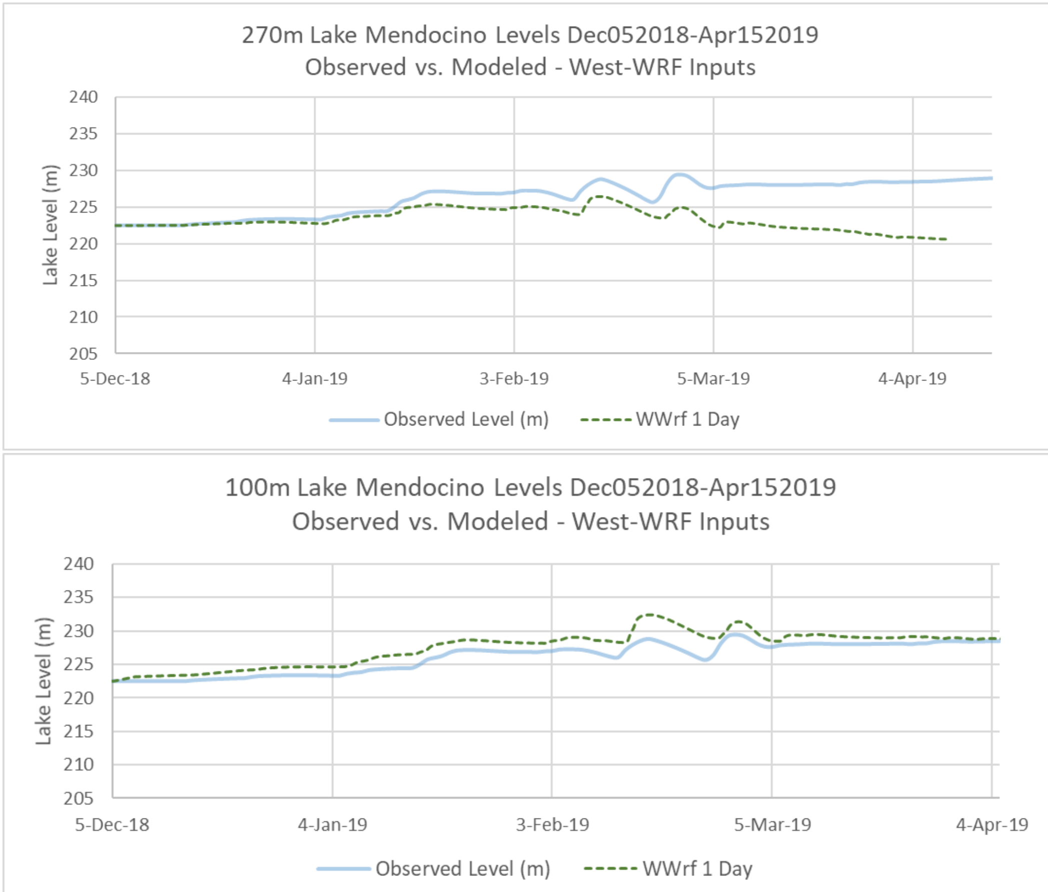

Figure 37. Simulated vs. Observed Lake Mendocino levels for the 270m and 100m resolution models with West-WRF 1-day forecasted forcing data.

5.1.2 Goodness of fit metrics

Table 31 and Table 32 include the goodness of fit metrics for the daily flows for all verification models at the USGS gauging stations located at Hopland, Calpella, and Ukiah, as well as the Lake Mendocino water levels.

For the verification simulations for models using the observed gage precipitation, NSE for the daily flows at the three USGS stations were all 0.80 or higher for both, the 270m and 100m resolution models, showing an excellent fit, and as good or better than the calibration statistics. NSE for the lake levels were 0.831 (270m) and 0.791 (100m), also showing a very good fit when the model is driven by the existing gage network. Both lake level and flows were simulated well with this model.

When driven by the 1D West-WRF forecast, the NSE for the flows at the USGS gages range from 0.550 to 0.628, still strongly positive, but not as high as when using the gage data. For the coarser resolution model, the lake levels are negative, mainly because there is not enough flow into the lake during this simulation and the actual and simulated levels diverge as the simulation proceeds. The finer resolution model does a fairly good job of simulating the lake levels, with a strongly positive NSE of 0.504.

Table 31. Goodness of fit metrics for the daily flows for the 270m verification models.

Station	Statistic	Gauge	West WRF 1-day
Hopland	NSE	0.854	0.601
	R^2	0.874	0.694
	RMSE, 10^6 m^3	2.146	3.549
	MAE, 10^6 m^3	1.467	1.999
Calpella	NSE	0.864	0.628
	R^2	0.932	0.688
	RMSE, 10^6 m^3	0.598	0.988
	MAE, 10^6 m^3	0.409	0.598
Ukiah	NSE	0.882	0.592
	R^2	0.921	0.679
	RMSE, 10^6 m^3	0.686	1.275
	MAE, 10^6 m^3	0.494	0.760
Lake Levels	NSE	0.831	-470.027
	R^2	0.849	0.004
	RMSE, m	0.925	48.926
	MAE, m	0.711	13.130

Table 32. Goodness of fit metrics for the daily flows for the 100m verification models.

Station	Statistic	Gauge	West WRF 1-day
Hopland	NSE	0.892	0.562
	R^2	0.906	0.617
	RMSE, 10^6 m^3	1.848	3.715
	MAE, 10^6 m^3	1.395	2.295
Calpella	NSE	0.854	0.610
	R^2	0.892	0.683
	RMSE, 10^6 m^3	0.618	1.011
	MAE, 10^6 m^3	0.405	0.580
Ukiah	NSE	0.903	0.550
	R^2	0.933	0.642
	RMSE, 10^6 m^3	0.621	1.339
	MAE, 10^6 m^3	0.475	0.832
Lake Levels	NSE	0.791	0.504
	R^2	0.887	0.879
	RMSE, m	1.031	1.587
	MAE, m	0.911	1.347

5.2 Model Assessment

Comparison with CNRFC Models

The performance of the Lake Mendocino GSSHA models was compared with a CNRFC operational model based on daily flow data at the Ukiah and Calpella gaging stations. The 2018 calibration period and the 2019 validation periods were taken into consideration in this analysis.

Figure 38 shows the daily volume hydrographs for the 1 day CNRFC forecast and the 270m GSSHA models (gauge and West-WRF forcings) for the Ukiah and Calpella gauging stations for the 2018 calibration period. These plots show that the response of the GSSHA models predict closer than the CNRFC model the observed daily flow volumes, particularly for large events.

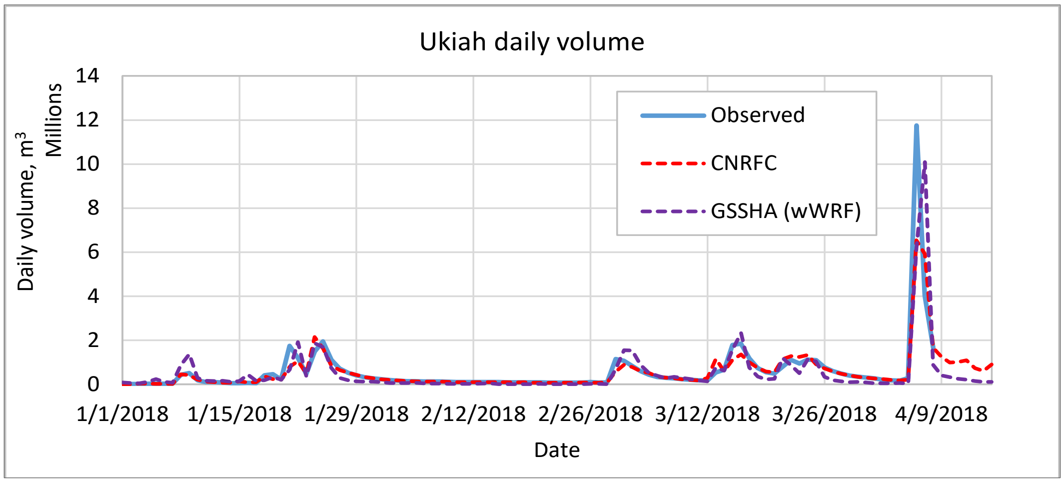

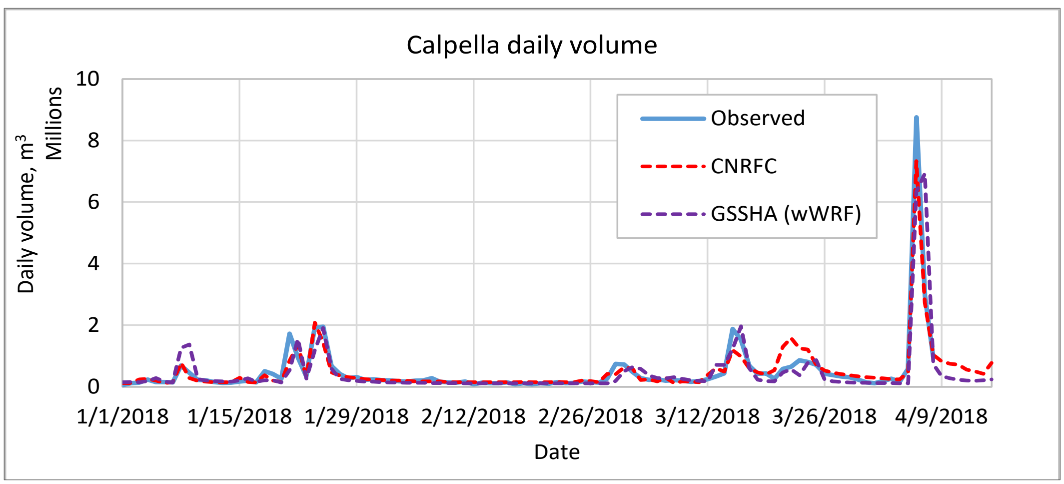

Figure 38. GSSHA and CNRFC simulated and observed daily volumes at Ukiah and Calpella.

Goodness of fit metrics for the daily volumes at Ukiah and Calpella are included in Table 33. Efficiencies for the GSSHA models are comparable with those of the CNRFC model at these two stations. For instance the efficiency at Ukiah for the 270m GSSHA model with gauge data is 0.790 and the corresponding value for the CNRFC model is 0.787. This indicates that the GSSHA models are as good predictors of the observed outcomes as the CNRFC model at this station. The same can be concluded when comparing the statistics for the Calpella station.

Table 33. Daily volume statistics for the CNRFC and GSSHA models for the 2018 calibration period.

Station	Statistic	CNRFC model	270m GSSHA w/ gauge	270m GSSHA w/ west-WRF (1day)
Ukiah	NSE	0.787	0.790	0.779
	R^2, m^3	0.819	0.869	0.796
	MAE, 10^3 m^3	149.7	241.0	0.269
	RMSE, 10^3 m^3	571.4	542.0	0.556
Calpella	NSE	0.927	0.772	0.879
	R^2, m^3	0.940	0.809	0.921
	MAE, 10^3 m^3	132.2	172.0	0.158
	RMSE, 10^3 m^3	251.5	387.0	0.282

Figure 40 shows the daily volume hydrographs for the CNRFC and the 270m GSSHA models (gauge, CNRFC, and West-WRF forcings) for the Ukiah and Calpella gauging stations for the 2019 verification period. In general, these plots show that the response of the GSSHA models and the CNRFC model compare reasonably well with one another.

Goodness of fit metrics for the daily volumes at Ukiah and Calpella are included in Table 34. Efficiencies for the GSSHA model with gauge forcing are slightly lower than the CNRFC model at these two stations. However, they are reasonably high such that this model can be considered a good simulator of observed values. The efficiencies for the 1d West-WRF forecast are reasonably good but not as close as those obtained with the CNRFC model and the GSSHA with gauge forcing. Other statistics for the models are shown in Table 34.

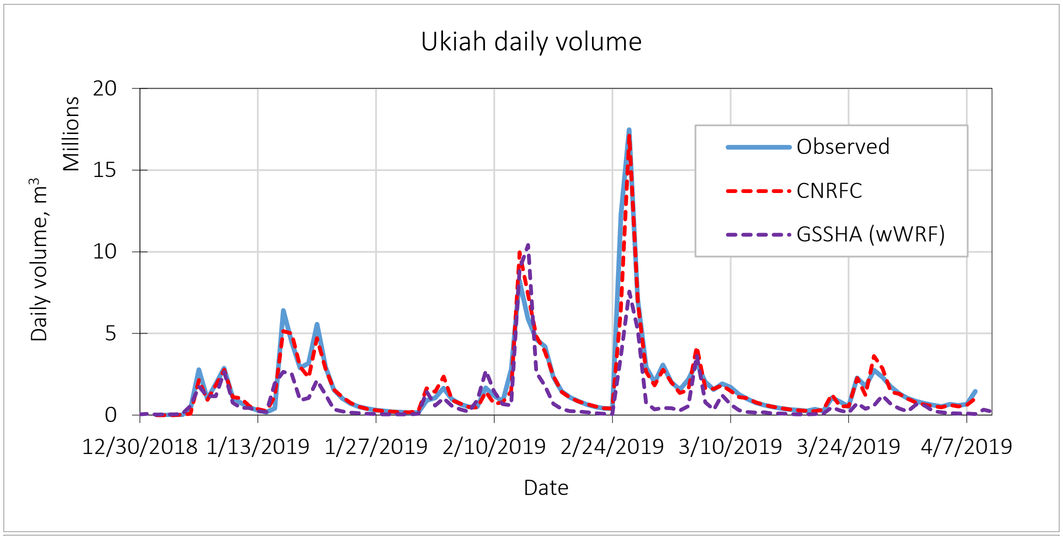

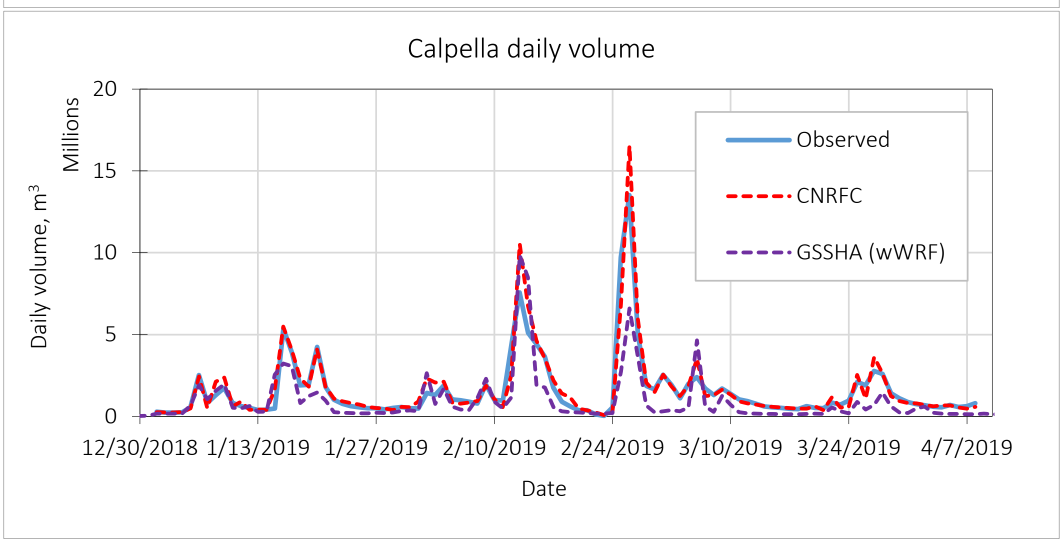

Figure 39. GSSHA and CNRFC simulated and observed daily volumes at Ukiah and Calpella.

Table 34. Daily volume statistics for the CNRFC and GSSHA models for the 2019 verification period.

Station	Statistic	CNRFC model	270m GSSHA w/ gauge	270m GSSHA w/ CNRFC	270m GSSHA w/ West-WRF 1-day
Ukiah	NSE	0.917	0.882	0.862	0.592
	R^2, m³	0.918	0.921	0.930	0.679
	MAE, 10^3 m³	699.1	686.0	741.0	1,275.0
	RMSE, 10^3 m³	274.2	494.0	547.0	760.0
Calpella	NSE	0.890	0.864	0.689	0.628
	R^2, m³	0.924	0.932	0.942	0.688
	MAE, 10^3 m³	636.0	598.0	903.0	988.0
	RMSE, 10^3 m³	310.3	409.0	478.0	598.0

6 Additional Analyses

6.1 Effect of Precipitation on GSSHA Simulated Flow and Lake Mendocino Water Levels

6.1.1 West-WRF Extended Forecasts GSSHA Models

The models verified using the 1d West-WRF forecast were driven with longer lead forecast data sets arranged in the same fashion as 1d forecast, that is the 3, 5, and 7 day forecast were strung together to produce a continual data set, and run for the verification period.

The results of this exercise for flow are shown in Figure 40 and Figure 41, and reservoir levels in Figure 42. As the West-WRF forecast period is extended beyond the 1-day forecast, the GSSHA models tend to under predict the flows and lake levels. The finer resolution model generally does a better job of simulating the flows and lake levels than the coarser resolution model, which tends significantly underestimate the flows, and lake levels, with the simulated lake levels diverging further and further from the observed as the simulation proceeds.

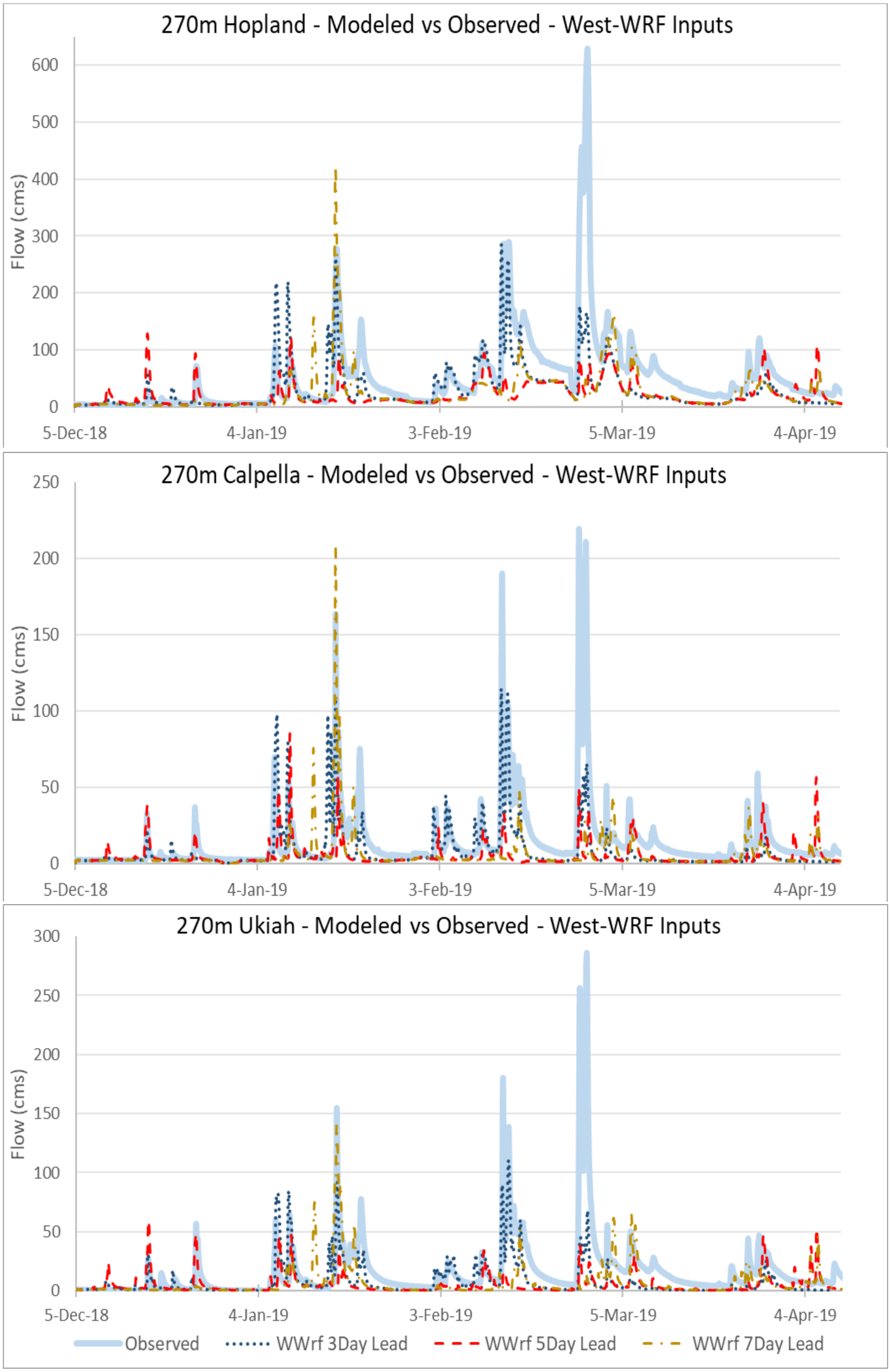

Figure 40. Simulated vs. Observed flow hydrographs for the 270m model resolution with West-WRF forecasted forcing data at Hopland, Calpella, and Ukiah for the 3, 5, and 7-day forecasts.

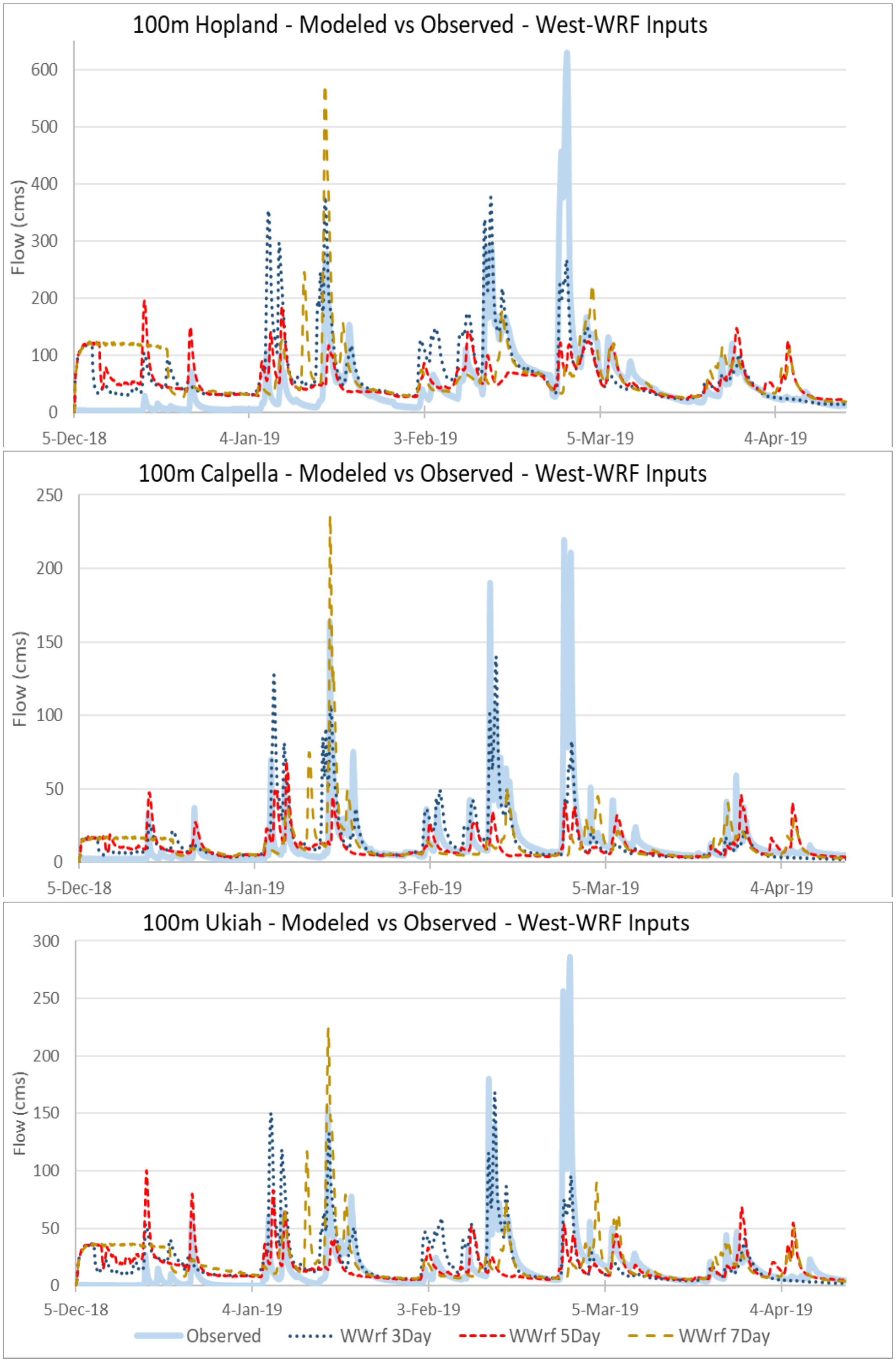

Figure 41. Simulated vs. Observed flow hydrographs for the 100m model resolution with West-WRF forecasted forcing data at Hopland, Calpella, and Ukiah for the 3, 5, and 7-day forecasts.

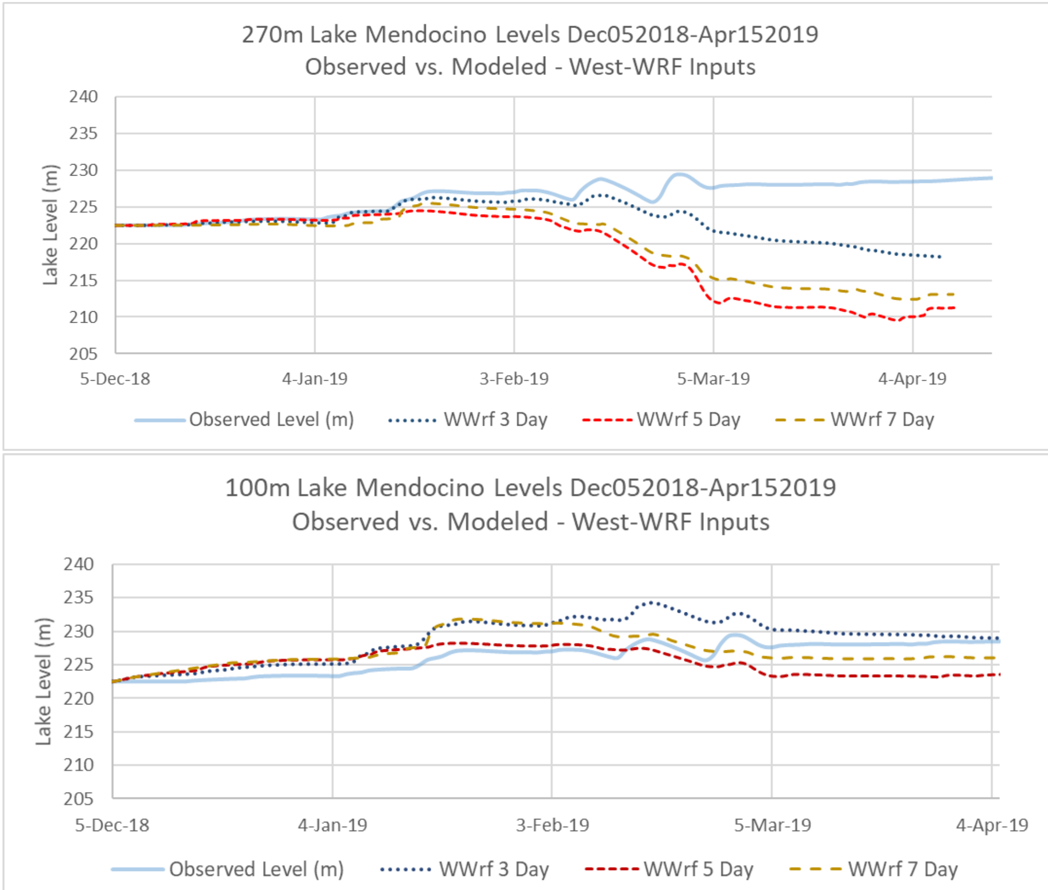

Figure 42. Simulated vs. Observed Lake Mendocino levels for the 270m and 100m resolution models with West-WRF forecasted forcing data for three different forecasts (3, 5, and 7 day).

6.1.2 CNRFC Forced GSSHA Models

The forcing inputs to these GSSHA models were the precipitation from CNRFC observation analyses; note these are observed (gauge) -based and ***not*** forecast datasets, so could not be used for forecasting purposes. (CNRFC conducts its streamflow forecasts through an observation and hydrology model initialization and then using operational numerical weather forecasts to drive the streamflow forecasts for short and medium lead forecasting purposes, and then more statistical approaches for long lead.). The flow hydrographs for the USGS gauging stations in Figure 43 show that the model fits reasonably well the observed data at these locations for the 270m resolution during this period. Also, when the model resolution was increased to 100m, the model still matches the observed flow rate magnitudes for different events at these locations (Figure 44).

Lake Mendocino water level predictions with these models are shown in Figure 45 where Lake Mendocino levels at both model resolutions are compared. In this case, the models at 270m resolution seem to predict better the observed Lake Mendocino water levels over the 100m model.

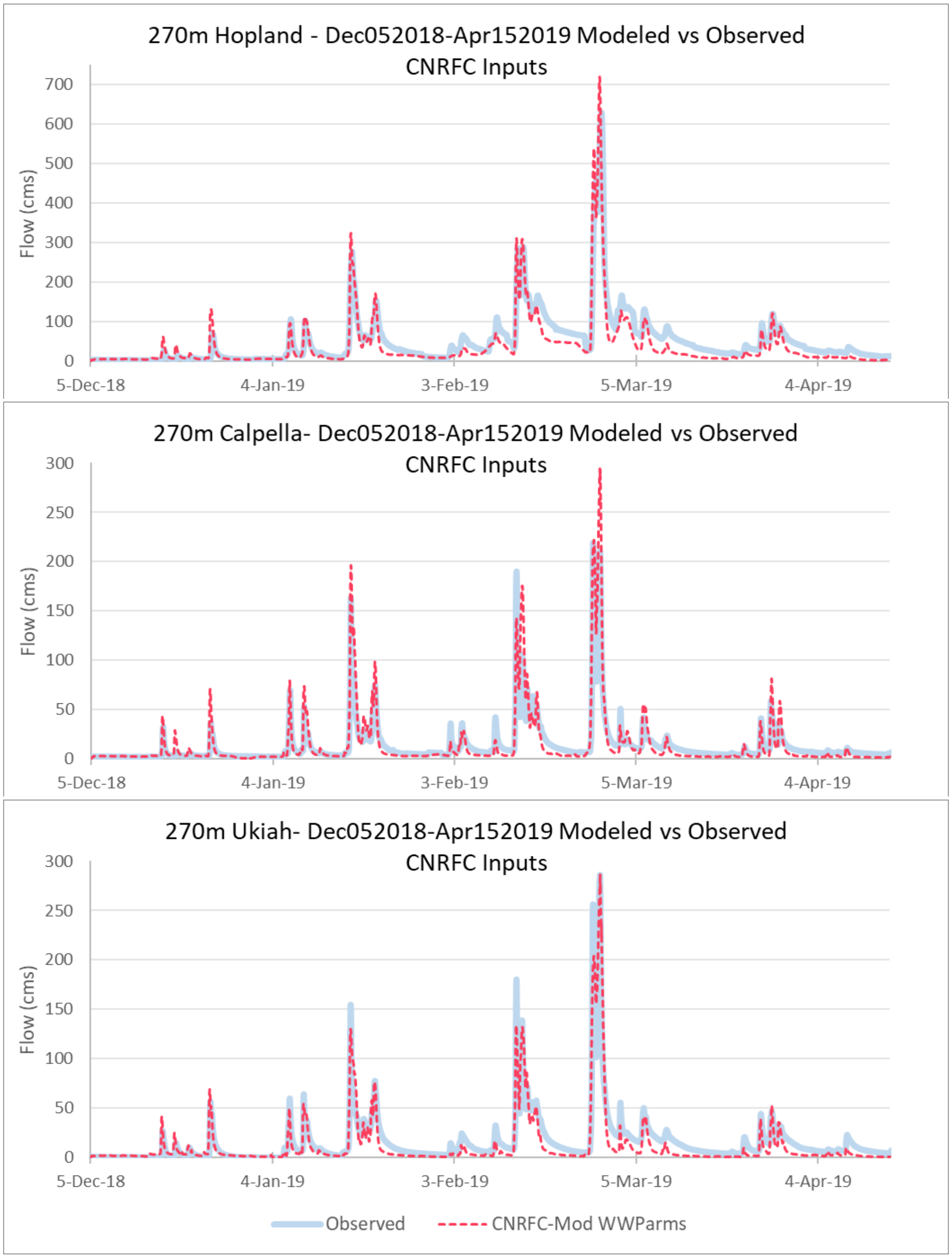

Figure 43. Simulated vs. Observed flow hydrographs for the 270m model resolution with CNRFC forcing data.

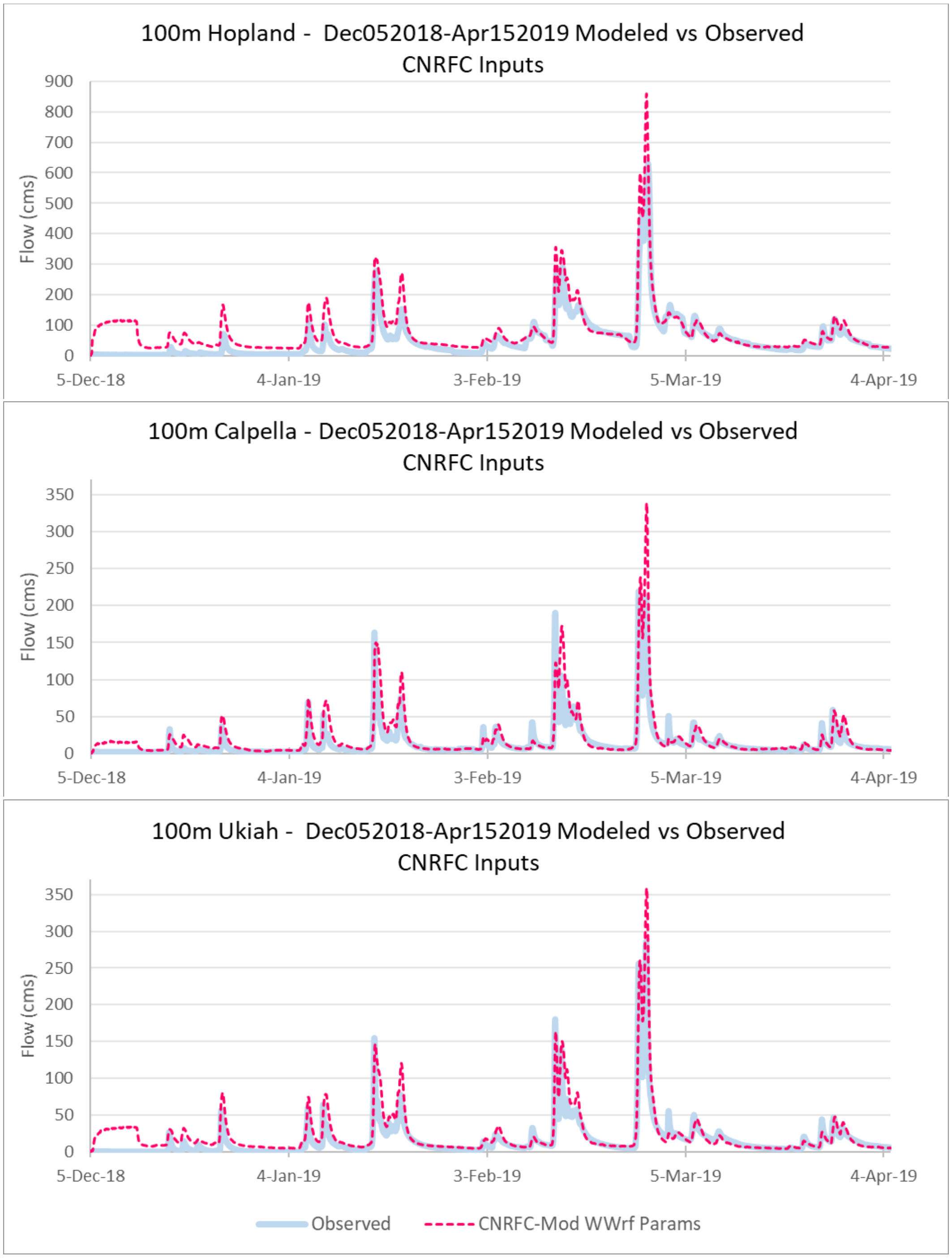

Figure 44. Simulated vs. Observed flow hydrographs for the 100m model resolution with CNRFC forcing data.

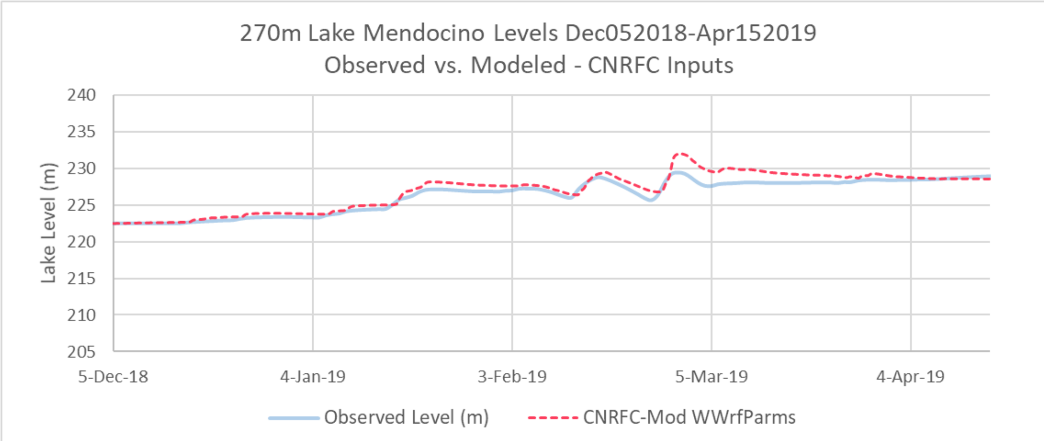

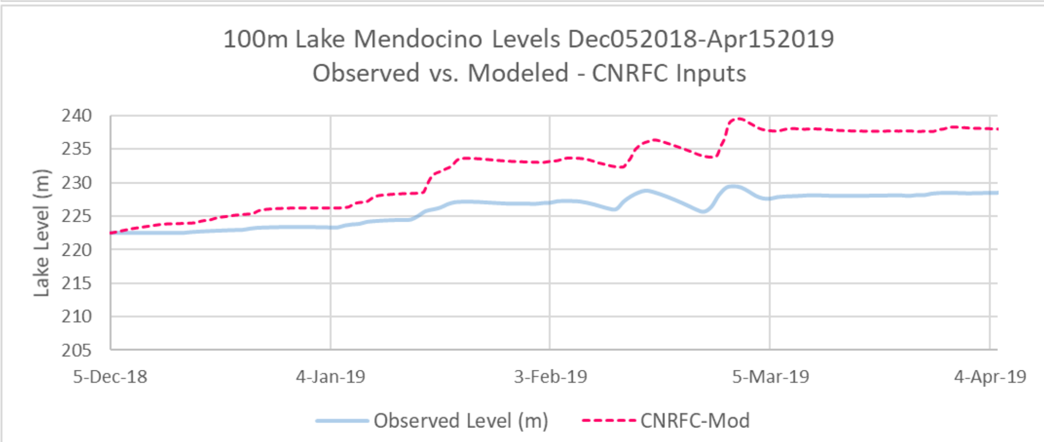

Figure 45. Simulated vs. Observed Lake Mendocino water levels for the 270m and 100m resolution models with CNRFC forcing data.

6.1.3 Discussion

Goodness of fit metrics are shown in Table 35 and Table 36. As shown in the tables, the models driven by the gage data, the 1d West-WRF forecast, and the CRNFC distributed gage data all produce very good simulations of flow and lake level. However, as the forecast lead time increases for the West-WRF precipitation, the results rapidly degrade, with the NSE efficiencies becoming low or negative as the forecast lead time increases.

Table 35. Goodness of fit metrics for the daily flows for the 270m verification models.

Station	Statistic	Gauge	West WRF 1-day	West WRF 3-day	West WRF 5-day	West WRF 7-day	CNRFC
Hopland	NSE	0.854	0.601	0.382	0.026	0.029	0.873
	R^2	0.874	0.694	0.500	0.279	0.192	0.907
	RMSE, 10^6 m^3	2.146	3.549	4.504	5.541	5.532	2.002
	MAE, 10^6 m^3	1.467	1.999	2.447	2.771	2.570	1.476

Calpella	NSE	0.864	0.628	0.398	-0.040	-0.086	0.689
	R^2	0.932	0.688	0.490	0.186	0.124	0.942
	RMSE, 10^6 m^3	0.598	0.988	1.284	1.651	1.687	0.903
	MAE, 10^6 m^3	0.409	0.598	0.729	0.854	0.824	0.478
Ukiah	NSE	0.882	0.592	0.292	-0.104	-0.103	0.862
	R^2	0.921	0.679	0.423	0.118	0.099	0.930
	RMSE, 10^6 m^3	0.686	1.275	1.719	2.098	2.097	0.741
	MAE, 10^6 m^3	0.494	0.760	0.921	1.093	1.020	0.547
Lake Levels	NSE	0.841	-1.953	-3.470	-19.711	-13.872	0.841
	R^2	0.956	0.004	0.031	0.452	0.338	0.956
	RMSE, m	0.900	3.845	4.726	10.193	8.637	0.900
	MAE, m	0.709	2.860	3.113	7.254	6.191	0.709

Table 36. Goodness of fit metrics for the daily flows for the 100m verification models.

Station	Statistic	Gauge	West WRF 1-day	West WRF 3-day	West WRF 5day	West WRF 7-day	CNRFC
Hopland	NSE	0.892	0.562	0.281	0.135	-0.276	0.646
	R^2	0.906	0.617	0.427	0.150	0.059	0.848
	RMSE, 10^6 m^3	1.848	3.715	4.761	5.224	6.342	3.341
	MAE, 10^6 m^3	1.395	2.295	2.976	3.134	3.658	2.249
Calpella	NSE	0.854	0.610	0.394	0.155	-0.113	0.360
	R^2	0.892	0.683	0.460	0.178	0.093	0.892
	RMSE, 10^6 m^3	0.618	1.011	1.260	1.488	1.707	1.295
	MAE, 10^6 m^3	0.405	0.580	0.698	0.798	0.854	0.617
Ukiah	NSE	0.903	0.550	0.207	-0.014	-0.376	0.571
	R^2	0.933	0.642	0.363	0.059	0.040	0.887
	RMSE, 10^6 m^3	0.621	1.339	1.777	2.010	2.341	1.308
	MAE, 10^6 m^3	0.475	0.832	1.117	1.208	1.309	0.759
Lake Levels	NSE	0.791	0.504	-0.858	-0.953	-0.370	-8.856
	R^2	0.887	0.879	0.682	0.008	0.158	0.971
	RMSE, m	1.031	1.587	3.073	3.150	2.639	7.077
	MAE, m	0.911	1.347	2.540	2.711	2.412	6.344

Figure 46 shows the relationship between the total of precipitation applied to the verification period models and the corresponding total simulated flows and helps explain the results shown in Figure 40 through 42 and Table 35 and 36. The Hopland gage represents flow from the entire watershed. The Calpella gage is indicative of the flow into the reservoir. Compared to the observed gage network, the CNRFC precipitation tends to overestimate the rainfall and thus the runoff. While the 1d West-WRF forecast compares very closely with the observed gage data, the West-WRF total precipitation tends to fall off as the forecast period is extended and the flows show a corresponding decrease. While calibrating the GSSHA models to the different West-WRF forecast periods may improve the results, as would running the model in a true forecasting mode with the model restarting from utilizing observed system states for each new forecast, the primary reason for the low flows, lake levels, and poor statistics for the GSSHA flows is the precipitous decline in precipitation as the West-WRF forecast lead is increased. Through the calibration and verification period, the GSSHA model has been shown capable of accurately simulating flows and reservoir levels given a good estimate of precipitation. The biggest potential for improvement in the GSSHA flows for the longer forecast lead times is improvement in the West-WRF precipitation forecast.

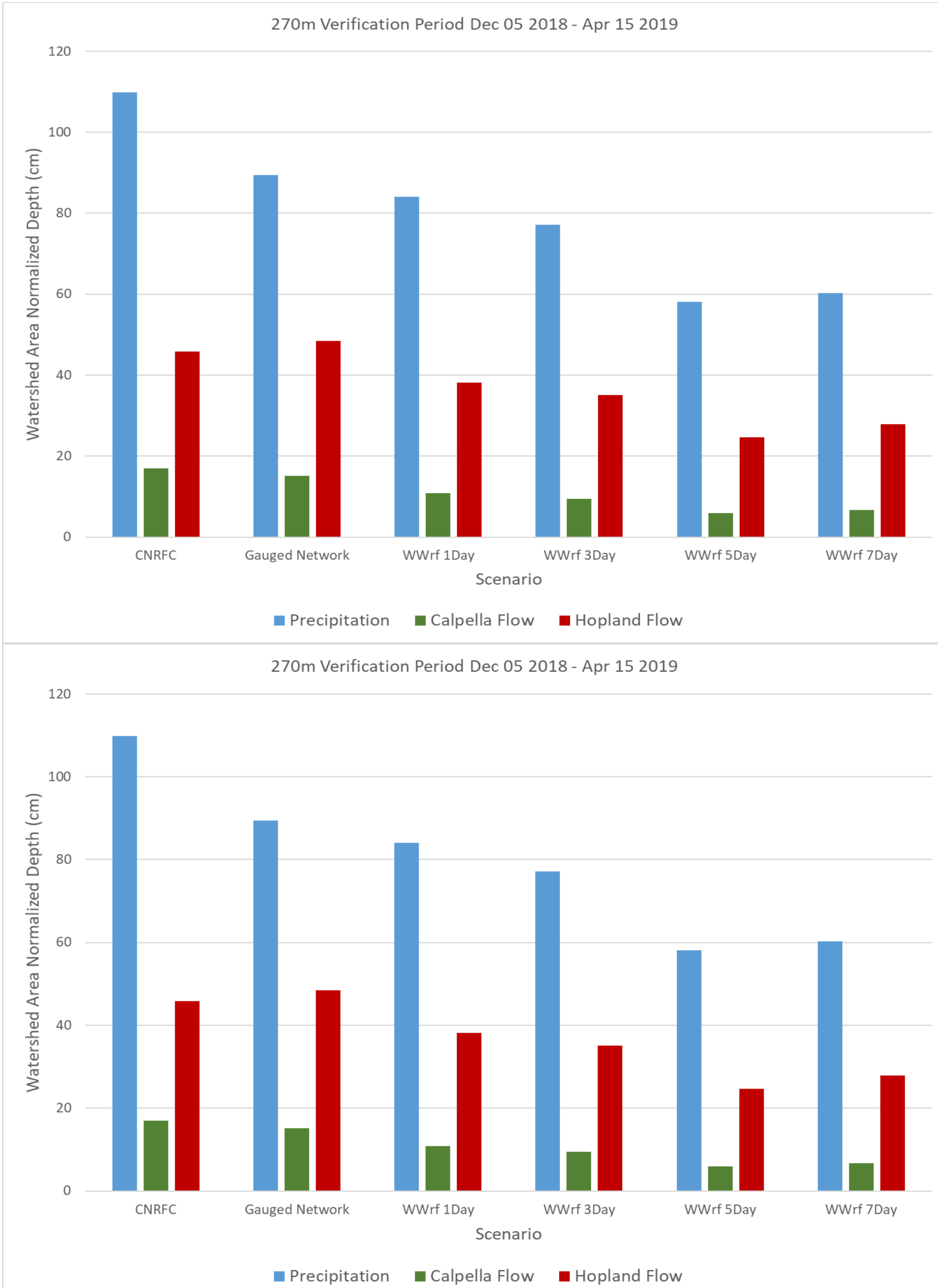

Figure 46. Precipitation, and simulated flows resulting from the various simulated scenarios, depth averaged over the watershed area for the 270 and 100 meter models.

6.2 Water Balance

The calibrated/verified 100m model was used to compute a yearly water balance for the watershed and the reservoir. The water year period of Oct 01, 2018 – Sep 30, 2019 was used for this analysis.

Figure 47 shows the water balance results for the October 01 2018 - September 30 2019 water year period for the watershed and lake processes of the 100m resolution model. Table 37 and Table 38 show the same information tabulated.

For the water year Oct 2018-2019 the watershed received 119.8 cm of rainfall. Of this, about half was infiltrated and half was discharged at the watershed outlet. Of the amount discharged at the outlet, the models indicated that approximately 10% was from groundwater, or baseflow. The model indicates that ET is was about equal to infiltration. Groundwater recharge was roughly 10%, about the same percent as the baseflow at the watershed outlet.

For the lake, the primary source of water to the lake is from surface water flows, approximately 250 m-km^2 for the year. Discharge was 208 m-km^2. The model indicates that precipitation to the lake is 7 m-km^2, with ET from the lake is approximately 6 m-km2, and the lake loses somewhere from 24 m-km^2 due to seepage to the groundwater, being the largest sink term to the lake, outside the releases.

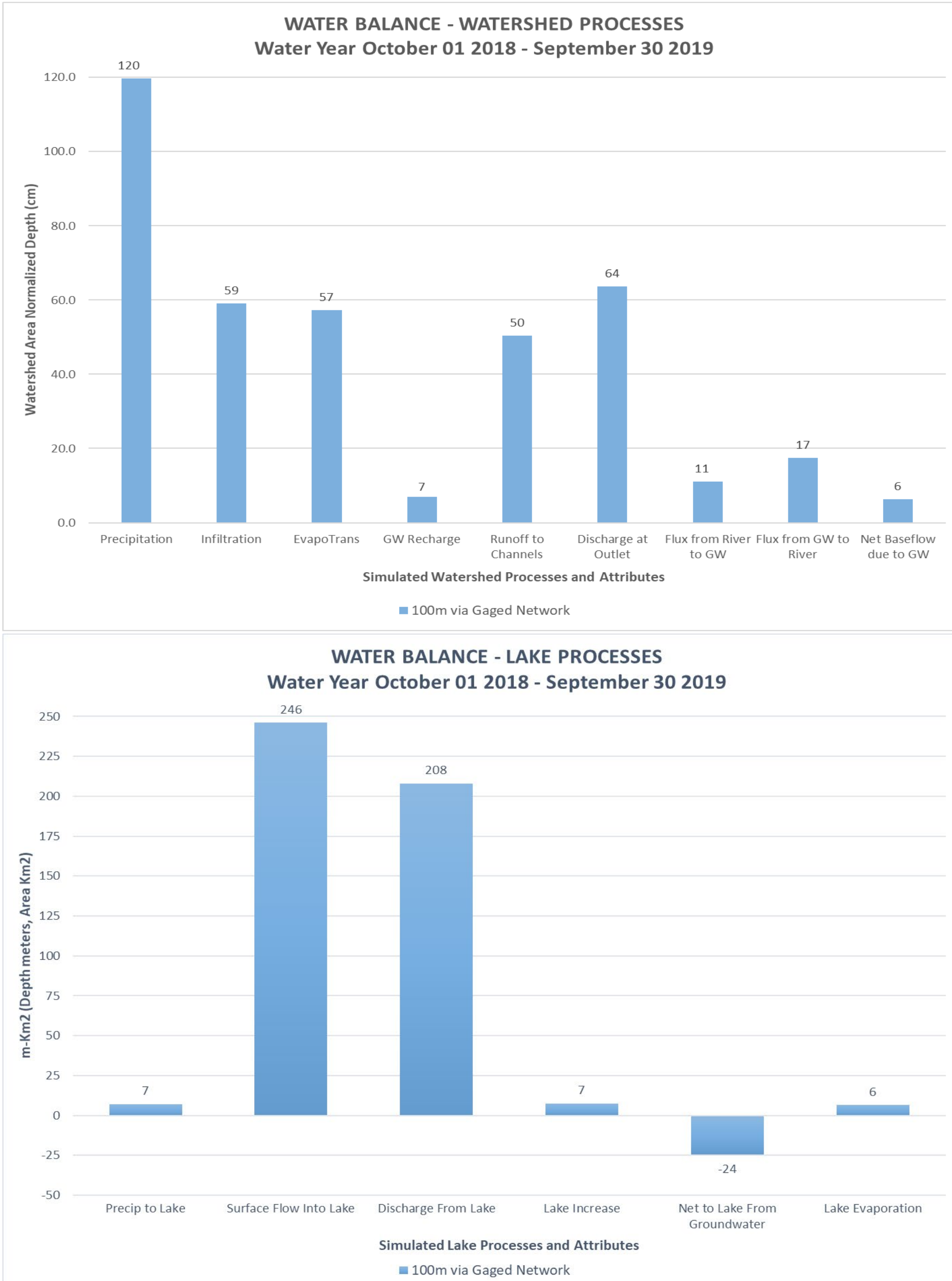

Figure 47. Comparison of October 2018 - September 2019 water year water balances of the simulated watershed and lake processes and attributes for the 100 meter model, run based on the gaged network input forcings.

Table 37. October 2018 - September 2019 water year water balance values for watershed processes, normalized by watershed depth.

Watershed Process	Totals Normalized by Watershed Depth (cm) 100m
Precipitation	119.8
Infiltration	59.1
Evapo-Transpiration	57.3
GW Recharge	6.9
Runoff to Channels	50.4
Discharge at Outlet	63.7
Flux from River to GW	11.1
Flux from GW to River	17.5
Net Baseflow due to GW	6.3

Table 38. October 2018 - September 2019 water year water balance values for lake processes.

Lake Process	m-Km2 (Depth m, Area Km^2) 100m
Precipitation to Lake	7.0
Surface Flow Into Lake	246.0
Discharge From Lake	207.8
Lake Increase or Decrease	7.3
Net to Lake From Groundwater	-24.5
Lake Evaporation	6.4

7 Conclusions and Recommendations

7.1 Summary and Conclusions

This study is a part of a multi-agency effort to assess the potential for improved stream flow predictions and Forecast-Informed Reservoir Operations (FIRO). The main goal of the program is to make water management more efficient in the face of extreme weather and climate events that typically lead to flooding or drought.

The focus of this report is the scientific and research component of the Final Viability Assessment for FIRO. In this case, a state of the art atmospheric and hydrologic model was developed for the Lake Mendocino watershed using GSSHA.

The tool was developed using point (i.e., gauge precipitation) and spatially distributed (i.e., soil type, land use, hydro-meteorology) gridded data sets. The Upper Russian River watershed was conceptualized in GSSHA by including significant physically based hydrologic process modules such as rainfall distribution, soil infiltration, groundwater flow, evapotranspiration, and others. Models developed at different grid resolutions were evaluated to test the effect on the simulated outcomes, discharge and Lake Mendocino levels.

Different combinations of forcing data sets with model resolutions were evaluated during model calibration efforts. Also, the calibration process was carried out in a staggered way such that a model with a single event on the surface water component was calibrated first, followed by models with increased levels of complexity and extended calibration time periods.

From these efforts, parameter data sets for the surface and groundwater components were determined based on comparisons of flow magnitudes on a daily basis and on event based volumes and peak flow rates. Models at 270m resolutions using forcing data derived from the West-WRF data sets, in general, better predicted the observed outcomes at key USGS and CW3E flow gauging stations. Also, although 100m resolution models matched reasonably well the observed flows at these stations, the long model run times at this resolution prevented them from making use of long (greater than 2 months) calibration time periods.

The calibrated parameters were used in models applied to a different time period (verification period) to assess the model capability on predicting stream flows and Lake Mendocino levels. From this exercise it was apparent that models at 270m resolution using gauge, CNRFC forcings, and West-WRF 1-day forecast data predicted the observed flows and lake levels better than other models assessed.

Water budgets, with low mass balance errors, accounted by each hydrological component from the integrated physical processes of the watershed model, explicitly provided an understanding that the deployed physics based processes are simulated correctly, and provides a better understanding of the watershed and the dominate physical processes in the watershed and the reservoir.

For short term forecast, 1D, comparisons of the outcomes of the GSSHA models with similar outcomes from other models in the area (CNRFC) showed that the GSSHA models developed as part of this study are reasonable predictors of daily volumes observed at the USGS gauging stations. The results indicate that the GSSHA/West-WRF driven model, as is, would be a useful tool for short term forecast in determining operations. However, as forecast lead time increased when utilizing the West-WRF forecast precipitation, the simulated flows and reservoir stages deviated from the observed with a general trend of decreasing precipitation, less flow, and lower reservoir stages indicating improvements would be needed to use the tools for longer forecast leads.

As the GSSHA model was demonstrated to reproduce runoff and reservoir stages when given a good representation of precipitation, the greatest potential for improved GSSHA forecast would be better precipitation forecast. Other measures, such as calibrating the model to the different forecast lead times, restarting the model with the observed system state for each new forecast, and utilizing observed data for data assimilation into the GSSHA, would also improve the model results.

7.2 Recommendations

Based on the outcomes of this study, the following are recommendations for the future application of the modeling tools to the FIRO study.

- 270m resolution models with West-WRF 1-day forecast seems to work reasonably well and could be used for forecast informed reservoir operations. An operational version of West-WRF/GSSHA should be developed and tested for utility.

- Model run times at 100m resolutions when the surface and groundwater components are fully coupled seem to be excessively long, which should be evaluated in any consideration of operational cycles' time constraints. Parallelization of some of the processes in the GSSHA model would possibly allow higher resolution models to be considered for operational models in subsequent phases of FIRO.

- Physics based hydrologic models require accurate precipitation forecast to produce accurate runoff and lake level forecast. The study highlights the need for more effort in developing more accurate long term meteorological forecast for use in FIRO. One option could be to modify weather forecast precipitation through, e.g., bias correction towards addressing decreasing precipitation volumes with increasing forecast lead times. Active research into improving the West-WRF forecasts are a part of the on-going FIRO project.

- To further the utility of longer forecast lead times, GSSHA model should be calibrated to their respective forcing inputs, and levels of uncertainty should be evaluated and communicated.

- Other recommendations to improve the model calibration would be to include the lake level as a calibration parameter and assess the impact of varying weights on various components in the automated calibration effort.

References

Anderson, S., W. Dietrich, D. Montgomery, R. Torres, M. Conrad, and K. Loague (1997) Subsurface flow paths in a steep, unchanneled catchment, Water Resources Research, vol. 33, no. 12, p 2637-2653, December, 1997.

Daly, C., R.P. Neilson, and D.L. Phillips (1994). A statistical-topographic model for mapping climatological precipitation over mountainous terrain. J. Appl. Meteor., 33, 140-158.

Dettinger, Michael, 2011. Climate Change, Atmospheric Rivers, and Floods in California – A Multimodel Analysis of Storm Frequency and Magnitude Changes. Journal of the American Water Resources Association (JAWRA) 47(3):514-523. DOI: 10.1111/j.1752-1688.2011.00546.x

Downer, C. W. (2002) Identification and modeling of important stream flow producing processes in watersheds, Ph.D. dissertation, Univ. of Conn., Storrs, 2002.

Downer, C.W. and F.L. Ogden (2006), Gridded Surface Subsurface Hydrologic Analysis (GSSHA) User's Manual Version 1.43 for Watershed Modeling System 6.1, available at: Gsshawiki.com

Ellis, C.J., S. Turnbull, C. Downer, A. Wilson, and H. Mix (2019). Russian River Watershed Hydrograph Separation using Stable Water Isotopes to Inform Watershed Models and Reservoir Operations. American Meteorological Association annual meeting poster. January 2019.

Flint, L. E., A. L. Flint, J. H. Thorne, and R. Boynton. 2013. Fine-scale hydrologic modeling for regional landscape applications: the California Basin Characterization Model development and performance. Ecological Processes 2:25.

Garbrecht, J., and L. W. Martz. 1999. TOPAZ: An Automated Digital Landscape Analysis Tool for Topographic Evaluation, Drainage Identification, Watershed Segmentation and Subcatchment Parameterization; TOPAZ Overview. U.S. Department of Agriculture, Agricultural Research Service, Grazinglands Research Laboratory, El Reno, Oklahoma, USDA, ARS Publication No. GRL 99-1, 26 pp., April 1999.

Nagel, D., S. Wollrab, S. Parkes-Payne, E. Peterson, D. Isaak, and J. Ver Hoef. 2017. National Stream Internet hydrography datasets for spatial-stream-network (SSN) analysis. Rocky Mountain Research Station, U.S. Forest Service Data Archive, Fort Collins, CO.

Martin, A., F.M. Ralph, R. Demirdjian, L. DeHaan, R. Weihs, J. Helly, D. Reynolds, and S. Iacobellis, 2018: Evaluation of Atmospheric River Predictions by the WRF Model Using Aircraft and Regional Mesonet Observations of Orographic Precipitation and Its Forcing. *Journal of Hydrometeorology*, **19**, 1097-1113, https://doi.org/10.1175/JHM-D-17-0098.1

Natural Resources Conservation Service (NRCS 2020) https://websoilsurvey.sc.egov.usda.gov/App/HomePage.htm

NLCD (2011). National Land Cover Database. https://www.mrlc.gov/

PEST (2020) Model-Independent Parameter Estimation and Uncertainty Analysis http://pesthomepage.org/

Ralph, F.M., and Dettinger, M.D. (2012) Historical and national perspectives on extreme west-coast precipitation associated with atmospheric rivers during December 2010: Bulletin of the American Meteorological Society, 93, 783-790.

Skamarock, W.C., et al. (2008) A Description of the Advanced Research WRF Version 3. NCAR Technical Notes, NCAR/TN-4751STR.

Sumargo, E., A.M. Wilson, F.M. Ralph, R. Weihs, A. White, J. Jasperse, M.A. Lamjiri, S. Turnbull, C. Downer, and L. Delle Monache, 2020: The Hydrometeorological Observation Network in California's Russian River Watershed: Development, Characteristics and Key Findings from 1997 to 2019. Bull. Amer. Meteor. Soc.

USGS (2019) USGS National Water Information System https://www.usgs.gov/nwis.

Appendix A - Daily Volume Hydrographs for the CW3E Stations for the 2018 Calibration Period with Gauge and 1-day West WRF Forcing Data

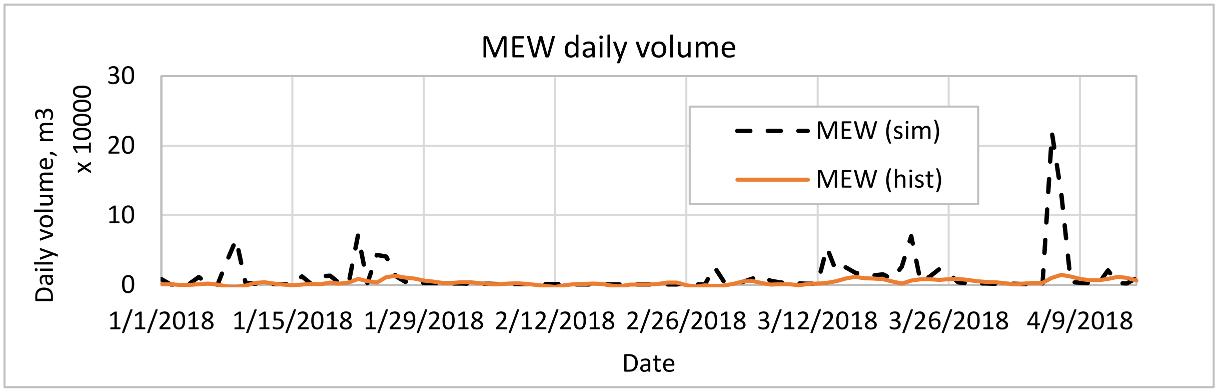

(a)

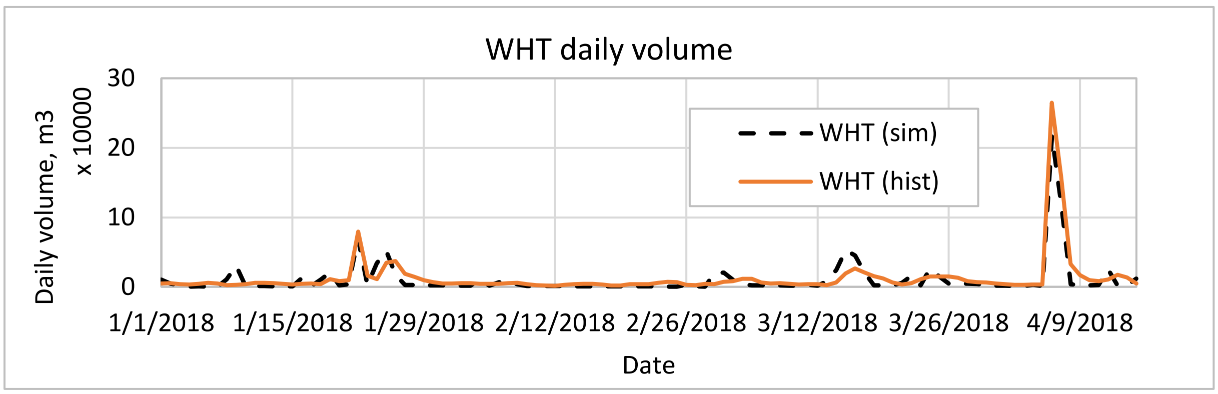

(b)

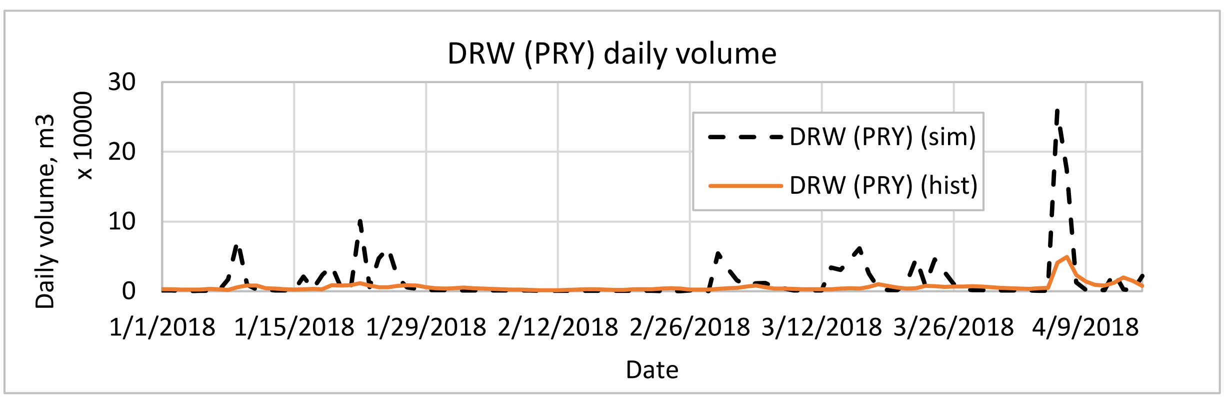

(c)

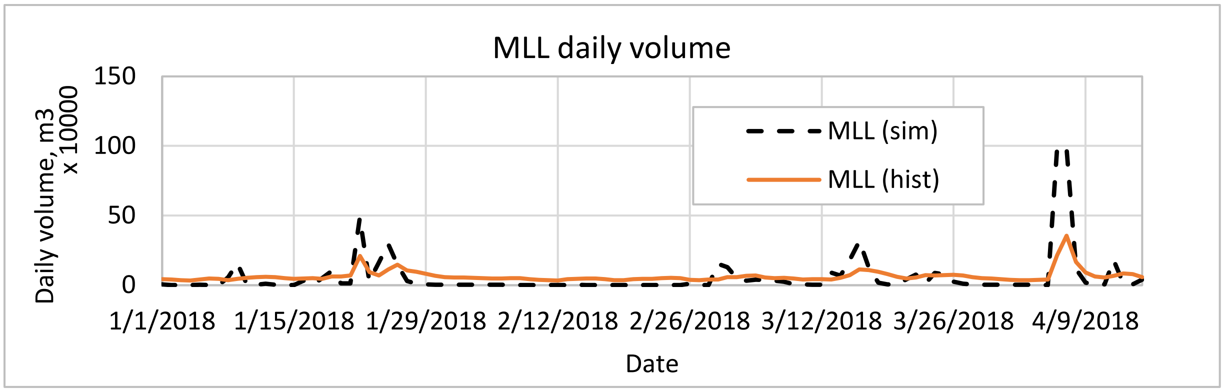

(d)

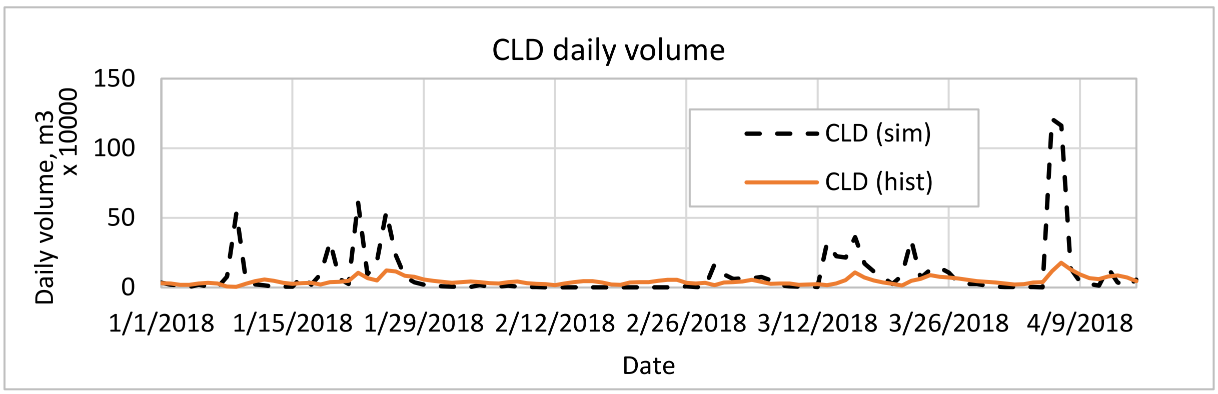

(e)

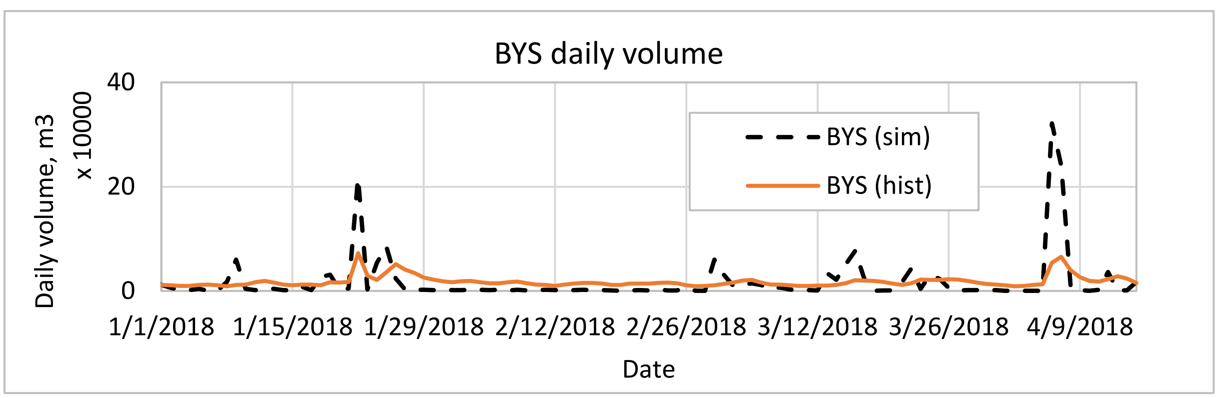

Figure A-1: Simulated vs. Observed daily flow hydrographs for the 2018 calibration period with gauge forcing data at (a) MEW; (b) WHT; (c) DRW; (d) MLL; (e) CLD; and (f) BYS gauging stations.

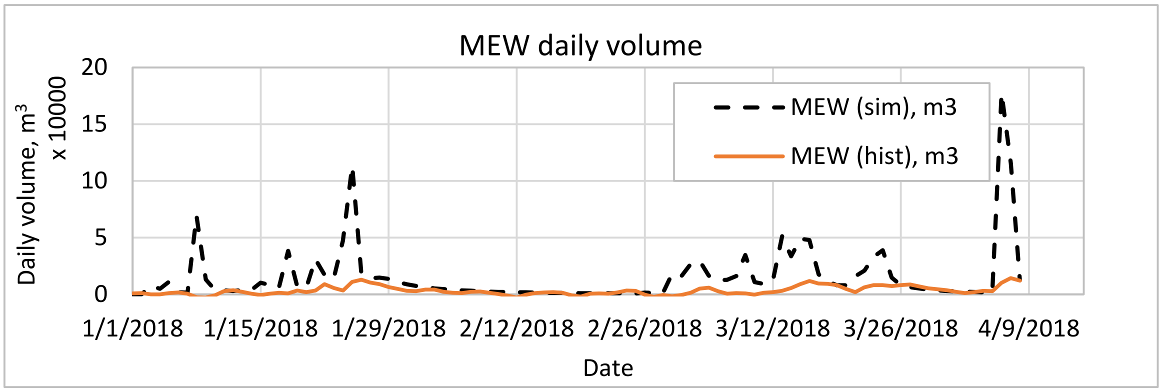
MEW daily volume
Daily volume, m³ x 10000
20
15
10
5
0
MEW (sim), m3
MEW (hist), m3
1/1/2018
1/15/2018
1/29/2018
2/12/2018
2/26/2018
3/12/2018
3/26/2018
4/9/2018
Date

(a)

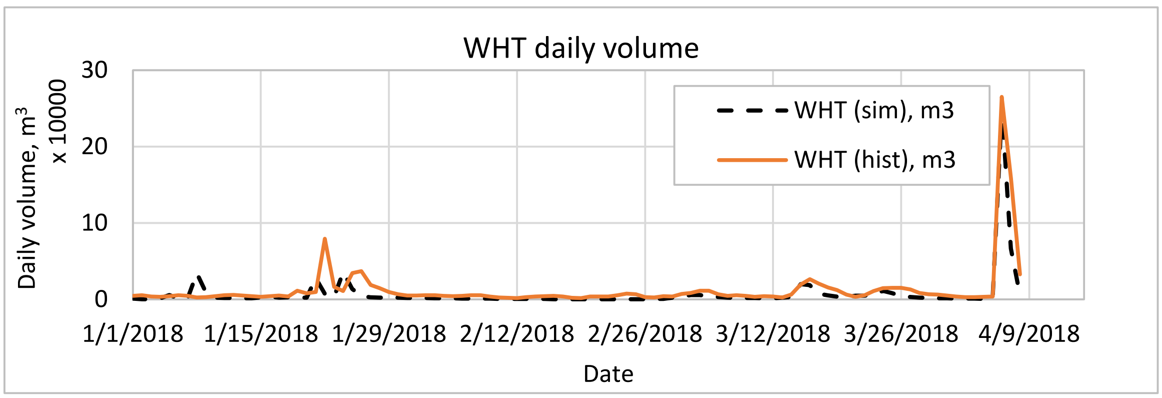
WHT daily volume
Daily volume, m³ x 10000
30
20
10
0
WHT (sim), m3
WHT (hist), m3
1/1/2018
1/15/2018
1/29/2018
2/12/2018
2/26/2018
3/12/2018
3/26/2018
4/9/2018
Date

(b)

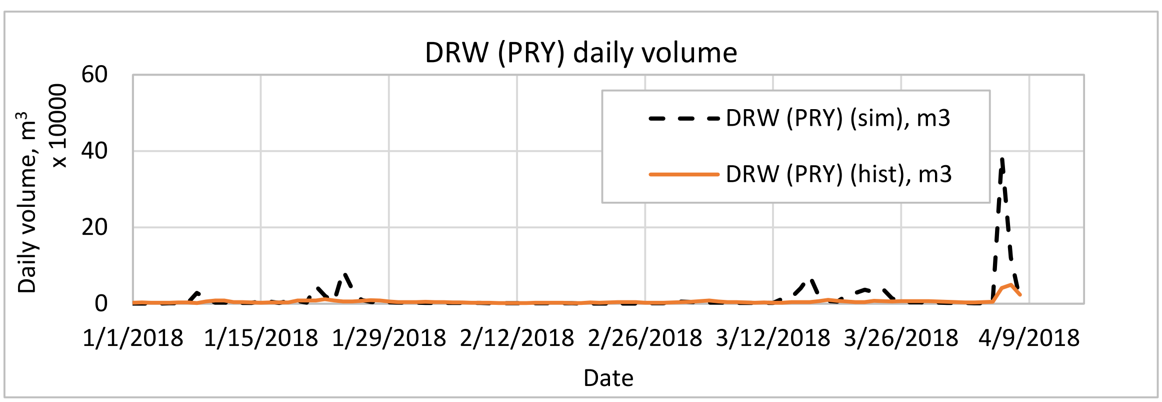
DRW (PRY) daily volume
Daily volume, m³ x 10000
60
40
20
0
DRW (PRY) (sim), m3
DRW (PRY) (hist), m3
1/1/2018
1/15/2018
1/29/2018
2/12/2018
2/26/2018
3/12/2018
3/26/2018
4/9/2018
Date

(c)

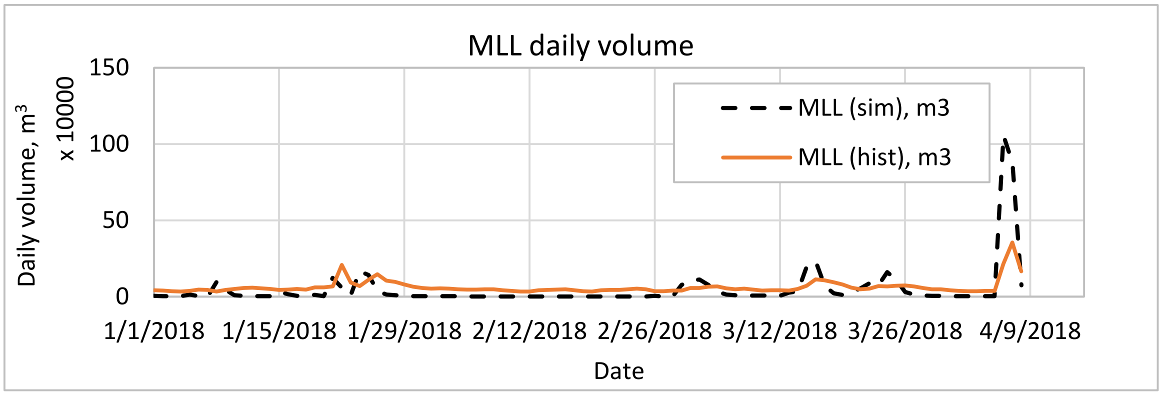

(d)

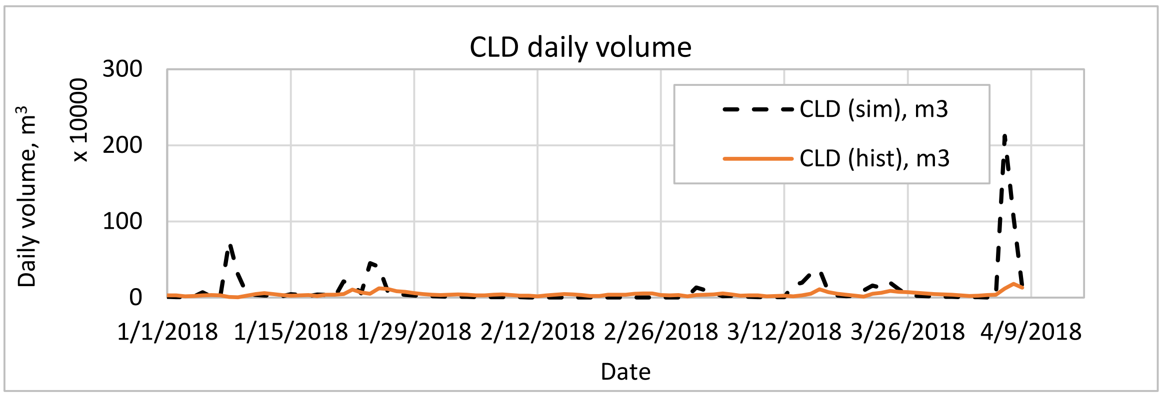

(e)

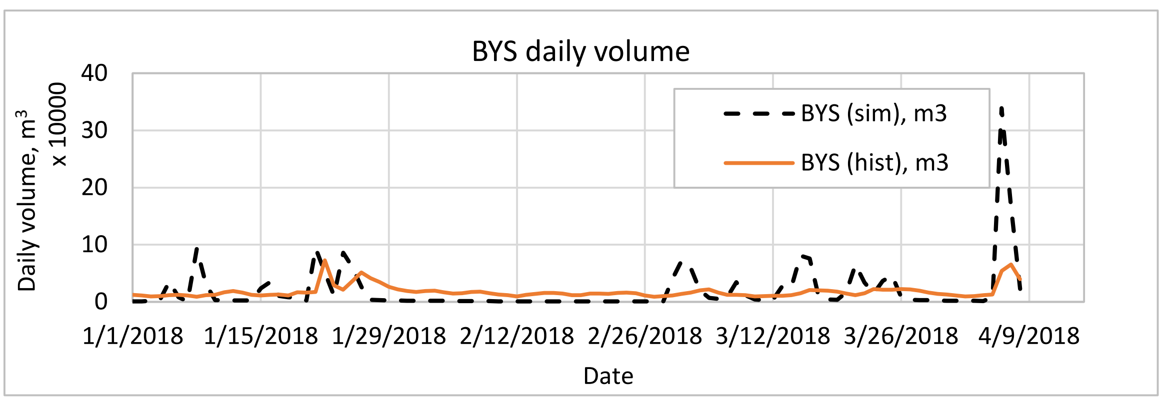

(f)

Figure A-2: Simulated vs. Observed daily flow hydrographs for the 2018 calibration period with 1-day West WRF forcing data at (a) MEW; (b) WHT; (c) DRW; (d) MLL; (e) CLD; and (f) BYS gauging stations.

Unit Conversion Factors

Multiply	By	To Obtain
acres	4,046.873	square meters
acre-feet	1,233.5	cubic meters
atmosphere (standard)	101.325	kilopascals
bars	100	kilopascals
cubic feet	0.02831685	cubic meters
cubic inches	1.6387064 E-05	cubic meters
cubic yards	0.7645549	cubic meters
degrees (angle)	0.01745329	radians
degrees Fahrenheit	(F-32)/1.8	degrees Celsius
feet	0.3048	meters
gallons (U.S. liquid)	3.785412 E-03	cubic meters
hectares	1.0 E+04	square meters
inches	0.0254	meters
microns	1.0 E-06	meters
miles (U.S. statute)	1,609.347	meters
square feet	0.09290304	square meters
square miles	2.589998 E+06	square meters
square yards	0.8361274	square meters
yards	0.9144	meters

EDITOR WILL INSERT SF298 REPORT DOCUMENTATION FORM BEFORE FINAL REVIEW.